1-1-2011

Bond characteristics of glass fibre reinforced polymer bars embedded in high performance and ultra-high performance concrete

Dave Ametrano
Ryerson University

BOND CHARACTERISTICS OF GLASS FIBRE REINFORCED POLYMER BARS EMBEDDED IN HIGH PERFORMANCE AND ULTRA-HIGH PERFORMANCE CONCRETE

By

Dave Ametrano

B.Eng. Civil Engineering, Ryerson University, Toronto 2008

A Thesis

Presented to Ryerson University

In the partial fulfillment of the degree of

Master of Applied Science

(Civil Engineering)

Toronto, Ontario, Canada, 2011

AUTHOR'S DECLARATION PAGE

I hereby declare that I am the sole author of this thesis.

I authorize Ryerson University to lend this thesis to other institutions or individuals for the purpose of scholarly research.

Author's signature _____   Date _____

I further authorize Ryerson University to reproduce this thesis by photocopying or by other means, in total or in part, at the request of other institutions or individuals for the purpose of scholarly research.

Author's signature _____   Date _____

BOND CHARACTERISTICS OF GLASS FIBRE REINFORCED POLYMER BARS EMBEDDED IN HIGH PERFORMANCE AND ULTRA-HIGH PERFORMANCE CONCRETE

Dave Ametrano

Master of Applied Science, Civil Engineering

RYERSON UNIVERSITY, Toronto, Canada, 2011

ABSTRACT

The use of fibre reinforced polymer (FRP) bars is increasing in construction as an alternative to conventional steel rebars. This thesis investigates the bond behaviour of glass fibre reinforced polymer (GFRP) bars embedded in high performance concrete (HPC) and ultra-high performance concrete (UHPC). In this study, the bond characteristics of sand coated GFRP bars embedded in 70 – 175 MPa concrete were explored. Beam and pullout tests were performed to determine the effects of the concrete strength, bar diameter, embedment length, and concrete cover on the bond behaviour of GFRP bars. Based on the analysis, the development lengths for the GFRP bars were determined and then compared to requirements provided by design codes. It was concluded that the design code lengths could be reduced by 20% while still maintaining a factor of safety of two over the development lengths determined through this study. This reduction can be applied when the GFRP bar is surrounded by sufficient transverse reinforcement, such that adding additional reinforcement would not affect the bond strength. Reducing the amount of GFRP reinforcing material needed, results in a lower overall cost of construction.

ACKNOWLEDGEMENTS

DEDICATED TO MY PARENTS

Table of Contents

List of Tables

List of Figures

Chapter 1

INTRODUCTION

1.1   Problem Statement

Steel reinforced concrete is the most widely used structural material for construction in the world. However, in the presence of corrosive environments, it is well known that the corrosion of steel rebar reinforcement may lead to the deterioration, or even the collapse, of structural elements. Billions of dollars are spent every year around the world on repairing and strengthening concrete structures whose reinforcement has deteriorated due to corrosion. In an effort to slow and/or prevent infrastructure deterioration, it has become a primary concern for scientists and engineers to mitigate the corrosion of steel rebars and to look for alternative reinforcing materials to use in place of steel to prevent corrosion altogether (Achillides and Pilakoutas, 2004).

Fibre reinforced polymers (FRPs) have emerged as a promising solution since they have been used successfully in other industries such as automotive, aerospace and sports manufacturing industries where their high strength and light weight characteristics are used to their advantage. Some of the commonly noted advantages of FRP materials over steel are their durability in various environments, non-corrosiveness, high strength-to-weight ratio, superior fatigue resistance, low thermal conductivity, nonmagnetic electrical insulation, small creep deformation, and specific gravity (Newhook and Svecova, 2006; Hao *et al.*, 2006). Subsequently, FRP reinforcement has been utilized for different concrete structures subjected to aggressive environments in order to increase their service lives and to reduce maintenance costs.

Despite the advantages of FRP reinforcement over steel reinforcement, due to various differences in the mechanical and physical properties between the two materials, a direct substitution is not

possible. The main issues that inhibit the vast use of FRP reinforcement for concrete structures include:

- High initial cost of FRP materials. Although the cost of FRP materials has reduced significantly in recent years as a result of improving manufacturing processes, most FRP materials remain more expensive than conventional reinforcing steel on an initial material cost basis.
- Lack of familiarity with FRPs as concrete reinforcement and limited availability of standards as compared with steel has delayed the adaptation of FRPs.
- FRPs exhibit a linear elastic behaviour until failure, thus they exhibit no ductility or yielding (Okelo and Yuan, 2005).
- The modulus of elasticity for some types of FRP, namely aramid fibre reinforced polymer (AFRP) and glass fibre reinforced polymer (GFRP) is much lower than steel. As a result, FRP-reinforced concrete structures are often governed by serviceability (deflection and crack widths) considerations, rather than strength requirements.
- The bond characteristics of FRP rebars with concrete and steel rebars with concrete are different due to the non-isotropic material properties and the different surface textures of the FRP rebars (ACI 440.1R-06).

The performance of a reinforced concrete member depends on the transfer of forces between the concrete and the reinforcement; this is the case for both the ultimate limit state (strength controlled) and the serviceability limit state (crack and deflection controlled). The transfer of forces between the concrete and the reinforcement depends on the quality of the bond between the two materials. The resistance of reinforced concrete members subjected to flexure, shear and torsion forces is directly related to the forces developed in their reinforcement. As a result, the development of adequate bond between the concrete and the reinforcement is always a critical aspect of the structural design.

Considerable experimental research has been conducted to understand the bond behaviour of FRP rebars in concrete. Due to the complexity of the parameters influencing the bond behaviour (i.e. the rebar diameter, embedment length, concrete cover, concrete confinement and concrete strength) and the different types of currently commercially available FRP rebars, a comprehensive understanding of the bond behaviour of FRP rebars with concrete has not yet been established (Okelo and Yuan, 2005). Design equations have been developed for designing concrete structures reinforced with FRP rebars

based on available experimental data up to 2002. Since then, considerable research has been conducted to assess the effects of different parameters on the bond performance of FRP rebars.

As the demand for stronger and more durable structures increases, high performance concrete and ultra-high performance concrete have been implemented as an alternative to conventional concrete for construction. The use of HPC and UHPC in conjunction with FRP materials requires modifications to the current design equations and provisions that determine the bond strength of FRP rebars and their required development length. Modifications are necessary in order to account for the effect of using HPC and UHPC on the bond properties between these materials. These modifications should be able to reduce the amount of FRP reinforcement needed which in turn will reduce the overall cost of the structure.

1.2   Research Objectives

The objective of this research project was to investigate the bond behaviour of GFRP rebars in high performance and ultra-high performance concrete with compressive strengths greater than 70 MPa. Within this objective, the research focussed on the effects that various parameters had on the bond behaviour which included: concrete strength, concrete cover, bar diameter, and embedment length.

The findings from this research were modeled to determine the development length requirement of the GFRP bars and then compared to code based equations.

1.3   Thesis Overview

This thesis is organized into six chapters. Chapter 1 gives an overview of the research. Chapter 2 provides an understanding of the components, manufacturing, properties, mechanics, durability, and applications of FRP materials. The parameters that affect the bond behaviour of FRP bars in concrete are also discussed in this section. As well, current design codes that are used to evaluate the bond strength of FRP along with the available methods used to model the bond behaviour of FRP are explained. Chapter 3 describes the materials used in this research study and the methodologies of the experimental testing program. Chapter 4 presents the experimental results and an analytical discussion on the findings. Chapter 5 provides a comparative analysis to existing code based equations and proposes modifications to the existing provisions. Chapter 6 provides the conclusions, limitations of this study, and recommendations for future research.

Chapter 2

BACKGROUND, LITERATURE REVIEW, AND DESIGN CODES

2.1   Fibre Reinforced Polymers

Fibre reinforced polymers (FRPs) are composite materials consisting of high strength fibres embedded in a polymer matrix. FRPs are composed of two distinct materials, thus the properties of the FRP system depend on those of the individual components. The fibres provide strength and stiffness to the composite and carry most of the applied loads, whereas the matrix acts to bond and protect the fibres and to transfer stress from fibre to fibre through shear stresses (ACI 440R-07). For structural engineering applications, the most common fibres used in FRPs are glass (GFRP), carbon (CFRP), and aramid (AFRP). FRP materials can be manufactured as sheets, plates and wraps for strengthening applications of existing structures, or as bars, rods, and tendons for internal reinforcement of concrete in new construction, or as a structural element itself. Figure 2.1 shows the typical FRP materials used for strengthening and rehabilitation of concrete structures.
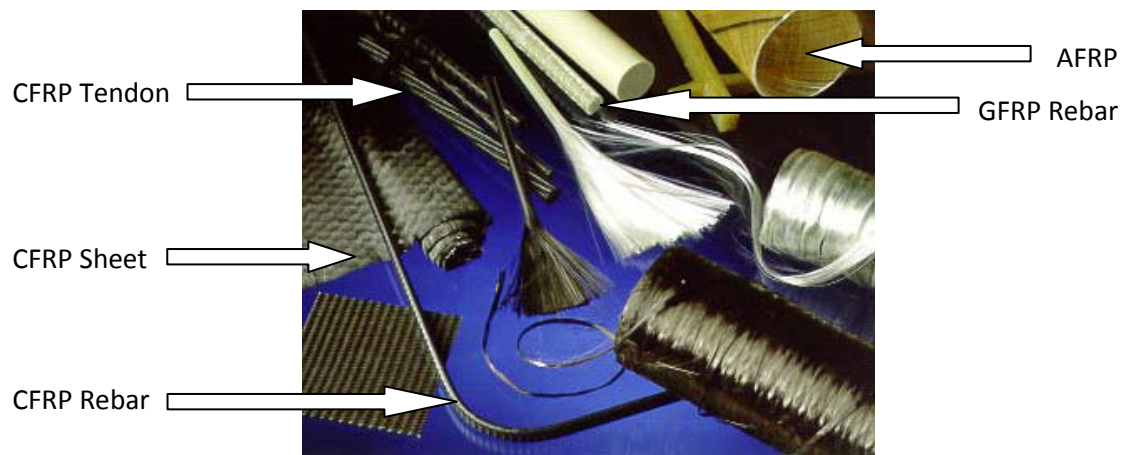
Figure 2.1: Various FRP products used for reinforcement of concrete structures.
(Source: Newhook and Svecova, 2006)

2.1.1 Resins

Selection of the appropriate matrix is essential in the manufacturing of FRPs. The physical and thermal properties of the matrix significantly affect the final mechanical properties as well as the manufacturing process of the FRP. In addition to coating and protecting the fibres from abrasion, the role of the matrix is to also transfers stresses between the fibres. The matrix transfers inter-laminar and in-plane shear stresses in the FRP, and provides lateral support to fibres against buckling when subjected to compressive loads (ACI 440.1R-03).

Matrix materials for FPRs can be grouped into two general categories: thermoplastics and thermosetting resins. Thermoplastics include polymer compounds such as polyethylene, nylon, and polyamides, whereas thermosetting materials include polyesters, vinylesters, and epoxies. For structural engineering applications, thermosetting materials are commonly used.

Thermoplastics matrix polymers are made from molecules in a linear structural form that are held in place by weak secondary bonds. The secondary bonds can be destroyed by heat or pressure and allow the thermoplastic to be reshaped though this could degrade its mechanical properties. Since thermoplastics display inferior thermal and physical properties when compared to thermosetting resins, they are not used as often as thermosetting resins, especially for structural engineering applications.

Thermosetting polymers are low molecular-weight liquids with very low viscosity, and their molecules are joined together by chemical cross-links forming a rigid, three-dimensional structure once cured (ACI 440.1R-06). Once the resins have hardened, they cannot be reshaped by applying heat or pressure. Thermosetting resins have good thermal stability and chemical resistance, and undergo low creep and stress relaxation. Thermosetting resins generally have good thermal stability at service temperatures, have good chemical resistance, and display low creep and relaxation properties in comparison with most thermoplastics. (Newhook and Svecova, 2006). Table 2.1 shows some mechanical properties of the thermosetting resins discussed below.

Polyesters – These are the most widely used polymers due to their relatively low cost and ease of processing since their resins cure at ambient temperatures. Several specific types of polyesters are available for use with varying degrees of thermal and chemical stability, moisture absorption, and shrinkage during curing.

Vinylesters – These are often categorized as a class of polyesters because of their similar processing procedures. Vinylesters are resistant to strong acids and alkalis, and are therefore commonly used as reinforcing bars for concrete since they are in a highly alkaline environment within the concrete. Furthermore, vinylesters offer lower moisture absorption and shrinkage when compared to polyesters however are slightly more expensive.

Epoxies – Theses are often used in wet lay-up applications of FRP plates and sheets due to their ability to cure at ambient temperature and exceptional adhesion characteristics. Epoxies have high strength, good dimensional stability, relatively good high-temperature properties, strong resistance to chemicals (except acids), and superior toughness. Epoxies are significantly more expensive than polyesters and vinylesters.

Table 2.1: Typical properties of thermosetting resins.

Resin	Specific Gravity	Tensile Strength (MPa)	Tensile Modulus (GPa)	Cure Shrinkage (%)
Vinyl Ester	1.12 – 1.32	73.00 – 81.00	3.00 – 3.35	5.40 – 10.30
Polyester	1.10 – 1.40	34.50 – 103.50	2.10 – 3.45	5.00 – 12.00
Epoxy	1.20 – 1.30	55.00 – 130.00	2.75 – 4.10	1.00 – 5.00

(Source: Newhook and Svecova, 2006)

2.1.2 Fibres

Fibres provide the strength and stiffness of an FRP. Since the fibres used in most structural applications are continuous and oriented in a specified direction, FRPs are orthotropic composites and are much stronger and stiffer in the direction of the fibres. The selection of fibres for specific applications depends on several factors including the required strength, the stiffness, durability concerns, cost limitations, and the fibre availability. For structural applications, the three most commonly used fibres are glass, carbon and aramid.

Glass fibres - Generally produced by a process called direct melt where the fibres are drawn from a glass melt with a diameter of 3-25 microns. Glass fibres are the most inexpensive and consequently are the most frequently used. The most common grade of glass fibre is E-glass. R-glass is stronger yet more expensive. Glass fibres are frequently used in the manufacturing of FRP rebars, pultruded FRP structural sections, FRP wraps for seismic applications, and filament wound FRP tubes.

Carbon fibres – Made from a process called pyrolysis, the formation of carbon fibres requires processing temperatures above 1000 °C (ACI 440R-07). Carbon fibres are notably more expensive than

glass fibres. They are extensively used in structural engineering applications such as prestressing tendons for concrete and structural FRP wraps for restoration and strengthening of reinforced concrete beams, columns, and slabs.

Aramid fibres – These are manufactured from a synthetic compound called aromatic polyamide in a process called extrusion and spinning (Newhook and Svecova, 2006). FRPs manufactured from aramid fibres have low compressive and shear strengths as a result of the anisotropic properties of the fibres. Furthermore, aramid fibres are susceptible to degradation from exposure to ultraviolet radiation and/or moisture.

Table 2.2: A qualitative comparison of the properties of carbon, aramid and glass fibres.

Criterion	Fibre Type		
	Carbon	Aramid	Glass
Tensile Strength	Very Good	Very Good	Very Good
Modulus of Elasticity	Very Good	Good	Adequate
Long Term Behaviour	Very Good	Good	Adequate
Fatigue Behaviour	Excellent	Good	Adequate
Bulk Density	Good	Excellent	Adequate
Alkaline Resistance	Very Good	Good	Adequate
Price	Adequate	Adequate	Very Good

(Source: Newhook and Svecova, 2006)

2.1.3 Manufacturing Process

The manufacturing of FRPs for structural applications is done by pultrusion, wet lay-up, and filament winding processes. Other methods to produce FRPs for non-structural applications include pull-winding, resin transfer moulding, vacuum bag moulding, and injection moulding. This section will focus on the methods used to produce FRP products for structural applications.

Pultrusion – This process is commonly used to fabricate FRP elements that have a constant cross-sectional profile such as bars, rods, tendons, plates, and structural sections that include bridge beams and decks. This is a continuous process that combines fibre reinforcements and thermosetting resin and is fully automated. Reinforcement materials, such as raw fibres (rovings), mats, or fabrics are pulled through a resin bath where the material is thoroughly coated or impregnated with a liquid thermosetting resin. The saturated reinforcements are then pulled through a heated die. As the fibres pass through the die, the polymer matrix hardens into the shape of the die and therefore produces a structural component. The FRP component is then pulled through the die from the cured end in a

continuous process, which in turn allows for FRP components of any length to be produced. As a result of this process, all of the fibres in the pultruded component are aligned in a single direction creating a unidirectional FRP. The process is driven by a system of caterpillar or tandum pullers located between the die exit and the cutoff mechanism (ACI 440R-07). Figure 2.2 shows a schematic of the pultrusion manufacturing process for a channel element.

Wet Lay-Up – This method is also referred to as hand lay-up or contact moulding. In this technique, a sheet of raw fibres is pressed into a mould covered with resin. In order to remove the entrapped air, a roller, brush or a squeegee is used to press the sheet into the resin. To achieve a desired thickness, additional layers of FRP can be added. For structural strengthening or rehabilitation applications, the mould is simply the structural member to be strengthened. The wet lay-up method is adequate for concrete, steel, aluminum, timber, and masonry structures. Once the resins have cured, the FRP sheet remains bonded to the structure. This technique is advantageous since it is performed quickly and easily in the field. Figure 2.3 shows a CFRP sheet and a bridge girder strengthened with and externally bonded CFRP sheets.
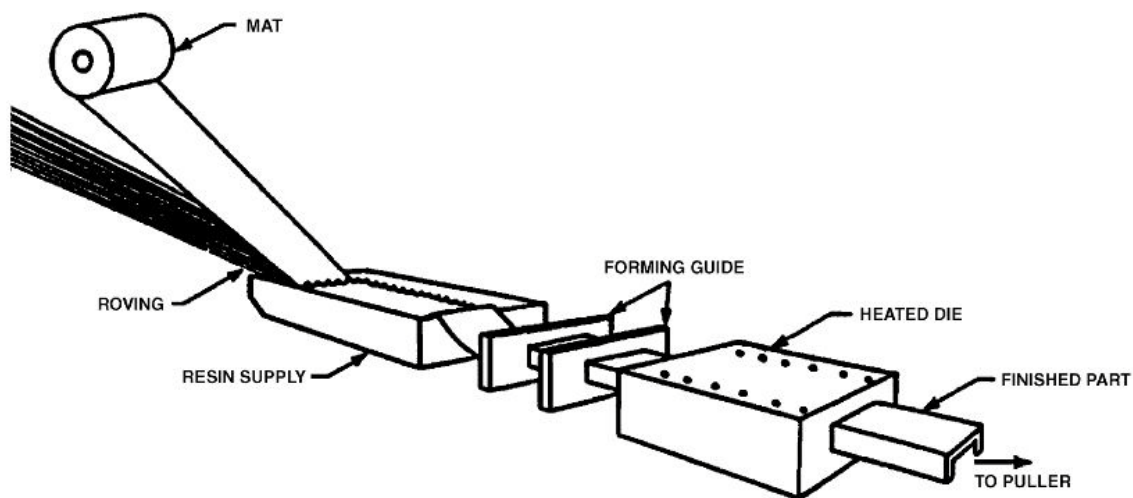
Figure 2.2: Schematic illustrating the pultrusion manufacturing process. (Source: ACI 440R-07)

Filament Winding – This process takes continuous raw fibres, impregnates them with matrix resin, and winds them onto a rotating mandrel. The resin-impregnated rovings move back and forth along the length of the mandrel (ACI 440R-07). The movement is controlled by a computer, which can allow the fibres to be placed with extreme precision and with desired orientations. The material is then cured on the cylinder and removed. FRPs made from filament windings can be used as stay-in-place formwork, such as for concrete piles. Figure 2.4 shows a schematic of the filament winding process.

<table>
<tr><td align="center">(a)</td><td align="center">(b)</td></tr>
</table>

Figure 2.3: FRP sheet: (a) CFRP sheet; (b) Strengthened bridge girder using CFRP sheets.
(Source: Bisby, 2006)
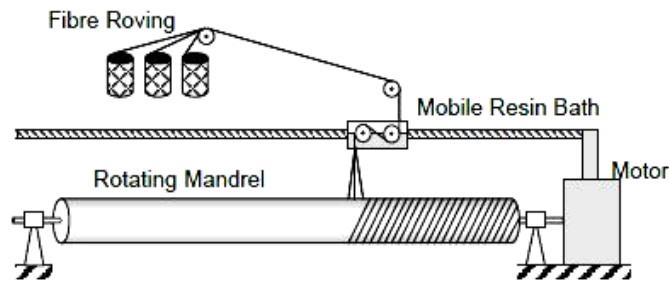
Figure 2.4: Schematic showing the filament winding manufacturing process.
(Source: Bisby, 2006)

2.1.4 Properties of FRP

The properties of FRP systems vary significantly depending on the relative proportions of fibre and matrix, the mechanical properties of the constituents, the fibre orientation within the matrix, and the manufacturing method. The mechanical properties of FRPs are highly directionally dependent, so the properties typically specified are in the direction of the fibres. All FRPs exhibit linear elastic tensile stress-strain behaviour in the direction of the fibres with no yielding prior to failure. Figure 2.5 shows the linear elastic behaviour of FRP from the typical stress-strain curve. The curves also show that FRP systems have a lower modulus of elasticity than that of steel, except for some CFRP systems.

The strength of FRP materials depends on whether the force being applied is tensile or compressive. Most FRPs are significantly more effective under tension; therefore, they are generally used as tensile reinforcement. The response of the FRP system depends on the failure strains of its fibres and matrix as illustrated in Figure 2.6. Table 2.3 and Table 2.4 show typical values for FRP reinforcing products and FRP strengthening products, respectively.

9
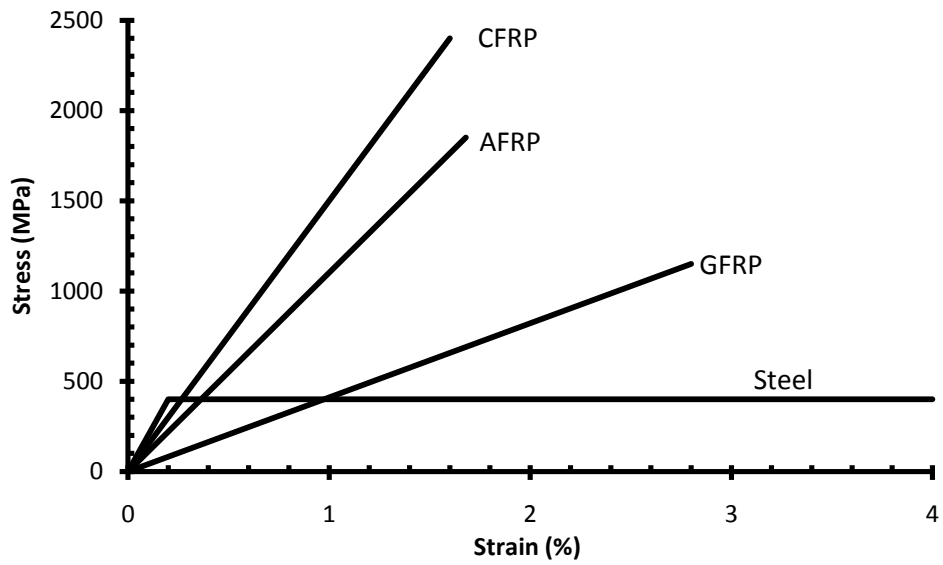
Figure 2.5: Stress-strain curves of FRP (Source: ACI 440R-96)
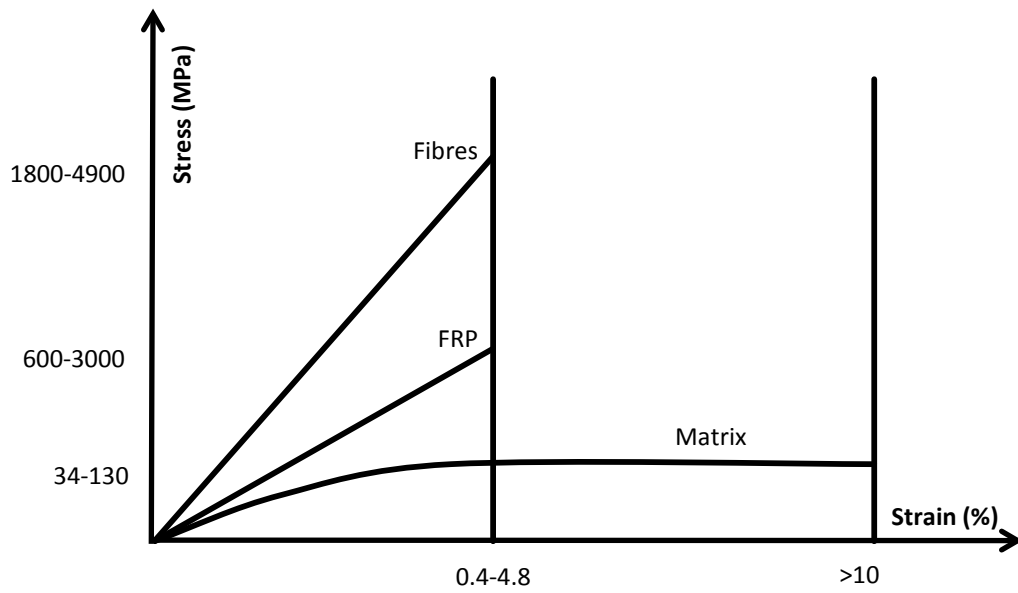
Figure 2.6: Stress-strain relationship for fibres, matrix and FRP
(Source: Bisby, 2006)

Table 2.3: Typical properties of FRP reinforcing products as reported by the manufacturer.

Reinforcement Type	Designation	Diameter (mm)	Area (mm^2)	Tensile Strength (MPa)	Elastic Modulus (GPa)
Deformed Steel	No. 3	9.5	71	420	208
Pultrall Inc. (2005)					
V-ROD CFRP Rod	3/8	9.5	71	1596	120
V-ROD GFRP Rod	3/8	9.5	71	852	43
Autocon Composites Inc. (2006)					
NEFMAC GFRP Rod	G10	N/A	79	600	30
NEFMAC CFRP Rod	C16	N/A	100	1200	100
NEFMAC AFRP Rod	A16	N/A	92	1300	54
Mitsubishi (2005)					
LEADLINE^{TM} CFRP Rod	Round	12	113	2255	147

(Source: ACI 440R-07)

Table 2.4: Typical properties of FRP strengthening systems.

FRP System	Fibre Type	Weight (g/cm^2)	Thickness (mm)	Tensile Strength (MPa)	Tensile Elastic Modulus (GPa)
Fyfe Co. LLC (2005)					
Tyfo SEH51 sheet	Glass	915	1.3	575	26.1
Tyfo SCH-35 sheet	Carbon	644	1.0	985	95.8
Sika Corp. (2007)					
Sika Wrap Hex 100G	Glass	913	1.0	531	23.6
Sika Wrap Hex 103C	Carbon	618	1.0	717	65.1
CarboDur S plate	Carbon	1800	1.2-1.4	2800	165
CarboDur M plate	Carbon	1900	1.2	2400	210
CarboDur H plate	Carbon	1900	1.2	1300	300
BASF (2006)					
MBrace EG 900 sheet	Glass	900	0.37	1517	72.4
MBrace AK 60 sheet	Aramid	600	0.28	2000	120
MBrace CF 130	Carbon	300	0.17	3800	227
MBrace CF 160	Carbon	600	0.33	3800	227
S&P 100/1.4	Carbon	---	1.4	2700	159

(Source: ACI 440R-07)

2.1.5 Applications of FRPs in Construction

FRPs are used in construction in various forms. Entire structures or structural elements can be fabricated entirely of FRP such as pedestrian bridges, utility poles, bridge deck panels, and girders. FRPs can also be used for new construction as internal rebars and prestressing tendons. FRP rebars and reinforcing grids have been used successfully as internal reinforcement in concrete beams and

slabs. The surface of FRP rebars are either sand coated, helically wound spiral outer surface, indented, braided, or ribbed. Figure 2.7 shows some commercially available FRP rebars with different surfaces. FRP tendons have also successfully been used as both internal and external prestressed reinforcement for concrete beams, slabs and bridge decks. FRP prestressing tendons were first used in Europe in the 1980s mostly to eliminate corrosion. However, the use of FRP prestressing tendons is still hindered since the use of the conventional steel anchor could not be used due to the low transverse strength of the FRP tendons (Erki and Rizkallak, 1993). Another application for FRPs is stay-in-place formwork. In these applications, the concrete formwork is fabricated from FRP and acts in a composite manner with the hardened concrete. The FRP formwork can be used as tensile reinforcement for slabs and beams. Columns and beams made from concrete-filled FRP tubes are an example of the stay-in-place formwork that has recently become popular. FRP tube formwork provides both tensile and confining reinforcement to the concrete (Bisby, 2006).

FRPs have also been used as a method for strengthening and rehabilitating concrete, steel, masonry, and timber structures. FRPs have the ability to increase the existing flexural, shear, and confinement strength of a structure. Materials used for these applications are either prestressing tendons, pre-manufacutred rigid FRP strips that are bonded to the surface of the structure with an adhesive, or wet lay-up sheets which are dry FRP sheets bonded to the surface using a polymer resin (Bisby, 2006). In addition, FRP strips, rods, and tendons can be inserted using an adhesive into grooves cut into structural members in applications called near-surface mounting (NSM).

(a)   (b)   (c)   (d)   (e)   (f)
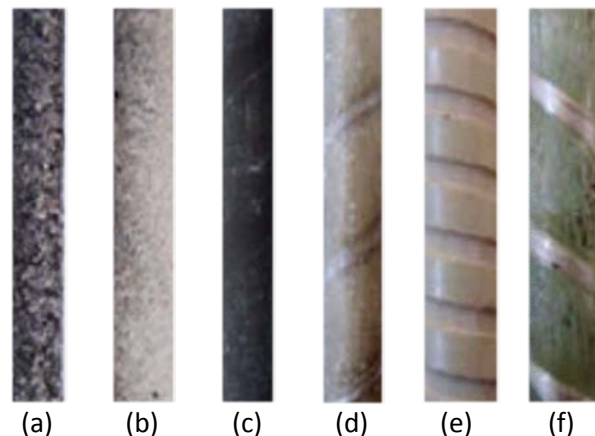
Figure 2.7: Commercially available FRP rebars: (a) sand coated CFRP bar; (b) sand coated GFRP bar; (c) surface textured CFRP bar; (d) helically wrapped - sand coated GFRP bar; (e) grooved GFRP bar; (f) helically wrapped GFRP bar. (Source: Baena *et al.,* 2009)

2.2   Bond Mechanism

The strength and stability of reinforced concrete structures depend on the bond strength between the concrete and its reinforcement. The compressive forces in a reinforced concrete member are resisted by the concrete, whereas the reinforcement resists the tensile forces. This indicates that there must be a force transfer or bond stress between the two materials. If the force transfer is not present, the reinforcement would pull out of the concrete and the structure would fail due to tensile loading (Alavi-Fard, 1999). In reinforced concrete, the transfer of forces between a reinforcing bar (Figure 2.8) and concrete occurs by three mechanisms: (1) chemical adhesion between the bar and the concrete, (2) frictional forces arising from the roughness of the interface, forces transverse to the bar surface, relative slip between the bar and surrounding concrete, and (3) mechanical anchorage or bearing arising from the textures or profile of the rebar surface (ACI 408R-03). The forces on the rebar are balanced by compressive and shear stresses on the concrete contact surfaces. These forces are resolved into tensile stresses that can result in cracking planes that are perpendicular to the reinforcement (radial splitting force) and parallel to the reinforcement (effective bond force).
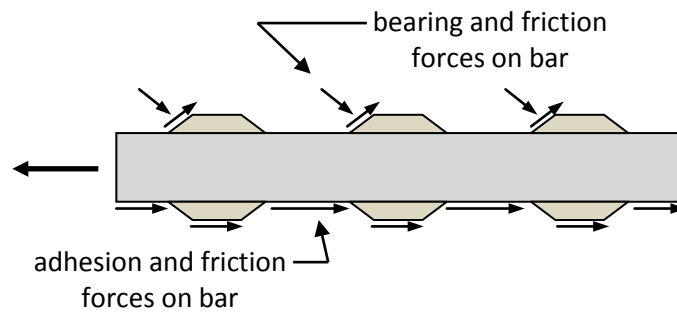
Figure 2.8: Bond force transfer mechanisms. (Source: ACI 408R-03)

To prevent bond failure, the rebar must be embedded deep enough into the concrete and should have enough confinement provided by the concrete cover and/or transverse reinforcement. Under these conditions, the radial and tangential stresses developed along the bar will be less than the capacity of the concrete and the reinforcing bar will achieve its design tensile strength and not undergo bond failure. If inadequate anchorage length or confinement is provided, radial and tangential stresses developed may be greater than the concretes capacity and can lead to bond failure.

2.2.1 Bond Failure Modes

Bond failures are divided into either splitting or pullout failure:

Splitting Failure – This failure mode occurs when the concrete surrounding the reinforcing bar develops transverse splitting cracks (Figure 2.9 a). Splitting failure results in cracking along planes that are both perpendicular and parallel to the reinforcement. As the reinforcing bars are loaded they exert radial pressure on the surrounding concrete. If the surrounding concrete and/or the transverse reinforcement are not adequate enough to resist this pressure, a splitting crack initiates at the concrete-rebar interface and propagates towards the surface, leading to the failure of the concrete by concrete cover splitting.

Pullout Failure – This failure mode occurs when the rebar pulls out of the concrete when the cover, bar spacing or transverse reinforcement is sufficient to prevent or delay a splitting failure. Pullout failure occurs when the radial forces from the loaded reinforcing bar are lower than what the surrounding concrete and/or transverse reinforcement can resist, and the tangential forcers are higher than what the concrete can resist. Pullout failure results in a shearing along a surface at the top of the ribs around the bars (Figure 2.9 b).

(a)   (b)
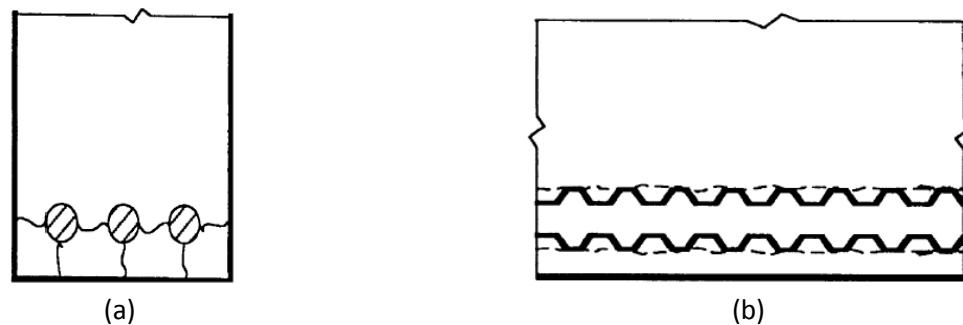
Figure 2.9: Cracking and damage mechanisms in bond: (a) End view showing splitting cracks between bars and concrete cover; (b) Side view of member showing shear crack and/or local concrete crushing due to bar pullout. (Source: ACI 408R-03)

For both splitting and pullout failures, it is common to observe crushed concrete in the region adjacent to the bearing surfaces of some of the deformations. Furthermore, both bond failures are related to the slip of the rebar relative to the concrete. In the pullout mode of failure, higher bond strength is achieved rather than in the splitting mode of failure since the concrete is well confined, and therefore, the radial splitting cracks need more energy to reach the surface of the concrete.

Bond force-slip and bond stress-slip curves can be used to better understand the nature of bond response as well as to determine the required embedment length for the rebar to achieve its desired strength prior to bond failure. Harajli *et al*. (2004) studied the effect of confinement of bond strength between steel bars and concrete, and produced a splitting and pullout failure bond stress-slip envelop for steel rebar in confined and plain concrete (Figure 2.10). For both failure modes, the stress-slip envelopes consist of four phases that explain bond behaviour during static loading.   Table 2.5 summarizes the phases for the splitting and pullout modes of failure.

Table 2.5: Summary of phases for the splitting and pullout modes of failure.

Phase	Failure Mode	
	Splitting	Pullout
First	First phase ends when an increase in the residual stress component of the bond force results in the development of splitting tensile cracks and the bond stress-slip relationship deviates from the pull out behaviour at s_α	First phase ends when the bond force is constant at a peak bond stress (u_1).
Second	Second phase ends when the crack has propagated to the surface and the splitting of the cover occurs indicating a complete deterioration of the bond ($s_{max,}u_{max}$).	The second phase is a constant bond following the peak bond stress (s_1 to s_2).
Third	The third phase shows significant drop in bond stress. (u_{max} to u_{ps} for confined concrete and u_{max} to βu_{max} plain concrete)	Third phase shows a significant drop in stress from s_2 to s_3.
Fourth	Fourth phase ends at zero bond stress and is a continuation of the third phase.	The fourth phase a constant bond for $s > s_3$.
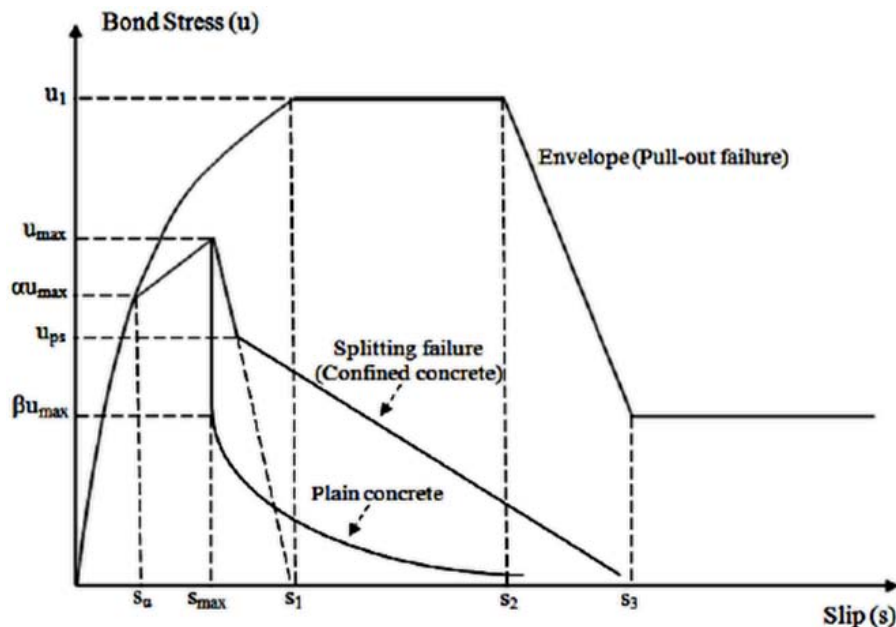
Figure 2.10: Bond stress-slip curve. (Source: Harajli *et al.,* 2004)

15

2.2.2 Bond Test Specimens

Two test methods to determine the bond strength of reinforcing bars are: pullout tests (Figure 2.11) and flexural bond tests (Figure 2.12). Pullout and flexural bond tests are the most common with the pullout test being the most popular method used by researchers for comparative bond assessment. In this test, a rebar is embedded in a concrete block or cylinder and pulled out under a tensile load. Although the stresses developed in the concrete during pullout tests rarely occur in practice, and the bond values developed under these tests differ substantially from those developed in reinforced concrete elements under practical conditions, these tests offer the simplest approach to determine the bond strength of rebars in concrete and therefore have been widely adopted (Achillides and Pilakoutas, 2004). Flexural bond tests, such as beam tests, resolve some of the stress field discrepancies that are present in pullout tests, and thus offer the advantages of representing the bond stress fields more accurately. Tighiouart et al. (1998) compared the results from pullout tests to beam tests and found that the results from the pullout tests showed higher bond strength that from the beam tests. The explanation is that the surrounding concrete around the rebar in the pullout test is under compression, reducing the cracking and therefore increasing the bond strength. Conversely, in the beam tests, the concrete surrounding the rebar is under tension, leading to cracking under low stress and therefore reducing the bond strength. The beam tests are more realistic in simulating the real behaviour of members in flexure. Direct axial tension tests have been used with concrete specimens having a continuous bar embedded in its centre (ACI 440R-07).
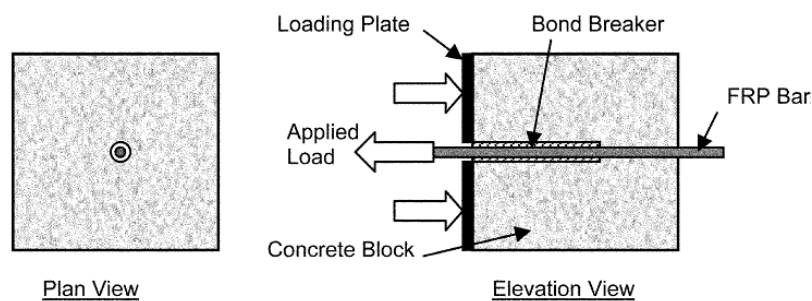
Figure 2.11: Pullout test specimen. (Source: ACI 440R-07)
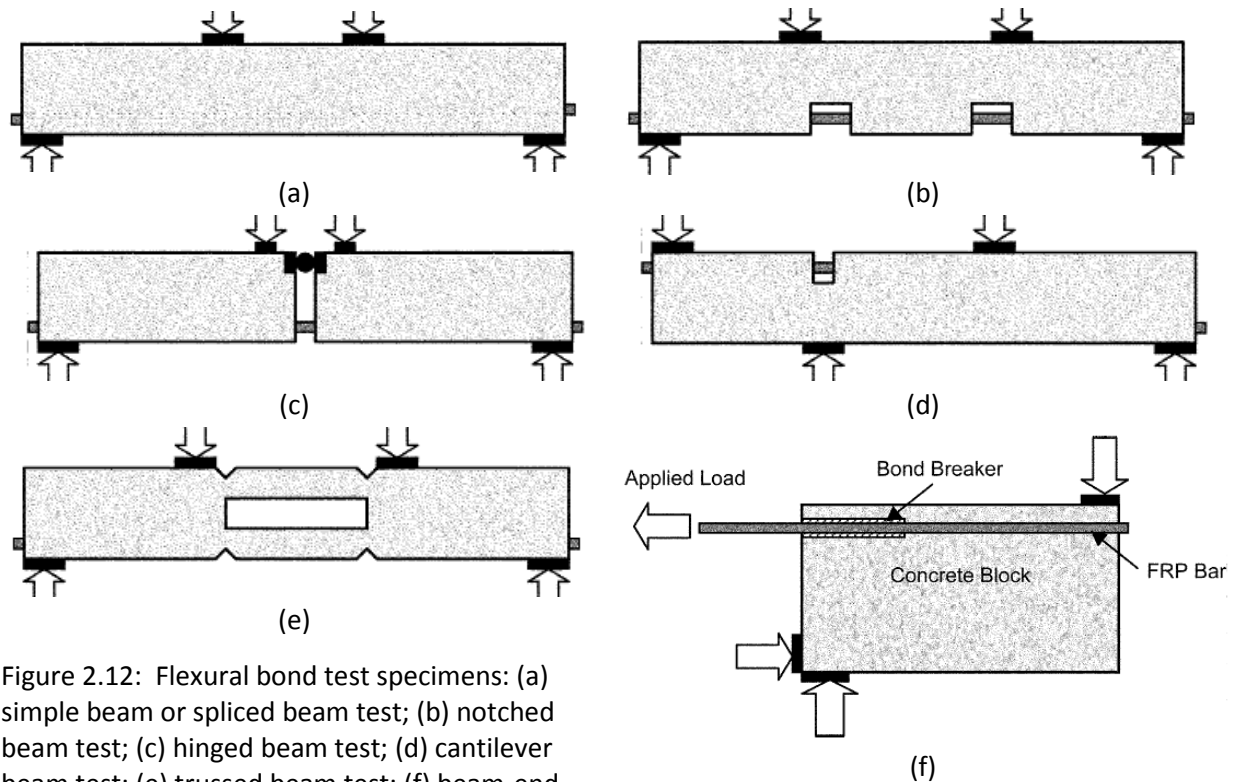
Figure 2.12: Flexural bond test specimens: (a) simple beam or spliced beam test; (b) notched beam test; (c) hinged beam test; (d) cantilever beam test; (e) trussed beam test; (f) beam-end test. (Source: ACI 440R-07)

2.2.3 Bond Behaviour of Steel Rebars

When a deformed bar moves with respect to the surrounding concrete, the surface adhesion is lost. At this instant, bearing forces acting on the ribs and friction forces acting on both the ribs and barrel of the rebar are activated. An increase in the bearing force results in an increase in the frictional force acting on the ribs. As the slip increases, the friction on the barrel reduces. This results in the bearing and frictional forces at the contact face between the ribs and the surrounding concrete to be the principal mechanism of force transfer (ACI 408R-03). However, in the case for plain bars (that is, with no deformation) frictional forces on the barrel play a significant role in force transfer. Any small shape variations of the bar and minor surface roughness causes transverse stresses which greatly affect the slip-induced friction on the bar.

2.2.4 Bond Behaviour of FRP Rebars

The bond behaviour of FRP rebars and concrete is not the same as that of steel bars because of the distinct differences in the force transfer and failure mechanisms of steel and FRP rebars. Their

17

different behaviour is attributed to the differences in material properties and their interaction mechanisms with concrete (Chaallal and Benmokrane, 1993). Steel is an isotropic, homogeneous, and elasto-plastic material, whereas FRP is an anisotropic, non-homogenous and linear elastic material. The anisotropic nature of the FRP rebar is due to the fact that its shear and transverse properties are influenced by the resins, whereas the longitudinal properties are influenced by the fibres (Cosenza et al., 1997). Material anisotropy leads to different physical and mechanical properties in both longitudinal and transverse directions; therefore, it is necessary for the anisotropic behaviour of FRP rebars to be considered in the development of design equations, and in the understanding of failure mechanisms (ACI 440.1R-06). The surface texture of FRP rebar is created by epoxy, fibres or sand coating and causes the rebars to be non-homogeneous. The non-uniform composition of FRP rebars results in a reduction in their bond performance. As a result, it has been observed that for FRP rebars the main force transfer mechanisms between the FRP rebar and concrete are through adhesion and friction (Benmokrane et al., 1996; Tighiouart et al., 1998).

2.3   Factors Affecting Bond of FRP Rebars in Concrete

There are several factors that affect the bond between FRP reinforcing bars and concrete. The major factors discussed in this section are divided into three major categories: bar properties, structural characteristics, and concrete properties. The bar properties addressed include bar size, fibre type, bar modulus, and bar surface condition. The structural characteristics discussed in this section include concrete cover and bar spacing, embedment length, bar cast position and transverse reinforcement. The concrete properties discussed include the compressive strength and fibre reinforcement.

2.3.1 Bar Properties

Bar Diameter – The relationship between bar size and bond strength of FRP rebars, in concrete has been investigated by Larralde and Silva Rodriguez (1993), Benmokrane et al. (1996), Tighiouart et al. (1998), Tighiouart et al. (1999), Achillides and Pilakoutas (2004), Okelo and Yuan (2005), Aly et al. (2006), Okelo (2007), Baena et al. (2009), and Hao et al. (2009). Their experimental research showed similar results obtained for steel rebar which was that the bond strength increased with the decrease in the bar diameter. Tigiouart et al. (1998) explained that the cause of decreasing bond strength with the increase in bar diameter was due to an increased amount of bleed water trapped beneath the

rebar which in turn created more voids than would form under a smaller bar. The presence of voids decreased the contact area between the rebar and the surrounding concrete and thus reduced the bond strength. In an investigation conducted by Achillides and Pilakoutas (2004), it was suggested that the reason for the decrease in bond strength for larger bars was because they developed less adhesion with the surrounding concrete than smaller bars. Baena *et al.* (2009) suggested that the Poisson effect may also influence the bond properties of FRP rebars since the diameter reduces when the bar is under tension. The diameter reduction increases with bar size, indicating that the Poisson effect had a greater influence on the larger bars with larger diameters, leading to a reduction in frictional and mechanical locking stresses.

Fibre Type – CSA S86-06, JSCE and ACI 440.1R-06 design codes do not distinguish between different types of fibres in the determination of bond strength, whereas the CSA S806-02 design code does make this distinction. CSA S806-02 specifies modification factors for each fibre type in the determination of bond strength. A value of 1.0 is assigned to CFRP and GFRP rebars, whereas a modification factor of 1.25 is assigned to AFRP bars in the determination of the required development length. This indicates that CFRP and GFRP develop similar bond strength whereas AFRP develops lower bond strength than CFRP and GFRP. Experimental research from Achillides and Pilakoutas (2004) found that both GFRP and CFRP developed 72% of the bond strength of steel, indicating that glass and carbon fibres had the same affect on bond strength. This agreed with the notion from the CSA S806-02 code that GFRP and CFRP develop similar bond strengths. Tigiouart *et al*. (1998) compared GFRP rebars to steel rebars and concluded that GFRP rebars exhibited lower bond strength than steel rebars. Findings from the study concluded that this was attributed to the differences in the surface deformation shapes of each type of rebar. Benmokrane *et al*. (1996) conducted research on GFRP rebars and found that the bond strength of GFRP rebars was 60 – 90% of steel rebars, which coincided with the findings from Tigiouart *et al.* (1998). Okelo (2007) conducted an investigation on CFRP bars by using beam test specimens and found that the bond strength of CFRP bars was 85% of steel bars.

Bar Modulus –Aly and Benmokrane (2005), and Aly *et al.* (2005, 2006) found that the bond strength of the FRP bars was related to the square root of the longitudinal modulus of the FRP bars. The Canadian Bridge Design Code, CSA S6-06, determines the required development length for an FRP bar by modifying the formula used for steel bars. This is done by multiplying the transverse reinforcement index by the modular ratio of FRP to steel bars (E_{frp}/E_s). The greater the modular ratio, the greater the

bond strength of the FRP bar, indicating that a higher FRP modulus will require a smaller development length. CSA S806-02, JSCE, and ACI 440.1R-06 do not take into account the modulus of elasticity of the FRP bar being developed. Very limited work has been done thus far and the effect of the bar modulus should be further investigated.

Rebar Surface – FRP reinforcing bars are manufactured with different surface textures, such as sand coated, spiral wrapped, helical lugged/ribbed, and indented. Similar to steel rebars, it is evident that deformed bars produce a significantly higher bond than plain bars due to the mechanical interlocking between the surface of the rebar and the surrounding concrete (Alunno Rossetti *et al. 1995;* Cosenza *et al.* 1997). CSA S806-02 provides modification factors for taking into account the different surface profiles of the FRP bars. A modification factor of 1.0 is assigned for roughened, sand-coated or braided surfaces; 1.05 is assigned to spiral patterned or ribbed surfaces; 1.80 for indented surfaces. This indicates that roughened, sand-coated, and braided surfaces provide the highest bond strength, followed by spiral patterned and ribbed surfaces, and lastly, indented surfaces with the weakest bond strength. Although CSA S806-02 suggests that the surface profile affects the bond strength of the FRP rebar, research by Mosley *et al.* (2008) suggested the opposite. Mosely *et al*. (2008) investigated the bond strength of FRP reinforcement through three series of beam tests using GFRP and AFRP, and showed that the deformation/surface texture of the FRP reinforcement did not significantly affect the bond strength or crack widths. Hao *et al.* (2009) performed tests on 90 pullout specimens to study the behaviour of GFRP rebars with ribbed surfaces with varying rib geometries in 28.7 MPa concrete. The research showed that when the rib height was kept constant at 5% or 6% of the rebar diameter, rib spacing equal to the rebar diameter was superior to rib spacing ranging from 0.5 to 3 times the rebar diameter. The research also showed with a rib spacing equal to the bar diameter, a rib height of 6% of the rebar diameter was superior to rib heights ranging from 3 – 9%. Research from Baena *et al.* (2009) concluded that when bond failure occurred at the rebar-concrete surface interface, the rebar surface treatment had a significant effect on the bond strength. Failure at the rebar surface occurred when the concrete strength was greater than 30 MPa. Since it is difficult to conclude that a definite relationship has been established for the effect of rebar surface on the bond strength, the effect of rebar surface should be further investigated as more information becomes available.

2.3.2 Structural Characteristics

Concrete Cover and Bar Spacing – The splitting and pullout modes of failure depend on the amount of concrete cover (Untrauer, 1965; Tepfers, 1973; Orangun *et al.,* 1977; Eligehausen, 1979; Darwin *et al*., 1996). For small cover and bar spacings, it is likely that splitting tensile failure will occur, whereas for large cover and bar spacing, it is possible to obtain a pullout failure mode resulting in higher bond strength (ACI 408R-03). Ehsani *et al.* (1996) conducted a test program with a total of 102 specimens with GFRP rebars. The research showed that the concrete cover had a significant effect on the type of bond failure. If the test specimen had a concrete cover of one bar diameter ($c = 1d_b$), the splitting mode of failure occurred. If the test specimen had a cover equal to, or exceeded, two bar diameters ($c \geq 2d_b$), pullout failure or rebar fracture was observed. Orangun *et al.* (1977) conducted splice tests on 62 unconfined and 54 confined specimens that all failed due to splitting. An equation was developed that related the average bond stress, normalized by the square root of the concrete compressive strength to the normalized cover to the center of the bar, and the normalized splice length using linear regression. This methodology was used by Wambeke and Shield (2006) to evaluate a compiled database of FRP rebar beam-end tests, notch-beam tests, and splice tests. A linear regression of the normalized average bond stress versus the normalized cover and embedment length showed that an increase in cover was accompanied by an increase in the bond strength. Furthermore, their relationship showed that the effect of concrete cover and bar spacing on the bond strength was non-linear. ACI 440.1R-06 uses Wambeke and Shield's relationship to determine the bond strength of an FRP rebar, which includes the effect of the cover. Similarly, CSA S6-06, CSA S806-02, and JSCE design codes all incorporate the effects of the cover and bar spacing in the determination of bond strength of an FRP bar.

Embedment Length – An increase in the embedment or splice length of a reinforcing bar will increase its bond capacity; however, this increase in capacity is not directly proportional to the increase in the bonded length. This is a result of the non-uniform bond forces along the length of the bar. Bond failure tends to be incremental, initiating in the area with the highest bond force per unit length.   The effect of embedment length of FRP rebars on the average bond stress in concrete was studied by Ehsani *et al.* (1995), Benmokrane *et al.* (1996), Sheild *et al.* (1997), Cosenza *et al.* (1997), Tigiouart *et al.* (1997, 1998), Achillides and Pilakoutas (2004), Aly *et al.* (2006), and Okelo (2007).   Their research showed that the maximum average bond strength decreases with the increase in embedment length, which was similar to the behaviour of steel rebars. This was attributed to the non-uniform distribution

21

of the bond stress along the length of the bar. For longer embedment lengths, Ehsani *et al.* (1995) reported that there was an increase in the initial tensile load and the initial stiffness of the bond stress-slip curve. Achillides and Pilakoutas (2004) found that the rate of bond stress increase was greater for smaller embedment lengths than for larger embedment lengths and attributed this behaviour to the non-uniform distribution of the bond stresses on the bar. Research by Okelo (2007) showed that for longer embedment lengths with higher compressive strengths, rebar fracture, concrete splitting, or shear compression failure takes place. The study also showed that for short embedment lengths, with low compressive strengths, and small rebar sizes, pullout of the rebar occurs.

Bar Cast Position – It has been observed that the bar position during concrete placement plays an important role in the bond strength between concrete and reinforcing bars. The effect of bar casting position on the bond behaviour of FRP rebars was investigated by Challal and Benmokrane (1993), Eshani *et al.* (1993), Alunno Rossetti *et al*. (1995), Benmokrane and Masmoudi (1996), Tigiouart *et al.* (1998) and Wambeke (2003).   It was observed that top cast bars showed weaker bond strength compared to bottom cast bars. The explanation was that during the placement of concrete, air, water, and fine particles migrate upwards and become trapped below the surface of the rebar. This caused a significant decrease in the bond strength, under horizontally placed rebars near the top of the concrete surface, due to the decreased contact area between the surrounding concrete and the bottom half of the rebar. Top cast bars generally refers to horizontal reinforcement with more than 305 mm (12 in.) of concrete below (ACI 440.1R-06). Tests from Ehsani *et al.* (1993) have shown that the bond strength of top bars is 66% of the bond strength of bottom bars. A decrease in the bond strength requires an increase in the required development length of the FRP bars; therefore, a modification factor is needed to account for the bar location when calculated the development length. ACI 440.1R-03 recommended a modification factor of 1.3 based on the available data from work by Chaallal and Benmokrane (1993) and Ehsani *et al.* (1996). ACI 440.1R-06 later revised its modification factor from 1.3 to 1.5 based on work done from Wambeke and Shield (2006). CSA S806-02 and CSA S6-06 and JSCE design codes recommend a bar location modification factor of 1.3.

Transverse Reinforcement – The use of transverse reinforcement provides confinement to developed and spliced bars by limiting the progression of splitting cracks and increases the force needed to cause bond failure (Tepfers 1973; Orangun *et al*., 1977; Darwin and Graham 1993a,b).   Transverse reinforcement added beyond what is need to provide the transition from splitting to pullout failure becomes less effective and eventually provides no increase in the bond strength (Orangun *et al*.,

1977). Limited research has been done thus far on the effect of confinement on FRP rebars in concrete. Research from Darwin *et al.* (1996) showed that confining steel bars with a high relative rib area (deformed bars with a relative rib area equal to 0.10 to 0.14) had increased bond strength compared to the same-size bars with smaller relative rib areas. Since FRP bars generally have a very low relative rib area, the confinement provided by transverse reinforcement may not increase the bond strength (Wambeke and Sheild, 2006). It was suggested that as more data becomes available, the effect of confinement on the bond strength of FRP rebars should be further investigated. The CSA S6-06 and JSCE design codes account for the effect of transverse reinforcement in evaluating the bond strength of FRP rebars, whereas CSA S806-02 and ACI 440.1R-06 do not.

2.3.3 Concrete Properties

Fibre Reinforcement – A reason for incorporating fibres into concrete is to increase its tensile strength. Wafa and Ashour (1992) reported an increase of 10 – 20% in the modulus of rupture of fibre reinforced concrete (FRC) over plain concrete with compressive strengths of 100 MPa. Even with this improvement, the compressive strength was still significantly larger than the tensile strength. The addition of fibres also increased the post-cracking resistance of the concrete, which was useful for applications where crack control was important. Fibres bridged across cracks and allowed some tensile stress to be transferred. At failure, the fibres pull out of the concrete, increasing the energy required to open and propagate the cracks (ACI 408R-03). The use of FRC should theoretically improve the resistance to splitting cracks and increase the bond strength. Studies have been done by Harajli and Salloukh (1997); Hamad *et al.* (2001); Harajli *et al.* (2002); and Dancygier *et al.* (2006, 2010) on the affect of fibres on the bond strength of steel rebars. Harajli and Salloukh (1997) performed an experimental study of the development/splice strength of steel reinforcing bars embedded in steel FRC. A bond strength increase of 55% for a volume fraction of fibres of 2% was reported. Hamad *et al.* (2001) found that steel fibre reinforcement improved the ductility of bond failure, and significantly increased the bond strength of steel rebars in high strength concrete. Harajli *et al.* (2002) showed that adding fibres in 1% and 2% by volume fraction increased the splitting bond strength by 26% and 33%, respectively. The addition of fibres also resulted in a significant improvement in the ductility of bond failure. However, in a study by Dancygier *et al.* (2010), the addition of steel fibres caused a reduction in the bond strength of up to 30% in normal strength concrete; whereas in high strength concrete, the addition of fibres increased the bond strength by 16%. The reduction in bond strength was attributed

to the fibres creating a local disturbance of the concrete matrix that prevented its proper compaction in the vicinity of the rebar which led to reduced bond strength. It was concluded that the disturbance of bond caused by the fibres was less pronounced in high strength concrete. Won *et al.* (2008) performed an experimental investigation on the effects of synthetic and steel fibres on high-strength concrete and FRP bars. The bond strength between the FRP bar and concrete increased by 5 – 70% as the volume fraction of fibre increased. Since most of the bond tests involving FRC have been pullout tests, as opposed to flexural tests, and because fibres affect the failure load for splice and development tests by changing the tensile properties of concrete, which in turn affects the bond strength, a significant amount of work is still needed before sufficient data is available to properly determine the effect of fibres on bond strength.

Compressive Strength – In most and design equations, the effect of the concrete properties on the bond strength is represented by using the square root of the concrete compressive strength ($\sqrt{f'}_c$) (ACI 408R-03). Since the tensile and shear properties of concrete greatly affect both the splitting and pullout modes of failure, and the tensile and shear properties of concrete are related the compressive strength concrete, the splitting and pullout modes of failure must also be influenced by the compressive strength of concrete. Performing a regression analysis on different experimental results showed that a good correlation exists between the bond strength of FRP rebars in concrete and $\sqrt{f'}_c$ (Ehsani *et al.,* 1996; Okelo and Yuan, 2005; Okelo, 2007). This representation has proven to be adequate for steel bars provided that the concrete strength is less than 55 MPa (ACI 408-03). Ehsani *et al.* (1995) conducted research to determine the effect of the concrete compressive strength on the bond strength of FRP bars. The researched showed that an increase in the compressive strength of concrete was accompanied by a slight increase in bond strength. It was also observed that the initial slip decreased as the concrete compressive strength increased. The effect of concrete strength on the bond behaviour was also studied by Makitani *et al.* (1993), Benmokrane *et al.* (1996), and Tighiouart *et al*. (1998). It was concluded that the bond strength increase was proportional to the square root of the compressive strength of concrete.

It has been observed that for concrete strength, $f'_c > 30$ MPa, the bond strength of FRP rebars does not depend on the compressive strength of concrete. This is a result of failure occurring at the interface between the FRP bar and the surrounding concrete. However, for concrete strength $f'_c < 15$ MPa, the compressive strength of concrete significantly influences the bond strength because failure

24

occurs in the concrete matrix away from the FRP rebar (Achillides, 1998; Achillides and Pilakoutas, 2004; Tepfers, 2006; Baena *et al.,* 2009).

The bond stress distribution for normal strength concrete (NSC) is significantly different from that of high strength concrete (HSC) (Azizinamini *et al.,* 1995). It was observed that for HSC, the bond stresses of deformed steel bars were highly non-uniform along the bars length, whereas the bond stresses between deformed steel bars and NSC appeared to be uniform. Azizinamini *et al.* (1993, 1995, 1999) concluded that for HSC, bond stresses were higher near the loaded end of the bar and they reduced moving away from this point. This was because the bond stresses develop only along the first few ribs of the deformed bar in HSC near the applied tensile force. In the case of NSC, as a tensile load is applied to the deformed bar, the first few lugs exert a bearing force on the concrete. As the load is increased, the concrete adjacent to the first few lugs crushes and this allows the next adjacent lug to come in contact with the concrete and participate in resisting the applied load. Design codes assume that there is uniform bond stress acting over the length of the rebar, which implies that all lugs bear against the concrete at the ultimate stage – which is a reasonable assumption to make for NSC and has been shown through experimental testing (Azizinamini *et al.,* 1995). However, experimental testing does not show the same behaviour for HSC. For HSC, as the first lug comes into contact with the surrounding concrete, a bearing force is generated. The horizontal component of the bearing force results in the bond stress, whereas the vertical component produces a radial stress that is responsible for splitting of the surrounding concrete, similar to the case with NSC. As the load is increased, the horizontal component of the bearing force is still less than that of the capacity of the concrete; however, the vertical component has now exceeded the capacity of the concrete and causes splitting failure to occur. This happens prior to achieving uniform load distribution along the bar length. Figure 2.13 illustrates the stress development at different stages of loading for NSC and HSC.

Since the surface deformations of FRP bars do not possess the same characteristics of steel reinforcing bars (high shear strength, high rigidity, deformation geometry), that provide enough lateral confinement through rib bearing, it follows that there is a lower bond strength for FRP reinforcing bars (Benmokrane *et al*., 1996). A study by Larralde and Silva-Rodriguez (1993) showed that the plane of failure for pullout test specimens showed little crushing or cracking in the concrete surrounding the reinforcing bars. This was an indication of low bearing stresses produced in the concrete by the action of the rebar deformations. A study by Cosenza *et al.* (2002) showed that for $f_c' < 30$ MPa, pullout failure was due to the breaking of the surrounding concrete, while the rebar was undamaged; when

$f_c' > 55 - 60$ MPa, failure was due to damage concentrated on the ribs of the FRP rebar, whereas the damage to the surrounding concrete was negligible; and for $30 < f_c' < 55$ MPa, damage of both the outer surface of the reinforcing bar and the surrounding concrete was observed.   Lee *et al.* (2008) also concluded that for NSC, bond failure occurred partly on the surface between the concrete and resin and partly between the resin and bar fibres; whereas for HSC, failure was mainly due to interlaminar delamination at the interface between the resin and fibres.   It is evident that the bond behaviour is dependent on the mechanical properties of the ribs of the FRP bar. This is significantly different from the bond between steel reinforcement and concrete where the concrete is always the weak element.

Figure 2.13: Behaviour of deformed steel rebars in concrete under tension: (a) low axial load causes nearest rib to come into contact with concrete; (b) increasing load causes adjacent ribs to contribute to the load resistance; (c) concrete crushes in front of ribs for NSC and causes load to be dispersed over full length; for HSC, only the first few ribs resist tensile load since the concrete has not crushed in front of first few ribs rendering the back ribs inactive. (Source: Azizinamini *et al.,* 1995).

2.4   Determination of Bond Strength

For several years, bond strength was represented in terms of the shear stress at the interface between the reinforcing bar and the concrete, essentially treating bond as a material property (ACI 408R-03). It is now understood that bond, anchorage, development, and splice strength are structural properties that are dependent on not only the materials, but also on the geometry of the reinforcing bar and the structural member itself.

The bond force, U, is defined as the change in tensile force per unit length ($U = dT/dl$). The tensile force in the bar, T, varies from a relatively high value at the location of cracks to a low value between cracks. When the concrete cracks around the rebar, the rebar carries the complete tensile load at the

location of the crack. At the uncracked locations, the tensile load is shared between the concrete and the rebar, thus causing the force in the bar to be lower. The real distribution of bond forces along the length of the bar cannot be determined because they depend on the location of the flexural cracks and the amount of tensile load shared by the concrete – neither of which can be evaluated. Figure 2.14 illustrates the variation of bond forces along the length of a rebar. Since the main focus of design is to ensure that the rebar is adequately anchored so that failure will not occur due to bond, it is convenient and realistic for design purposes to assume that bond forces are uniform over the anchored, developed or spliced length of the reinforcement (ACI 408R-03).
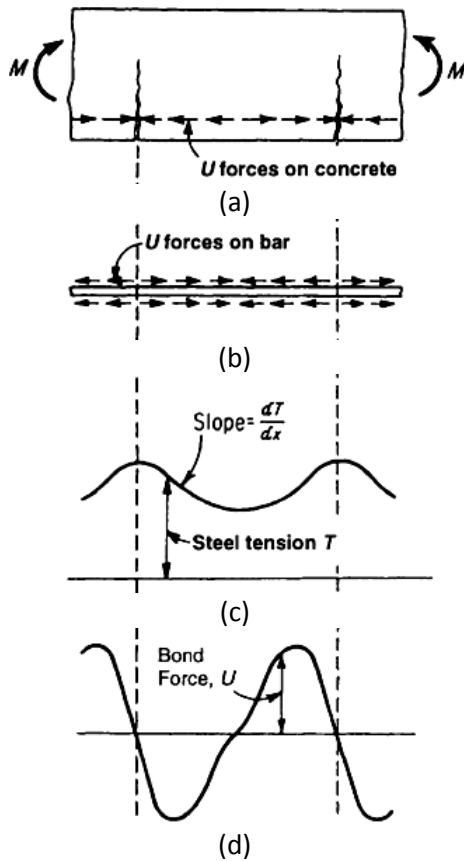
Figure 2.14: Variation of bond force along length of rebar in reinforced concrete member: (a) cracked concrete member; (b) bond forces on rebar; (c) variation of tensile forces along rebar; (d) variation of bond force acting on reinforcing bar, determined from dT/dl. (Source: ACI 408R-03)

Assuming a uniform distribution of stress, the force on the rebar is resisted by an average bond stress, u, acting on the surface of the rebar. Thus, an equilibrium condition can be established for a rebar embedded in concrete with a length l:

$$l\pi d_b \mu = A_b f_s$$
<div align="right">Equation 2.1</div>

where, l = embedment length of rebar (mm); d_b = rebar diameter (mm); μ = average bond stress (MPa); A_b = area of rebar; f_s = stress in rebar (MPa). From Equation 2.1, the average bond strength can be expressed as:

$$\mu = \frac{A_b f_s}{l \pi d_b} = \frac{d_b f_s}{4l}$$

Equation 2.2

2.5 Bond Strength and Development Length Equations in Design Codes

When used in design, development lengths and splice lengths are understood to represent the length of embedded reinforcement required to develop its design strength at a critical section (ACI 318-02). Design codes always specify the development length required to develop the design stress in the rebar because it is easier to apply by engineers. The development length can be related to the bond strength by using Equation 2.2. The following sections discuss the development length equations for FRP bars provided by CSA S806-02, CSA S6-06, ACI 440.1R-06, and JSCE.

2.5.1 CSA S806-02

The Canadian Standards Association (CSA S806-02) recommends the use of the following equation to determine the development length of the FRP rebars:

$$l_d = 1.15 \frac{k_1 k_2 k_3 k_4 k_5}{d_{cs}} \frac{f_F}{\sqrt{f'_c}} A_b$$

Equation 2.3

where:
l_d = Development length of FRP bars in tension, mm.
k_1 = Bar location factor: 1.3 for horizontal reinforcement placed so that more than 300 mm of fresh concrete is cast in the member below the development length or splice; 1.0 for all other cases.
k_2 = Concrete density factor: 1.3 for structural low-density concrete; 1.2 for structural semi-low-density concrete; 1.0 for normal density concrete.
k_3 = Bar size factor: 0.8 for A_b < 300 mm²; 1.0 for A_b > 300 mm².
k_4 = Bar fibre factor: 1.0 for CFRP and GFRP; 1.25 for AFRP.
k_5 = Bar surface profile factor. Can be taken as less than 1.0, but not less than 0.5, if this value has been shown by experiment. In the absence of direct experimental results the following values are used: 1.0 for surface-roughened or sand coated surfaces; 1.05 for spiral pattern surfaces; 1.0 for braided surfaces; 1.05 for ribbed surfaces; 1.80 for indented surfaces.
d_{cs} = The smaller of: (a) the distance from the closest concrete surface to the centre of the bar being developed; or (b) two-thirds of the centre-to-centre spacing of the bars being developed. The value shall not be taken greater than $2.5d_b$, mm.

f_F	=	Design stress in FRP tension reinforcement at ultimate limit state, MPa.
$\sqrt{f'_c}$	=	Square root of concrete compressive strength, MPa. Maximum permissible value of $\sqrt{f'_c}$ shall be 8 MPa.
A_b	=	Area of an individual bar, mm^2.

Substitution of Equation 2.3 into Equation 2.2 gives the following expression for the average bond strength:

$$\mu = \frac{d_{cs}\sqrt{f'_c}}{1.15 k_1 k_2 k_3 k_4 k_5 \pi d_b}$$
<div align="right">Equation 2.4</div>

From Equation 2.4, it is apparent that the bond stress is a function of the concrete cover, the compressive strength of concrete, the bar diameter, the bar location, the concrete density, the fibre type, and the bar surface profile.

2.5.2 CSA S6-06

The Canadian Highway and Bridge Design Code (CSA S6-06) modified the development length equation for steel by multiplying the transverse reinforcement index by the modular ratio of FRP to steel bars to determine the development length of FRP bars. The development length equation for an FRP bar is given as follows:

$$l_d = 0.45 \frac{k_1 k_4}{\left(d_{cs} + k_{tr}\frac{E_{frp}}{E_s}\right)}\left(\frac{f_{frp}}{f_{cr}}\right) A_{frp}$$
<div align="right">Equation 2.5</div>

where:

l_d	=	Development length of FRP bars in tension, mm.
k_1	=	Bar location factor: 1.3 for horizontal reinforcement placed so that more than 300 mm of fresh concrete is cast in the member below the development length or splice; 1.0 for all other cases.
k_4	=	Bar surface factor representing the ratio of bond strength of FRP to that of steel rebar having the same cross-sectional area, but not greater than 1.0. In absence of manufacturer or test data, 0.8 shall be used.
d_{cs}	=	The smaller of: (a) the distance from the closest concrete surface to the centre of the bar being developed; or (b) two-thirds of the centre-to-centre spacing of the bars being developed, mm.
E_{frp}	=	Modulus of elasticity of FRP, MPa.
E_s	=	Modulus of elasticity of steel, 200 x 10^3 MPa.
f_{frp}	=	Stress in FRP reinforcement, MPa.
f_{cr}	=	Flexural cracking strength of concrete, MPa. Equal to: (a) $0.4\sqrt{f'_c}$ for normal density concrete; (b) $0.34\sqrt{f'_c}$ for semi-low density concrete; (c) $0.30\sqrt{f'_c}$ for low-density

concrete. The value of $\sqrt{f'_c}$ used to compute f_{cr} must be less than 8 MPa.

A_{frp} = Area of FRP bar, mm^2.

k_{tr} = Transverse reinforcement index, mm. $\qquad k_{tr} = \dfrac{A_{tr}f_y}{10.5sn}$

However, $\left(d_{cs} + k_{tr}\dfrac{E_{frp}}{E_s}\right) \leq 2.5d_b$

where:

A_{tr} = Area of transverse reinforcement normal to the plane through the anchored bars, mm^2.
f_y = Yield stress of steel, Mpa.
s = Spacing of transverse reinforcement, mm.
n = Number of bars being developed or spliced.

Combining Equation 2.5 with Equation 2.2 gives the following expression for average bond strength:

$$\mu = \frac{\left(d_{cs} + k_{tr}\dfrac{E_{frp}}{E_s}\right) f_{cr}}{0.45k_1k_4\pi d_b} \qquad\qquad \text{Equation 2.6}$$

Equation 2.6 shows that CSA S6-06 considers the bond strength of an FRP bar to be a function of the concrete cover, the confinement provided by transverse reinforcement, the modulus of elasticity of the FRP, flexural compressive strength – which is related to the concrete density and compressive strength, the bar location, bar surface, and the bar diameter.

2.5.3 ACI 440.1R-06

The bond strength provided by the American Concrete Institute (ACI 440.1R-06) is based on research from Wambeke and Sheild (2006). A relationship for the bond strength of FRP bars was developed similar to the way that Orangun *et al.* (1977) developed an equation for the bond strength of steel bars and concrete. Wambeke and Shelid (2006) compiled a database of 269 beam bond tests, mostly consisting of GFRP specimens and a few AFRP specimens, which was limited to beam-end tests, notch-beam tests, and splice tests with compressive strengths ranging from 28-45 MPa. A linear regression of the normalized average bond stress versus the normalized cover and embedment length resulted in the following relationship:

$$\mu = \left(0.33 + 0.025\frac{C}{d_b} + 8.3\frac{d_b}{l_e}\right)\sqrt{f'_c} \qquad\qquad \text{Equation 2.7}$$

where:

C = Is the lesser of the cover to the center of the bar or one-half of the center-on-center spacing of the bars being developed.
d_b = Diameter of the bar, mm.

l_e = Embedment length of bar in concrete, mm.
f'_c = Compressive strength of concrete, MPa.

In the database, the bar surface (spiral wrap versus helical lug) did not appear to affect the results, nor did the presence of transverse reinforcement, however it was concluded that the affect of confinement should be further investigated.

Wambeke and Sheild (2006) developed a subset of their full database to determine a factor of safety for use with their equations. This database included both splitting and pullout failure with specimens having embedment lengths of at least $19d_b$. The C/d_b ratio was limited to 3.5 so that the same equation could be used to predict developable bar stresses for both failure modes. This limit was decided upon because specimens that had a C/d_b greater than 3.5 and embedment lengths greater than $19d_b$ always failed by rebar pullout. The following equation was developed for predicting the developable bar stress for a given cover and embedment length:

$$f_{fe} = \frac{0.083\sqrt{f'_c}}{\alpha}\left(13.6\frac{l_e}{d_b} + \frac{C}{d_b}\frac{l_e}{d_b} + 340\right) \leq f_{fu} \qquad \text{Equation 2.8}$$

where:
C/d_b = Cover to diameter ratio. Should not be taken larger than 3.5.
α = Bar location factor: 1.5 for horizontal reinforcement place above 300 mm of concrete; 1.0 for bars with less than 300 mm of concrete below.
l_e = Embedment length of bar in concrete, mm.
f'_c = Compressive strength of concrete, MPa.
f_{fu} = Design tensile strength of FRP, MPa.

Based on the tests in the Wambeke and Shild (2006) database, the bond of AFRP bars is similar to GFRP bars. There was no data for CFRP bars, however, it is anticipated that the much larger stiffness of the CFRP bars will likely decrease the required development length – resulting in a lower material modification factor. A material factor of 1.0 recommended for CFRP bars.

The bond between FRP bars and concrete according to ACI 440.1R-06 is dependent on the concrete cover, bar diameter, embedment length, the concrete compressive strength, and bar location. The bond relationship presented in the study by Wamebeke and Shield (2006) was developed primarily on GFRP bars. Very few of the test specimens in the data base contained transverse reinforcement, therefore its effectiveness is difficult to judge based on few results. Furthermore, the bond relationship was developed using specimens with concrete compressive strengths ranging from 28-45

MPa. No limits have been placed the concrete compressive strength as there are in the other codes. It is still necessary to further investigate the suitability of ACI 440.1R-06 equation for bond strength by studying the effects of transverse reinforcement, fibre type, and effect of concrete strength.

2.5.4 JSCE Design Recommendation

The Japanese Design Recommendation (JSCE, 1997) is similar to the CSA S6-06 design code in that they both make modifications to equations used to determine the required development lengths for steel bars and applied it to FRP. The basic development length of tensile reinforcement which will undergo bond splitting failure is calculated by the following equation:

$$l_d = \alpha_1 \frac{f_d}{4\,f_{bod}}\,d_b \qquad \text{provided that } l_d > 20d_b \qquad\qquad \text{Equation 2.9}$$

where:
l_d =   Development length of FRP bars in tension, mm.
f_d =   Design tensile strength of FRP, MPa.
d_b =   Diameter of FRP bar, mm.

α_1 =   1.0 (where $k_c \leq 1.0$);
           0.9 (where $1.0 < k_c \leq 1.5$);
           0.8 (where $1.5 < k_c \leq 2.0$); $k_c = \dfrac{c}{d_b} + \dfrac{15A_t}{sd_b}\dfrac{E_t}{E_0}$
           0.7 (where $2.0 < k_c \leq 2.5$);
           0.6 (where $2.5 < k_c$).

where:
c =   The smaller of: downward cover of main reinforcement; or half of the space between the anchored reinforcement, mm.
A_t =   Area of transverse reinforcement which is vertically arranged to the assumed splitting failure surface, mm^2.
s   =   Distance between the centers of the transverse reinforcement, mm.
E_t =   Young's modulus of transverse reinforcement, MPa.
E_0 =   Standard Young's modulus, 200,000 MPa.
f_{bod} =   Design bond strength of concrete, MPa. $f_{bod} = 0.28\alpha_2 f'^{2/3}_{ck}/\gamma_c \leq 3.2$

where:
α_2 =   Modification factor for bond strength of FRP: 1.0 where bond strength is equal to or greater than that of deformed steel bars; otherwise value shall be reduced according to test results.
f_{ck} =   Compressive strength of concrete, MPa.
γ_c =   Characteristic value for the concrete compressive strength taken as 1.3.

JSCE Design Recommendation specifies that when the reinforcement to be anchored is placed such that there is more than 300 mm of concrete below, and the bar placement is at an angle less than 45° from the horizontal, the development length determined from Equation 2.9 should be multiplied by a factor of 1.3.

Combining Equation 2.9 with Equation 2.2 provides the following expression for average bond strength:

$$\mu = \frac{f_{bod}}{\alpha_1} \qquad \qquad \text{Equation 2.10}$$

According to the JSCE Design Recommendation from Equation 2.10, it can be seen that the bond strength between FRP bars and concrete is dependent on the bar location, compressive strength of concrete, concrete cover, bar diameter, and the confinement provided by the transverse reinforcement.

2.6   Bond Stress-Slip

Bond between reinforcement and concrete can be analytically described by means of a constitutive bond stress-slip $(\tau - s)$ relationship that can be introduced in the solution of problems, such as the calculation of the development length (Cosenza *et al.,* 1996). Even with the numerous existing formulations for steel rebars, FRP rebars still require an extensive research effort to determine an analytical model of the bond stress-slip constitutive law. The available formulas that do exist for FRP rebars are intended to establish a general law, which is validated by determining its parameters by curve fitting. No specific formulation for the different types of rebars have been developed so far (Cosenza *et al.*, 1997). The following sections present an overview of the available bond stress-slip relationships of FRP rebars in concrete.

2.6.1 Malvar Model

The first modeling of the bond phenomenon in the case of FRP bars was given by Malvar (1994). The objective of this study was to develop an understanding of bond-slip behaviour for FRP rebars with various deformation geometries and radial confining stresses. Based on the experimental data, an analytical expression for the bond stress-slip curve was developed for generic confinement and different concrete strengths. The developed expression is derived in a two-step procedure. First, the peak on the bond stress-slip curve was defined as a function of confinement as follows:

$$\frac{\tau_m}{f_t} = A + B\left(1 - e^{-C\sigma/f_t}\right)$$

Equation 2.11

$$\delta_m = D + E\sigma$$

Equation 2.12

where:

τ_m	=	Peak bond stress.
σ	=	Confining axisymmetric radial pressure.
f_t	=	Tensile concrete strength.
δ_m	=	Slip at peak bond stress.
A,B,C,D,E	=	Emperical constants determined for each bar type.

Second, the complete normalized bond stress-slip curve is expressed as $\tau = \tau(\delta, \sigma)$:

$$\tau = \tau_m \frac{F\left(\frac{\delta}{\delta_m}\right) + (G-1)\left(\frac{\delta}{\delta_m}\right)^2}{1 + (F-2)\left(\frac{\delta}{\delta_m}\right) + G\left(\frac{\delta}{\delta_m}\right)^2}$$

Equation 2.13

where: F,G = Empirical constants for each bar type.

2.6.2 Bertero, Popov, and Eligehausen Model (BPE Model)

The well-known bond stress-slip analytical law for deformed steel bars failing by rebar pullout was proposed by Eligehausen *et al.* (1983). According to this model, the bond stress-slip of steel rebars shows four distinct branches (Figure 2.15): the initial ascending branch of the bond stress-slip relationship up to the maximum bond stress,τ_1, for $s \leq s_1$; a second branch of constant bond ($\tau = \tau_1$) up to slip ($s = s_1$); a linearly descending branch from (s_2, τ_1) to (s_3, τ_3); and a horizontal branch for $s > s_3$ with a value of τ equal to the development of frction ($\tau = \tau_3$).
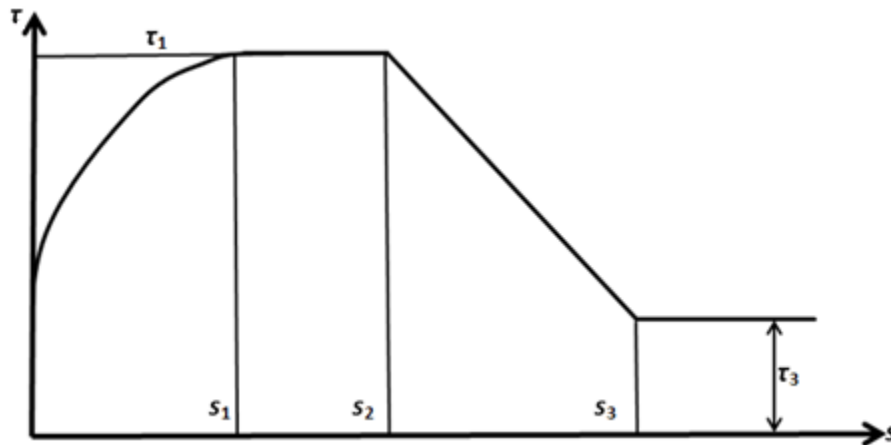
Figure 2.15: BPE Model. (Source: Eligehausen *et al.,* 1983)

The ascending branch of the BPE model is expressed as follows:

$$\frac{\tau}{\tau_1} = \left(\frac{s}{s_1}\right)^\alpha$$
Equation 2.14

where, τ_1= maximum bond stress; s_1= slip corresponding to maximum bond stress. Values for s_2, s_3 and τ_3 in Figure 2.15 are determined based on experimental results. In Equation 2.14, α is a curve-fitting parameter that must not be larger than 1 to be physically meaningful. Eligehausen *et al.* (1983) proposed a value of $\alpha = 0.40$ for steel bars.

Application of the BPE model to FRP rebars has been done by Faoro (1992), Aluno Rossetti *et al.* (1995), Focacci *et al.* (2000), and Pecce *et al.* (2001). When the BPE model was applied to FRP rebars, it was determined that the original BPE model had shown a lack of the second branch. Cosenza *et al.* (1996) investigated the bond stress-slip behaviour of FRP rebars and proposed a modification to the BPE model which presented the same ascending branch, neglected the second branch, and a softening branch having the slope p $\cdot$ τ_1/s_1 from (s_1, τ_1) to (s_3, τ_3) which is given by:

$$\frac{\tau}{\tau_1} = 1 - p\left(\frac{s}{s_1} - 1\right)$$
Equation 2.15

The third branch, where s $>$ s_3, is horizontal and has a value representing the friction component τ_3. The modified BPE model appears more suitable for FRP rebars than the original BPE model. The modified BPE model is shown in Figure 2.16.
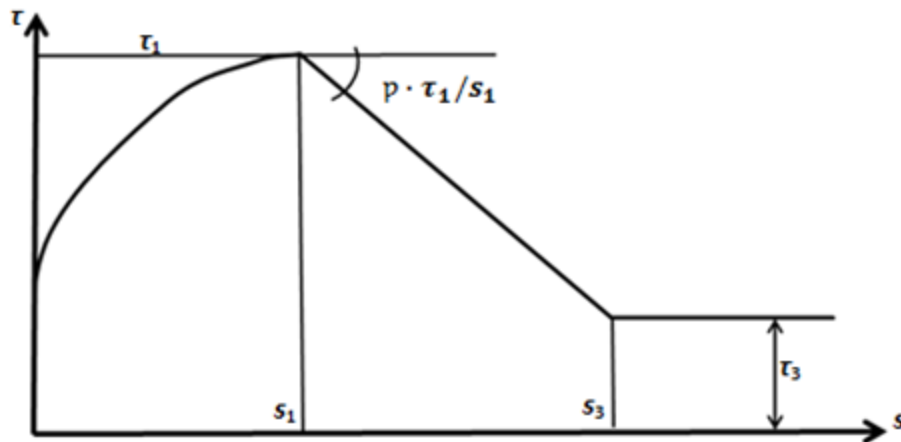
Figure 2.16: Modified BPE Model. (Source: Cosenza *et al.* 1997)

2.6.3 Cosenza, Manfredi, and Realfonzo Model (CMR Model)

Since most structural problems are to be dealt with at the serviceability state level, a refined modeling of the bond stress-slip curve is needed for the ascending branch only (Cosenza *et al.,* 1997). A new model has been proposed by Cosenza *et al.* (1995) for the ascending branch of the stress-slip curve which represents and alternative to the BPE model and is defined by the following:

$$\frac{\tau}{\tau_m} = \left(1 - e^{-\frac{s}{s_r}}\right)^{\beta} \qquad\qquad\qquad\qquad \text{Equation 2.16}$$

where τ_m= peak bond stress and s_r and β are based on curve-fitting parameters from of the actual data. In an experimental study on the bond behaviour of GFRP bars in concrete conducted by Tigiouart *et al.* (1998), values of -1/4 and 0.5 were proposed for s_r and β, respectively for the CMR model.

Chapter 3

EXPERIMENTAL INVESTIGATION

3.1   Introduction

The use of high performance concrete (HPC) and ultra-high performance concrete (UHPC) with fibre reinforced polymers (FRP) in construction is an emerging technology. The use of FRP as reinforcing materials in HPC and UHPC resolves the typical issues associated with steel reinforced conventional concrete such as: corrosion of steel leading to premature deterioration, increased reinforcement requirement, and larger dimensions needed for structural elements. Attempts to reduce the weight and size of concrete structures are increasing in response to current architectural trends for massive concrete structures (Mazloom *et al.* 2004). When compared to conventional concrete, HPC and UHPC have far superior durability and strength. The strength, and consequently durability, improvement is a result of increasing the density of the concrete matrix, generally by reducing the water-to-cementitious materials ratio while increasing the calcium oxide – silicon dioxide ratio by adding mineral admixtures containing silica fume (Won *et al.* 2008).

Results from experimental studies have shown that the bond behaviour between FRP reinforcement and concrete is dependent on factors such as: the bar properties, structural characteristics, and the concrete properties. In this investigation, experimental work was carried out with the intention of investigating the bond behaviour of FRP bars embedded in a high strength HPC, and an ultra-high strength UHPC, determined through a series of pullout and beam tests. This chapter provides a summary of the experimental study conducted to investigate the bond behaviour of FRP bars embedded in HPC and UHPC. The experimental program, bond test specimen manufacturing process, material properties, and test configurations are discussed in detail in this section.

3.2   Experimental Program

The experimental stage of this study was designed such that the bond properties of sand coated glass fibre reinforced polymer bars (GFRP) embedded in high strength, HPC and ultra-high strength, UHPC could be determined. The variable parameters that were used to determine the bond behaviour include: bar diameter, compressive strength, embedment length, and concrete cover. 32 beam tests and 72 pullout tests were carried out to study the bond behaviour of GFRP rebars.

To evaluate the effect of the compressive strength on the bond behaviour, four different concrete compressive strengths were used in this study that ranged from 70 – 175 MPa. 15.9 mm and 19.1 mm GFRP bar diameters were used to determine the effect of the bar diameter on the bond strength. The effect of embedment length on bond strength was also investigated by varying the embedment length from three times the bar diameter to seven times the bar diameter; however, eight pullout specimens also had embedment lengths of ten times the bar diameter. The effect of concrete cover was investigated through the pullout test specimens. Concrete covers of 40 mm and 60 mm were used in this study. For all configurations with embedment lengths of five and ten times the bar diameter, two duplicate specimens were casted whereas for all other configurations, one specimen was casted. The list of bond test specimens is presented in Appendix A.

3.2.1 Beam Specimen Geometry and Configuration

The beam geometry was based on the beam test recommendation established by RILEM/CEB/FIP (1982).   The beam test was comprised of two parallelepiped reinforced concrete blocks, interconnected at the bottom by the rebar whose bond was to be investigated and at the top by a steel hinge. The dimensions of the bond test beams were dependant on the diameter of the rebar being investigated. In the recommendation, two beam types are given which are dependent on the diameter of the rebar: Type A and Type B. For the smaller 15.9 mm diameter GFRP rebars, Type A beams were used, whereas Type B beam specimens were used for the larger 19.1 mm diameter GFRP bars. Table 3.1 and Figure 3.1 and show the dimensions of the specimens for Type A and Type B.

The unbonded length was created by placing foam pipe insulation around the GFRP rebar to prohibit the concrete from bonding to the bar. Table 3.2 shows the length of foam needed to create three, five, and seven times the bar diameter embedment lengths for each half of the beam specimens. The

foam lengths were cut in half and placed, as shown in Figure 3.1, such that the bonded portion of the GFRP rebar was located at the center of each beam block.

Table 3.1: Dimensions of beam specimens.

Beam Type	Type A	Type B
Bar Diameter, d_b	15.9 mm	19.1 mm
Embedment lengths, $3d_b/5d_b/7d_b$	47.7mm/79.5mm/111.3mm	57.3mm/95.5mm/133.7mm
Thickness of concrete blocks	100 mm	150 mm
Depth of concrete blocks	180 mm	240 mm
Length of concrete blocks	375 mm	600 mm
Distance between concrete blocks	50 mm	60 mm
Total length of beams	800 mm	1260 mm
Length of bars tested	1000 mm	1500 mm
Distance between centre-line of bar and centerline of hinge	100 mm	150 mm
Distance between centre-line of bar and underside of beam	50 mm	50 mm
Spacing of the loads	150 mm	200 mm
Spacing of the bearing supports	650 mm	1100 mm
Dimensions of the steel hinges	See Figure 3.2a	See Figure 3.2b

	Type A	Type B
A	375mm	600mm
B	650mm	1100mm
C	180mm	240mm
D	100mm	150mm
E	50mm	50mm
F	50mm	60mm
G	100mm	150mm
H	150mm	200mm

(a)

(b)
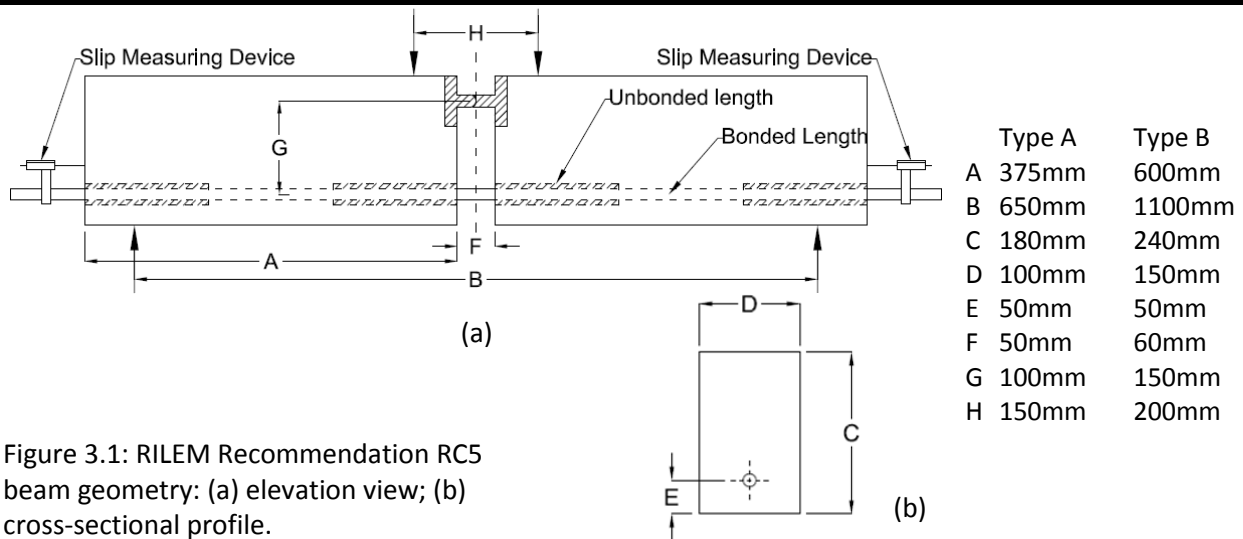
Figure 3.1: RILEM Recommendation RC5 beam geometry: (a) elevation view; (b) cross-sectional profile.

Table 3.2: Foam lengths needed for beam specimens.

Embedment length (xd_b)	Embedment length (mm)		Foam length (mm)	
	Type A Beam Specimen	Type B Beam Specimen	Type A Beam Specimen	Type B Beam Specimen
$3d_b$	47.7	57.3	327.3	542.7
$5d_b$	79.5	95.5	295.5	504.5
$7d_b$	111.3	133.7	263.7	466.3
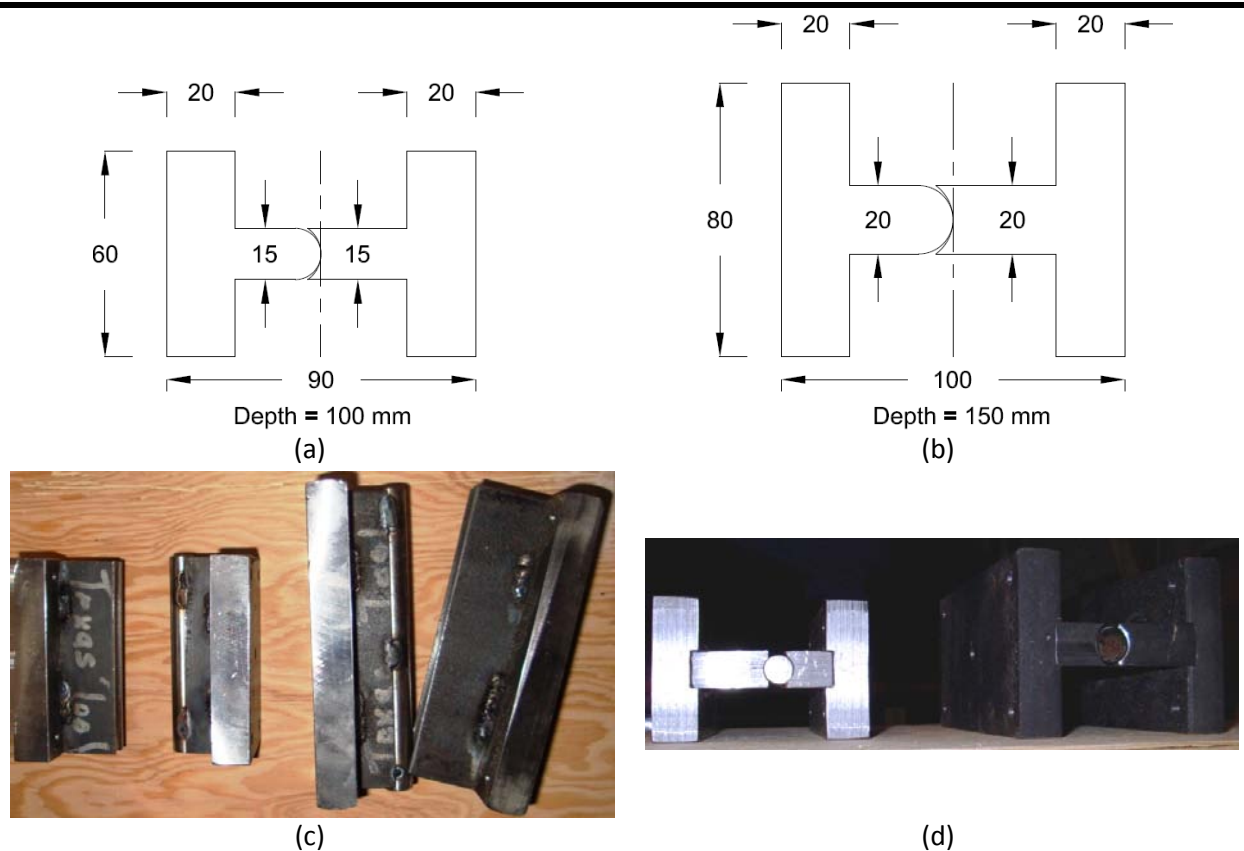
Figure 3.2: Beam specimen hinges: (a) Type A hinge; (b) Type B hinge; (c) top view; (d) elevation view.

The auxiliary reinforcement for the beams specimens consisted of plain, mild steel bars. Details of the reinforcement are given in Figure 3.3 and Figure 3.4 for Type A and Type B beam specimens, respectively. Reinforcing cages were produced using three layers of longitudinal steel reinforcement with five evenly spaced closed stirrups for Type A specimens and seven evenly spaced closed stirrups for Type B specimens. The longitudinal steel reinforcement was 5/16" (7.94 mm) in diameter and the transverse reinforcement was 1/4" (6.35 mm) in diameter. The stirrups at the end of the reinforcement cages were spot welded at the top and bottom to the longitudinal reinforcement such that the cage would not become distorted during casting. Cable ties were used to secure the transverse reinforcement to the longitudinal reinforcement. Figure 3.5 shows a reinforcement cage for a Type B specimen. Less reinforcement was used for the beam specimens than is suggested by the RILEM/CEB/FIP Recommendation.

The following reasons for justify the reduction of the auxiliary reinforcement provided in the beam specimens:

- Orangun e*t al.* (1977) concluded that providing additional amounts of reinforcement beyond what is needed to cause the transition from the splitting mode of failure to the pullout mode of failure becomes progressively less effective, eventually providing no increase in the bond strength. Therefore, as long as it was ensured that a pullout failure was always achieved in the beam specimens, the lower amount of reinforcement used could be justified as it would not affect the bond strength.

- The sand coated GFRP rebars produce lower radial stresses than that of deformed steel bars, which are used in the RILEM/CEB/FIP Recommendation. Since radial stresses are the cause of splitting failure, a lower amount of radial stress can be accompanied by a lower requirement for internal reinforcement.

- The embedment lengths used in this study were a maximum of seven times the bar diameter. In the RILEM/CEB/FIP Recommendation, embedment lengths of ten times the bar diameter are used. Since a shorter embedment length was used in this study, a lower amount of force was required to cause bond failure by pullout. With a reduced failure load, the pullout failure mode becomes more probable and lessens the likelihood of the beam specimen failing due to shear, or bending moment, and as mentioned previously, bond failure due to splitting thus the amount of reinforcement could be reduced.

- Finally the compressive strength of the concrete used in the RILEM/CEB/FIP Recommendation for the beam specimens is between 23-33 MPa, depending on the dimensions of the control specimens. In this investigation, the compressive strength of the concrete used was over 70 MPa.   This indicates that the concrete used in this study has a higher radial stress capacity, thus the amount of reinforcement required could be lowered.
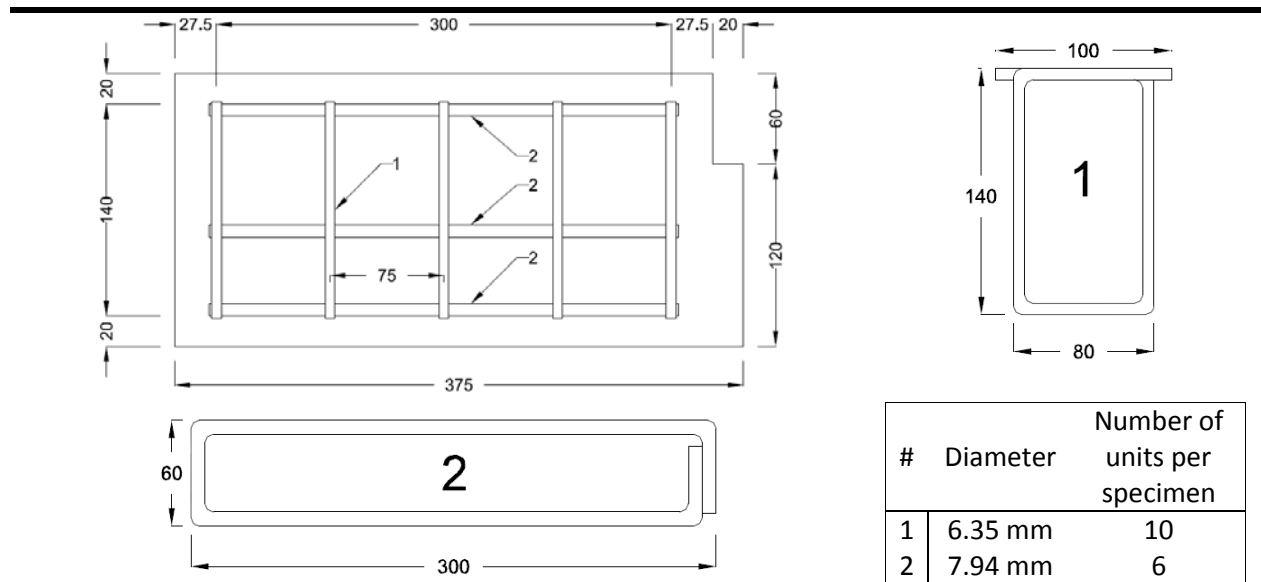
Figure 3.3: Auxiliary reinforcement for Type A specimen.

#	Diameter	Number of units per specimen
1	6.35 mm	10
2	7.94 mm	6
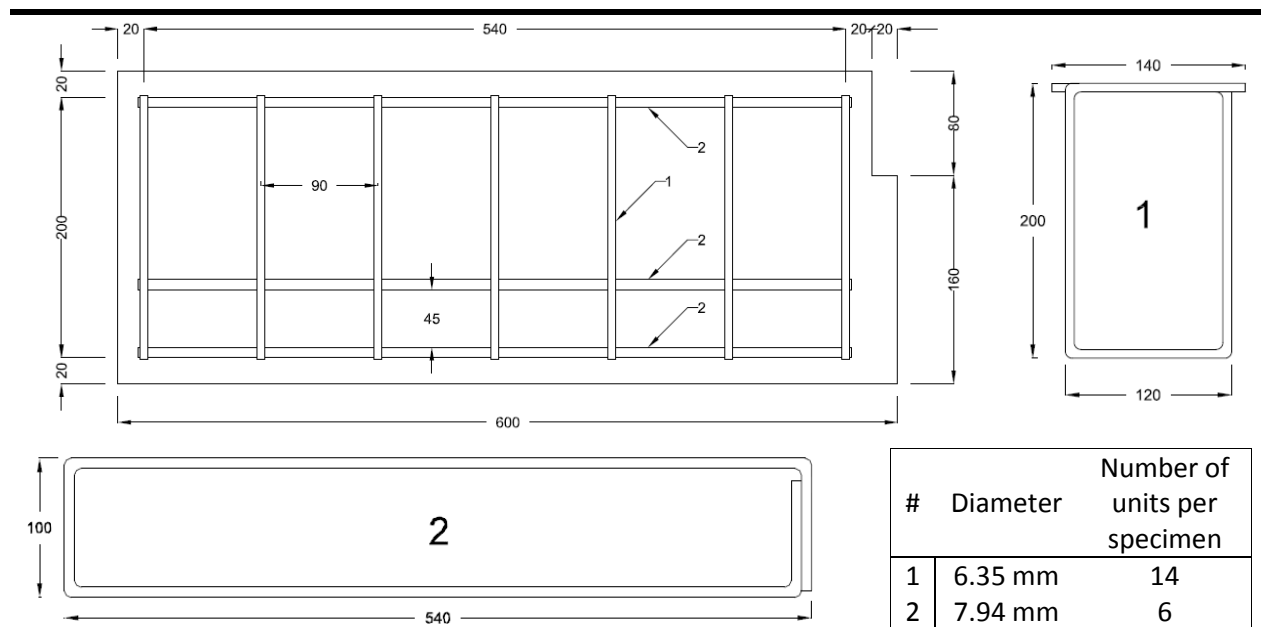
Figure 3.4: Auxiliary reinforcement for Type B specimen.

#	Diameter	Number of units per specimen
1	6.35 mm	14
2	7.94 mm	6

Figure 3.5: Reinforcement cage for Type B specimen.

3.2.2 Pullout Specimen Geometry and Configuration

The configuration of the pullout specimens used in this study was based on Annex D of CSA S806-02. The pullout test comprised of a GFRP rebar embedded inside of a concrete prism. The lengths of the GFFR bars were all 1000 mm. Concrete covers of 40 mm and 60 mm were used for each configuration of embedment length and concrete strength. The dimensions of the pullout test specimens were dependant on the embedment length of the rebar being tested. Table 3.3 and Figure 3.6 show the dimensions of the pullout specimens used in this study.

The unbonded segments of the pullout specimen were created by placing foam pipe insulation around the GFRP bar, as was done to the beam specimens, to prevent the concrete from bonding to the bar in these regions. A 25 mm unbonded section was created on the segment of the bar nearest to the applied load. The remaining amount of foam needed to produce the desired embedment length was placed at the rear of the specimen. Table 3.4 shows the length of foam needed to create three, five, seven, and ten times the bar diameter embedment lengths for the pullout specimens.

Table 3.3: Dimensions of prisms for pullout specimens.

Embedment length (xd_b)	Width	Height	Depth
$3d_b$	150 mm	150 mm	175 mm
$5d_b$	150 mm	150 mm	120 mm
$7d_b$	150 mm	150 mm	175 mm
$10d_b$	150 mm	150 mm	250 mm

Table 3.4: Foam lengths needed for pullout specimens.

Embedment Length (xd_b)	Prism Depth (mm)	Embedment Length (mm)	Front Foam Length (mm)	Rear Foam Length (mm)
15.9 mm GFRP Bar				
$3d_b$	175	47.7	25	102.6
$5d_b$	120	79.5	25	15.5
$7d_b$	175	111.3	25	38.7
$10d_b$	250	159	25	66
19.1 mm GFRP Bar				
$3d_b$	175	57.3	25	92.7
$5d_b$	120	95.5	25	0
$7d_b$	175	133.7	25	16.3
$10d_b$	250	191	25	34
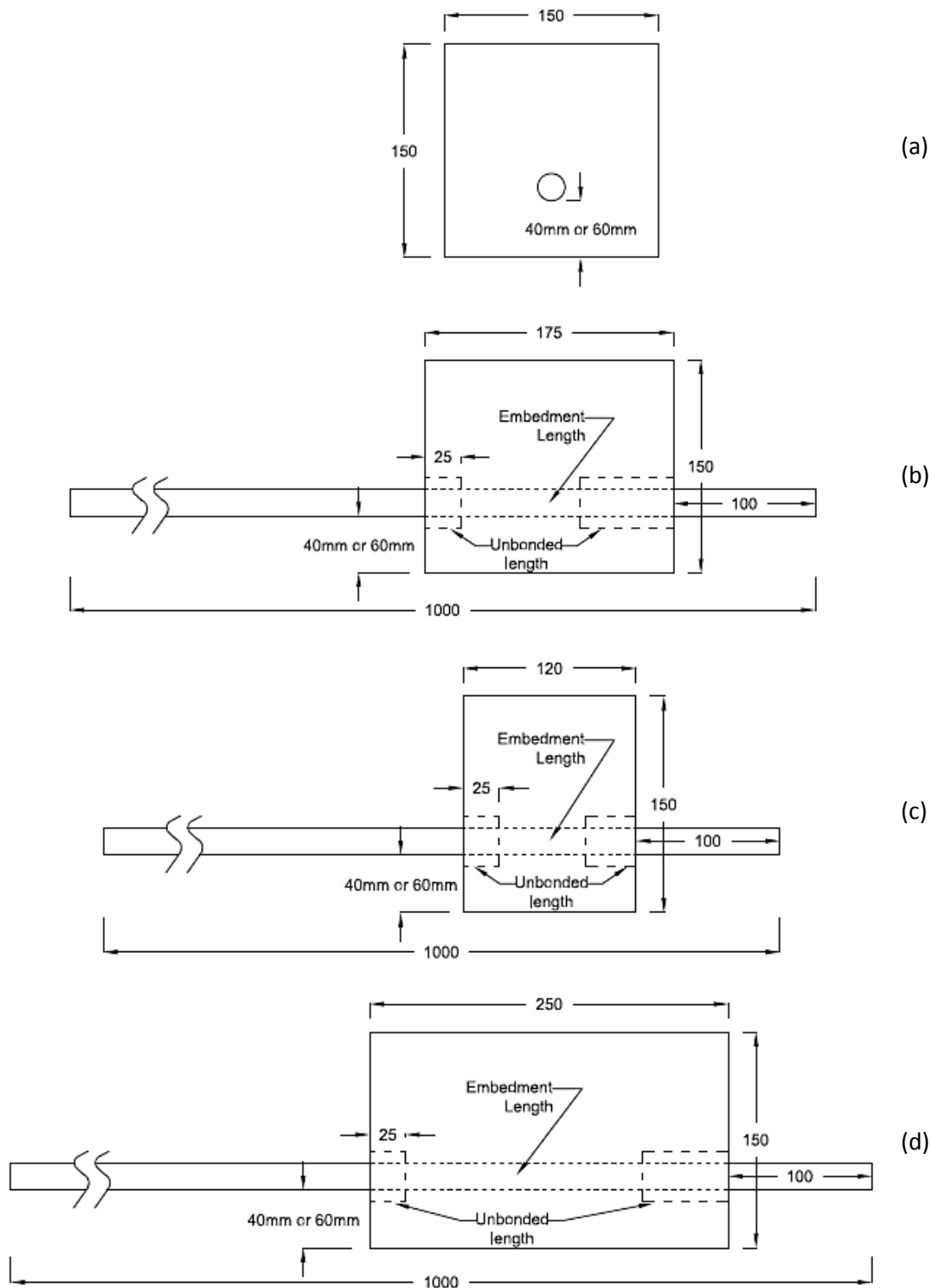
Figure 3.6: Pullout Specimen Configuration: (a) cross section perpendicular to longitudinal axis of bar; (b) $3d_b$ and $7d_b$ specimen dimensions; (c) $5d_b$ specimen dimensions; (d) $10d_b$ specimen dimensions.

3.3   Materials

The following sections discuss the materials used in this study and their corresponding properties. This section is divided into three subsections: GFRP Rebar, Commercial Concrete, and Ryerson Concrete, which discuss the properties of the GFRP rebars and the different concretes used in this investigation. The properties of the Ryerson Concrete mix will be discussed with further detail than the commercialized concretes since it was developed for this project, whereas the properties of the commercial concretes are available from the manufacturer.

3.3.1 GFRP Rebar

V·Rod^{TM} GFRP bars manufactured by Pultrall Inc. were used in this study. The surface of the GFRP bars were sand coated, which inhibited the longitudinal movement of the bar relative to concrete. The matrix resins were composed of modified vinyl ester with a maximum volume fraction of 35%. The fibre reinforcement was comprised of continuous E-glass fibres with a minimum volume fraction of 65%. In order to determine the affect of the bar size on the bond behaviour between GFRP and the surrounding concrete, two bar sizes were used in this study: 15.9 mm and 19.1 mm diameter. Properties of the GFRP bars are provided in Table 3.5 and Table 3.6.

Table 3.5: Nominal diameter and sectional area of GFRP V·Rod^{TM}.

US Size	Soft Metric Size	Nominal Diameter (mm)	Area, (mm^2)	Weight (g/m)
#5	#16	15.875	197.9	425.5
#6	#19	19.050	285.0	614.5

(Source: Pultrall Inc., 2007)

Table 3.6: Tensile properties GFRP V·Rod^{TM}.

US Size	Soft Metric Size	Tensile Modulus of Elasticity E_T (GPa)	Ultimate Tensile Strength F_U (MPa)	Guaranteed Design Tensile Strength f_{fu} (MPa)	Shear Strength F_S (MPa)	Ultimate Strain in Tension ε_{fu} (%)	Poisson's Ratio μ
#5	#16	48.2	751	683	195	1.56	0.25
#6	#19	47.6	728	656	200	1.53	0.25

(Source: Pultrall Inc., 2007)

3.3.2 Commercial Concrete

Two commercial concretes were selected for use in the production of the bond test specimens: HP-S10 Concrete and Ductal®. HP-S10 Concrete was used to provide compressive strength at the lower end of the investigated range and Ductal® was used to provide compressive strengths at the higher end of the investigated range. The concrete mix descriptions, proportions, mixing procedures and properties are discussed below.

HP-S10 Concrete:

The HP-S10 Concrete used in this study is a high performance, high strength, rapid hardening, pre-blended, and pre-packaged concrete material. HP-S10 Concrete is manufactured by King Packaged Materials Company. It contains Portland cement, silica fume, air-entraining admixture, 10 mm stone and other carefully selected components. HP-S10 Concrete came in pre-blended bags weighing 30 kg, each producing a yield of approximately 14 litres. It was recommended by the manufacturer to use a maximum of 2.4 litres of water with each 30 kg bag.

The HP-S10 Concrete was mixed using either a 75 litre capacity concrete pan mixer or a 60 litre rotating drum mixer, depending on the volume of concrete needed for the batch. Figure 3.7 shows the two mixers used for mixing HP-S10 Concrete. There was no noticeable difference between the batches produced by each mixer. The water content used to mix HP-S10 Concrete was 2.4 kg of water for 30 kg of pre-blended material. The mixing procedure for HP-S10 Concrete was as follows:

Step 1 - With the mixer turned off, 75% of the required water was placed into the mixer followed by the pre-blended material.
Step 2 - The mixer was turned on and remaining amount of water was slowly poured in while the mixer was running.
Step 3 - Mixing continued for 8 minutes and then the mixer was shut off.

(a)   (b)

Figure 3.7: Mixers used for HP-S10 Concrete: (a) 75 litre pan mixer; (b) 60 litre rotating drum mixer.

HP-S10 Concrete is a high-slump concrete mix. Slump tests were performed according to ASTM Standard C143. The slump for the mix was 250-260 mm. Air content tests were performed according to ASTM Standard C231 and a values ranging from 5-7% were obtained. Figure 3.8 shows the HP-S10 Concrete upon completion of mixing.

Figure 3.8: HP-S10 Concrete after mixing.

Immediately after mixing, the concrete was placed into the bond test specimen moulds and consolidated using a vibrating table according to ASTM Standard C192. 4-6 control cylinders, having dimensions of 100 mm x 200 mm, were produced with each batch of HP-S10 Concrete. Once the test specimens and control cylinders were casted, they were sealed using plastic sheeting and placed into the moist curing room. Figure 3.9 shows the casting of the beam and pullout test specimens. The test specimens and control cylinders were demoulded 24 hours after casting and placed back into the moist curing room until they achieved their maximum strength, which came 21-25 days after casting. Any additional elapsed time produced zero to negligible increases in strength. This provided flexibility in the testing schedule and eliminated any time constraints for testing the specimens.

The compressive strength development of HP-S10 Concrete was determined from the control cylinders produced while casting the bond test specimens. The compressive strength development of HP-S10 Concrete is shown in Figure 3.10. The compressive strength attained for HP-S10 Concrete was 71.2 MPa. The control cylinders were capped with a standard sulphur capping compound according to ASTM Standard C617 in order to carry out compressive strength tests which were performed according to ASTM Standard C39. The control cylinders had a standard deviation of 3.59 MPa and a coefficient of variation of 5.0%.

(a)   (b)

Figure 3.9: Bond test specimen casing with HP-S10 Concrete: (a) Beam test specimen; (b) pullout test specimen.
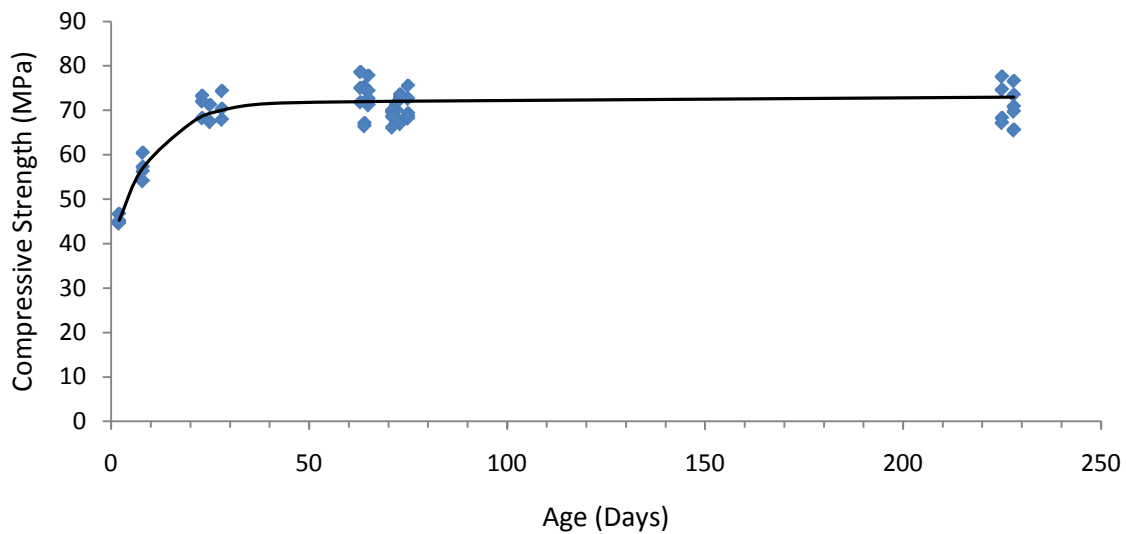
Figure 3.10: HP-S10 Concrete compressive strength development.

Ductal®:

Ductal® was the second commercial concrete used in this study. Ductal® is an ultra-high performance, ultra-high strength concrete produced by Lafarge that was developed in a joint venture with Rhodia and Bouygues. Due to the confidentiality agreement with Lafarge, only minimal information will be provided in the following sections. As a result, specific material properties and names will be omitted from this report along with the mixing procedure.

Ductal® was used to provide concrete strengths in the upper range of our investigation. Two Ductal® mixes were used, which were named Ductal1 and Ductal2. Ductal1 was produced to provide compressive strengths above 140 MPa and Ductal2 was produced to provide compressive strengths above 170MPa. In order to generate the increase in strength from Ductal1 to Ductal2, the water and admixture content were reduced by 10%. The general mix proportions are provided in Table 3.7 for Ductal1 and Ductal2.

Table 3.7: Ductal1 and Ductal2 mix proportions.

Mix	Ductal® Premix	Water	Admixture	Fibres
Ductal1	2194	155	30	156
Ductal2	2194	139.5	27	156

*all values in kg/m^3

Ductal® was mixed using a Mortarman® 750 MBP mixer (Figure 3.11). This is a vertical shaft mixer which mixes using a stirring action as opposed to a flipping motion. As mentioned previously, the mixing procedure has been omitted from this section.

Figure 3.11: Mortarman® 750 MBP mixer used to batch Ductal®.

Both Ductal® mixes were self-consolidating. Upon completion of the mixing sequence, the concrete was poured into the bond test specimens. 4-9 control cylinders were produced with each batch of Ductal®. Figure 3.12 shows casting of the bond test specimens. Immediately after the specimens were casted, they were sealed with a sheet of tough, durable impervious plastic to prevent evaporation of water from the unhardened concrete (Figure 3.13).

<center>(a)   (b)</center>
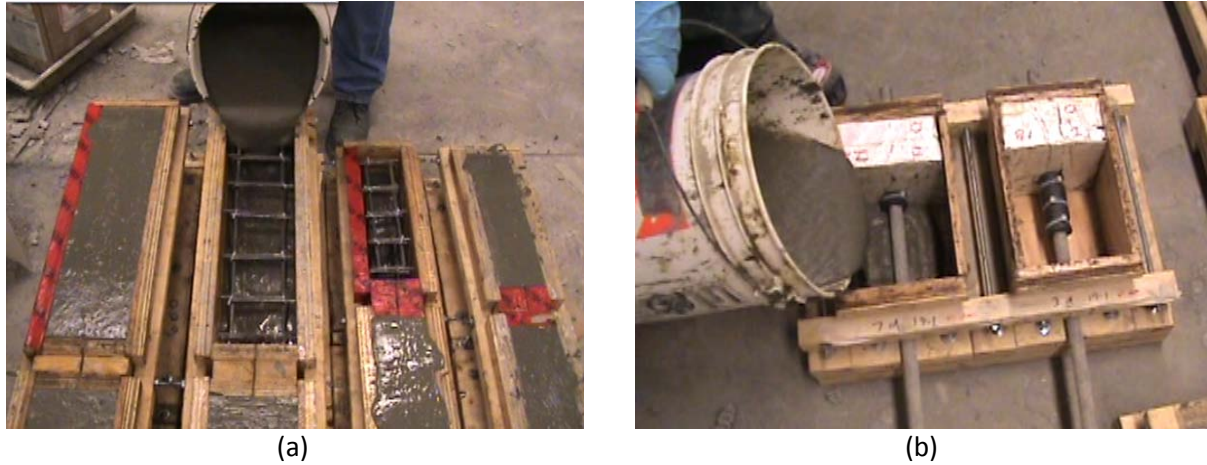
Figure 3.12: Bond test specimen casing with Ductal®: (a) beam test specimen; (b) pullout test specimen.

The test specimens and control cylinders were demoulded 48 hours after casting (Figure 3.14). The demoulded specimens were left in the laboratory without providing any special curing conditions. This was done so the specimen testing and casting schedule could be optimized because it was not desirable for the Ductal® specimens to attain their design strength too rapidly, or risk surpassing it. Ductal1 specimens reached their maximum strength 21 days after casting, whereas Ductal2 specimens reached their maximum strength 35 days after casting. Similar to HP-S10 Concrete, any additional elapsed time produced zero to negligible increases in strength and thus, provided flexibility in the testing schedule of the specimens.

The compressive strength development of Ductal® was determined from the control specimens produced along with the bond test specimens. In order to prepare the cylinders for testing, 15 mm were cut off of each end using a high-speed concrete cutting saw with a carbide-tipped blade to achieve a smooth surface free of any deformations. The compressive strength development of Ductal® is shown in Figure 3.15. The compressive strength attained for Ductal1 specimens was 147.8 MPa and the compressive strength attained for Ductal2 specimens was 174.5 MPa. The control cylinders had a standard deviation of 6.19 MPa and 8.77 MPa, and a coefficient of variation of 4.1% and 5.0% for Ductal1 and Ductal2 cylinders, respectively.

Figure 3.13: Sealed Ductal® specimens after casting.

Figure 3.14: Demoulding of beam specimen.
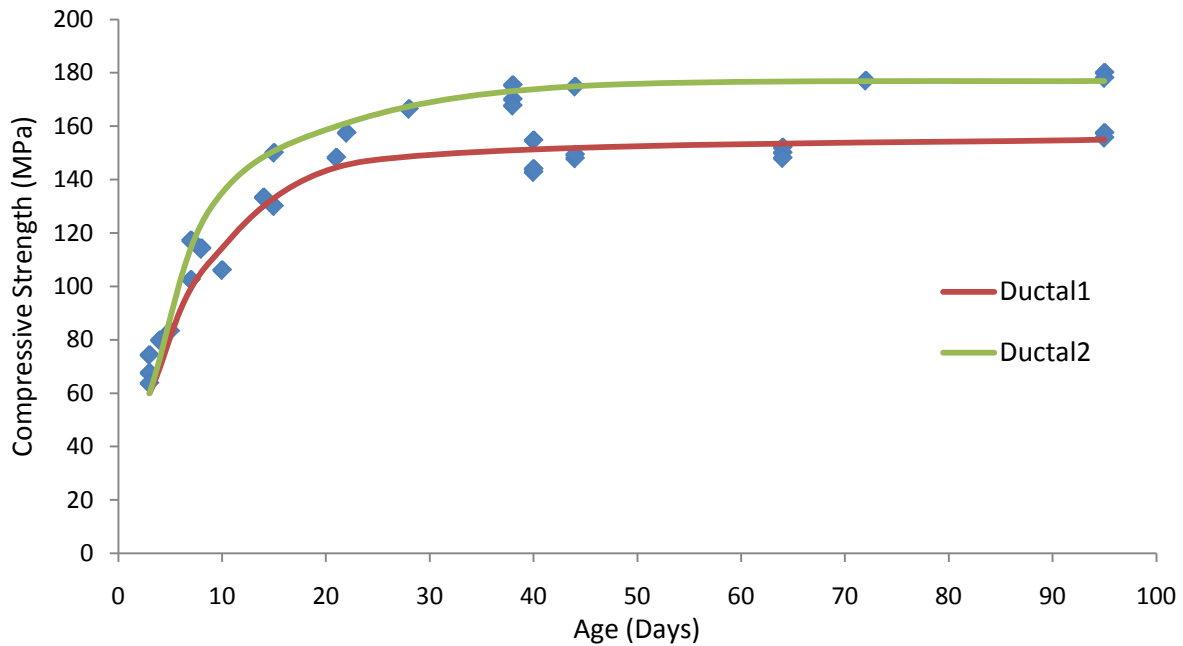
Figure 3.15: Ductal® compressive strength development.

3.3.3 Ryerson Concrete Mix

The mix developed at Ryerson University was designed to have a compressive strength between 115-130 MPa. Ryerson Concrete is a self-consolidating UHPC produced from cement, silica fume, silica sand, steel fibres, superplasticizer, and water. The material properties and mix proportions are shown in Table 3.8 and Table 3.9, respectively.

Table 3.8: Materials used for Ryerson Concrete.

Material:	Cement
Product:	GU Lafarge Portland Cement
Company:	Lafarge North America Inc.
Description:	Complies with ASTM Standard C150.
Material:	Silica Sand
Product:	F-110 Silica Sand Natural Grain
Company:	U.S. Silica Company
Description:	See Figure 3.16 for grain size distribution.
Material:	Silica Fume
Product:	Microsilica Grade 971-U
Company:	Elekem Materials Inc.
Description:	Undensified silica fume, coarse particles > 45 microns = 0.2%.
Material:	Superplasticizer
Product:	ADVA® Cast 575
Company:	Grace Construction Products
Description:	Polycarboxylate-based ASTM C494 Type F and ASTM C1017 Type I plasticizer.
Material:	Steel Fibres
Product:	Dramix® OL 13/0.2
Company:	Bekaert
Description:	Straight fibres, length = 13 mm, diameter = 0.2 mm.
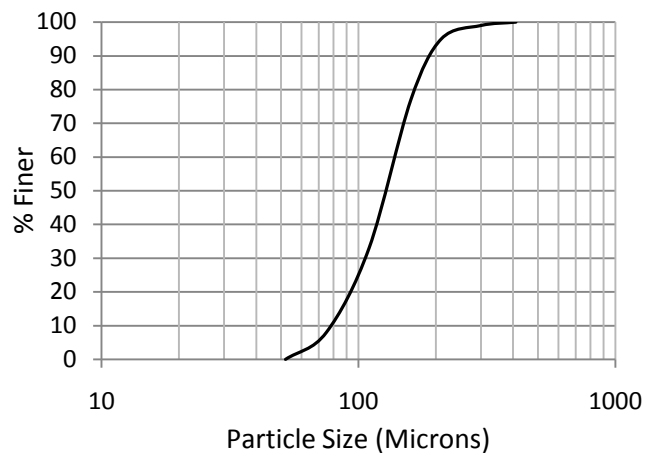
Figure 3.16: F-110 particle size distribution.

Table 3.9: Ryerson Concrete mix proportions.

Material	Quantity (kg/m^3)
Cement	818
Silica Sand	899
Silica Fume	204
Steel Fibres	164
Superplasticizer	26.0
Water	221.8

Ryerson Concrete was mixed using the 75 litre pan mixer shown in Figure 3.7a. The mixing sequence for the Ryerson Concrete mix was as follows:

Step 1 - The dry powders were mixed for a minimum of two minutes or until a homogenous distribution of the powders was achieved.

Step 2 - The water was slowly introduced with half of the superplasticizer and mixed for 4 minutes.

Step 3 - The second half of the superplasticizer was introduced slowly.

Step 4 - When the mixture became self-consolidating, usually 3-5 minutes after the addition of the second half of the superplasticizer, the fibres were dusted over the mix to allow for even

dispersion, and to avoid fibre clumping. The concrete was mixed for one minute after the inclusion of the fibres.

In order to evaluate the fresh properties of the mix, the slump-flow, T_{500} time, V-funnel time, and L-box passing ability tests were performed on the fresh mix. Appendix B describes the details of the test procedures. Table 3.10 summarizes the results from these tests for Ryerson Concrete. Based on visual observations, the fibres were evenly distributed and there were no signs of fibre clusters. The slump-flow produced a smooth circle indicating that the viscosity was even throughout the mix. The L-Box test showed no segregation or signs of blockages.

Table 3.10: Fresh properties of Ryerson Concrete.

Slump-Flow	T_{500}	V-funnel Time, T_v	L-Box (3 bar test), PA
910 cm	1.8 seconds	4.6 seconds	0.93 (H_1 = 7.6, H_2 7.1)

Immediately after mixing, the self-compacting concrete was poured into the bond test specimen moulds. 4-6 control cylinders, having dimensions of 100 mm x 200 mm, were produced with each batch of Ryerson Concrete in addition to 6-15 cube specimens having dimensions of 50 mm x 50 mm. One hour after the bond test specimens and control specimens were cast, they were covered with wet burlap for the first 24 hours in order to maintain high humidity on the exposed surface of the specimen. Ryerson Concrete forms a semi-solid thin film/skin on the exposed surface, preventing any moisture from escaping the specimen. As a result, no bleed water was observed at the surface. This layer also allowed for the placement of the wet burlap without the risk of increasing the water content while the specimens were still fresh. Figure 3.17 and Figure 3.18 show bond test specimens being cast with Ryerson Concrete and then covered with wet burlap, respectively. 24 hours after casting, the specimens were demoulded and left in the laboratory without providing them with any special curing conditions as Ryerson Concrete was able to develop its hardened state properties without any curing methods. Since the Ryerson Concrete was supposed to provide compressive strengths between 115-130 MPa, the specimens needed to be tested between 23-24 days after casting when they attained an average compressive strength of 128.6 MPa. It was essential to test the specimens within that time frame, or consequently, the specimens would continue to gain strength and exceed their desired compressive strength range.

The compressive strength development of Ryerson Concrete was determined from the control specimens produced while casting the bond test specimens. Similar to the preparation for the Ductal®

cylinders for compression testing, 15 mm were cut off of each end using a high-speed concrete cutting saw. The compressive strength development of Ryerson Concrete is shown in Figure 3.19. The compressive strength attained for Ryerson Concrete appeared to reach a maximum value of 152 MPa after 75 days. The control cylinders had a standard deviation of 5.62 MPa and a coefficient of variation of 4.4%. The control cubes had a standard deviation of 4.91 MPa and a coefficient of variation of 3.8%. It can be seen that the strength values between the cylinders and cubes are nearly identical after 28-30 days. The 1-2 day cylinder strength appears to be higher than the 1-2 day strength of the cube specimens. However, the 3-28 day strength is greater for the cubes than for the cylinders. The higher strength of the cylinders during the first two days can be attributed to the greater volume of concrete, which produced a much higher heat of hydration, which in turn accelerated the strength gain of the cylinders. After two days of casting, the heat produced from hydration significantly dissipated, and the rate of strength gain was significantly reduced. The strength of the cubes was much less than the cylinders during the first two days because there was far less heat produced during the initial stages of hydration. However, because the cube has less volume and the larger relative surface area compared to the cylinder, the elevated temperatures in the laboratory where the specimens were stored affected the cubes more than the cylinders and caused them to hydrate at a faster rate, resulting in the cubes reaching their maximum strength sooner than the cylinders.

(a)   (b)

Figure 3.17: Bond test specimen casing with Ryerson Concrete: (a) beam test specimen; (b) pullout test specimen.

Figure 3.18: Wet burlap placed on Ryerson Concrete specimens following casting.
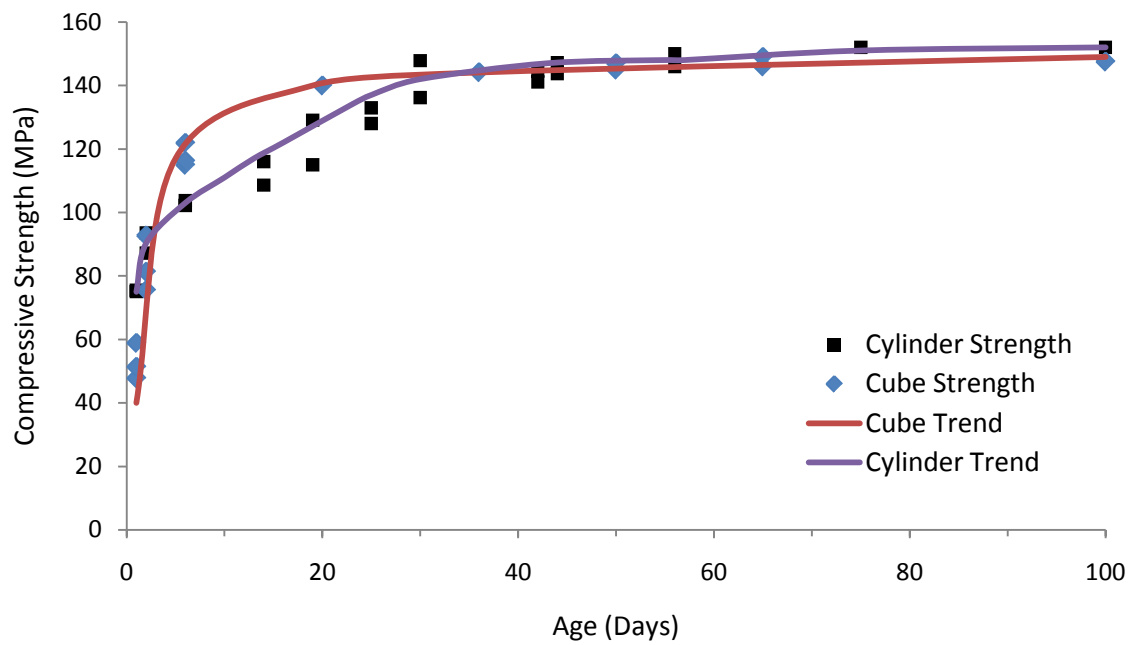
Figure 3.19: Ryerson Concrete compressive strength development.

3.4   Test Setup and Procedure

The bond test specimens were tested once the control cylinders had reached the desired compressive strength. As mentioned in the previous section, testing for the HP-S10 Concrete and Ductal® specimens were tested anytime after their control cylinders reached their maximum strength, whereas the Ryerson Concrete specimens had to be tested 23-24 days after casting. The following sections describe the setup, equipment, and methodology used to carry out the tests, whereas the data gathered from these test is presented in the next chapter.

3.4.1 Beam Test

The beam test specimens were carried out as specified according to the recommendation by RILEM/CEB/FIP (1982). The locations of the supports and load applications were placed as indicated in Figure 3.1. The test setup is shown in Figure 3.20.
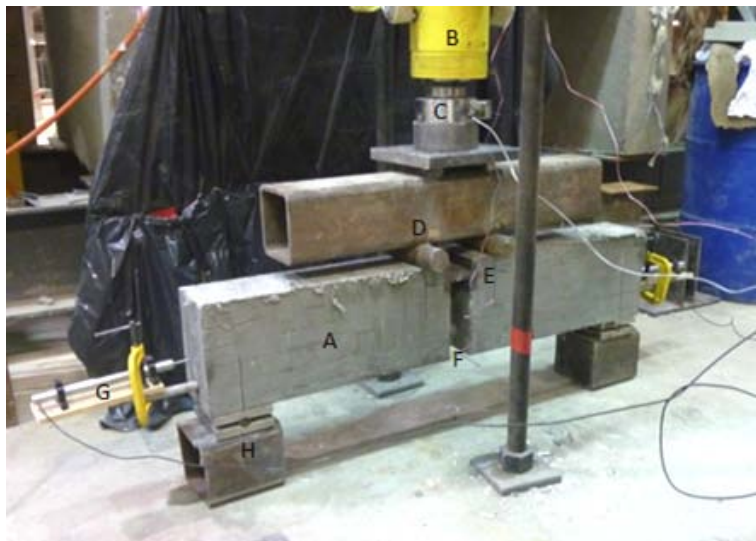
A   Test Specimen
B   Hydraulic Jack
C   Load Cell
D   Point of Load Application
E   Steel Hinge
F   Strain Gauge on GFRP Rebar
G   LVDT Measuring Free-End Slip
H   Roller Support

Figure 3.20: Test setup for beam specimen.

The loading was applied in consecutive increments corresponding to stresses in the bar successively equal to 80 MPa, 160 MPa, 240 MPa, 320 MPa, 400 MPa, etc. For each rebar stress increment, the following expression was used to determine the total load applied to the specimen:

$$F = \frac{A_s \sigma_s}{1.25} \quad \text{for Type A Specimens} \qquad \text{Equation 3.1a}$$

$$F = \frac{A_s \sigma_s}{1.5} \quad \text{for Type B Specimens} \qquad \text{Equation 3.1b}$$

Based on Equation 3.1 the following load increments were followed:

Table 3.11: Load increments for beam test specimens.

Type A	Type B
0	0
12.5	15
25	30
37.5	45
50	60
62.5	75
75	90
Continued until failure…	Continued until failure…

*all values in kN

The load was increased from one stage to the next increment evenly over the span of 30 seconds. Once the next increment was reached, the load was kept constant for two minutes. After two minutes, the load was increased to the next increment over a span of 30 seconds and maintained for another two minutes. This process was repeated until bond failure of the specimen.

A data acquisition system was used to record data from the load cell, which measured the applied load accurate to 0.01 kN, the linear variable displacement transducers (LVDTs) located at each end of the beam specimen providing free end slip measurements accurate to 0.01 mm, and from the strain gauge to measure the micro-strain at the center of the GFRP bar.

3.4.2 Pullout Test

A critical concern when testing FRP reinforcing bars is their low transverse strength; therefore, they could not be tested using the traditional wedge-shaped grip system employed for steel rebar bond tests. If an FRP rebar is loaded using a traditional wedge-shaped frictional grip, the combination of high compressive stresses and mechanical damage caused by the serration from the wedge surfaces would lead to premature failure in the gripped region. For this study, a steel grip was fabricated such that the applied force would not be enough to damage the GFRP bar, yet large enough to ensure that the grip does not fail prior to the bond failure of the pullout specimen. The grip used in this study consisted of two grooved halves which encompassed the rebar that were bolted together using high-strength steel bolts. The grips were secured together using a torque gun powered by compressed air. The amount or torque applied was limited such that the transverse strength of the GFRP bar could not

be exceeded. Figure 3.21 shows the grip used in this study. The distance of the unbonded length was always greater than 400 mm. Figure 3.22 shows the dimensions of the test setup.

(a)
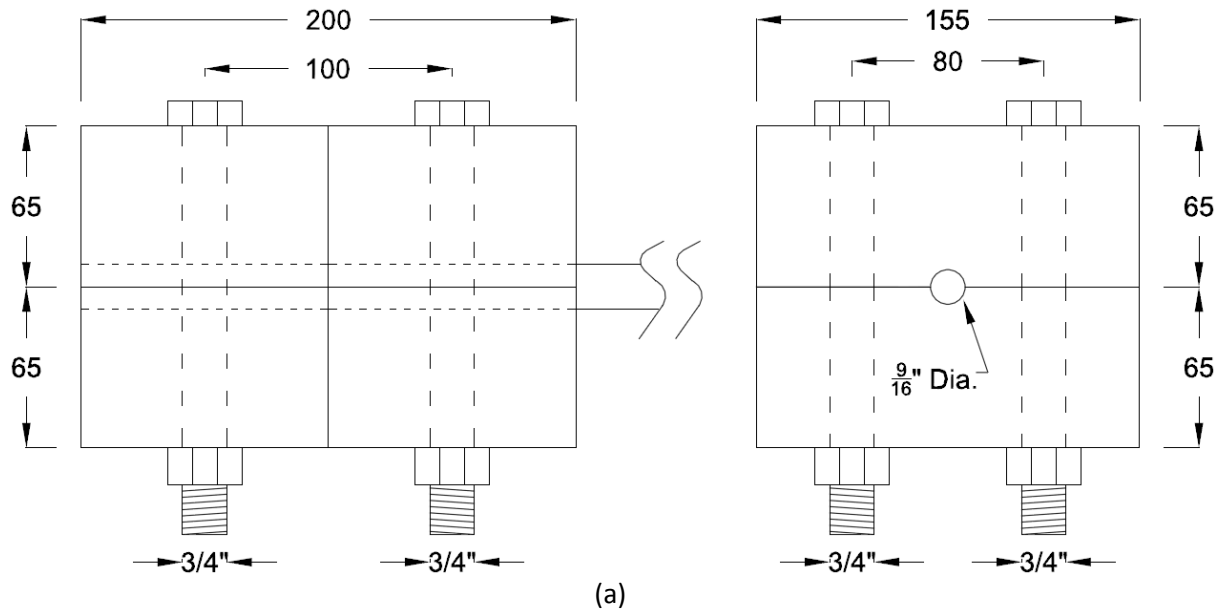
(b)   (c)

Figure 3.21: Steel grip used to secure GFRP bar during pullout test: (a) grip dimensions; (b) front view of grip; (c) side view of grip.

The pullout test specimens were setup according to the recommendation by RILEM/CEB/FIP (1982). The test setup is shown in Figure 3.23.   In addition to the fabricated grip, a wedge-shaped grip was placed at the end of the specimen to provide extra strength. Spacers were used as needed such that the fabricated grip could act in unison with the wedge-shaped grip at the end. The wedge-shaped grip

was only used for specimens with embedment length of five times the bar diameter or greater for the 19.1 mm GFRP bars, and for specimens with embedment lengths of seven times the bar diameter or greater for the 15.9 mm GFRP bars. If the wedge grip was not used, the manufactured grip was placed at the far end of the GFRP bar and spacers were used as needed.

The load was applied based on the recommendation provided in CSA S806-02 at a rate of 90 kN/min for the 19.1 mm diameter bar, and at a rate of 60 kN/min for the 15.9 mm diameter bar. The load was increased until the specimen reached bond failure.

A data acquisition system was used to record data from the load cell which measured the applied load accurate to 0.01 kN, and from the LVDT located at the free end end of the pullout specimen provided free end slip measurements accurate to 0.01 mm.
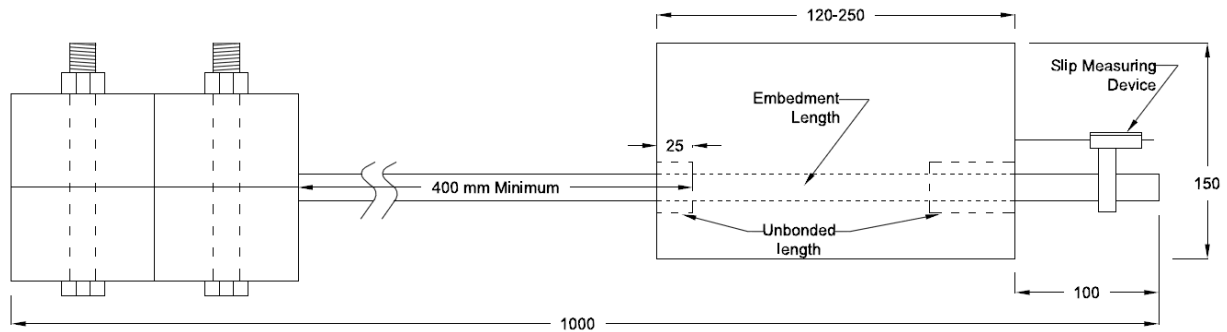
Figure 3.22: Dimensions of pullout test setup.
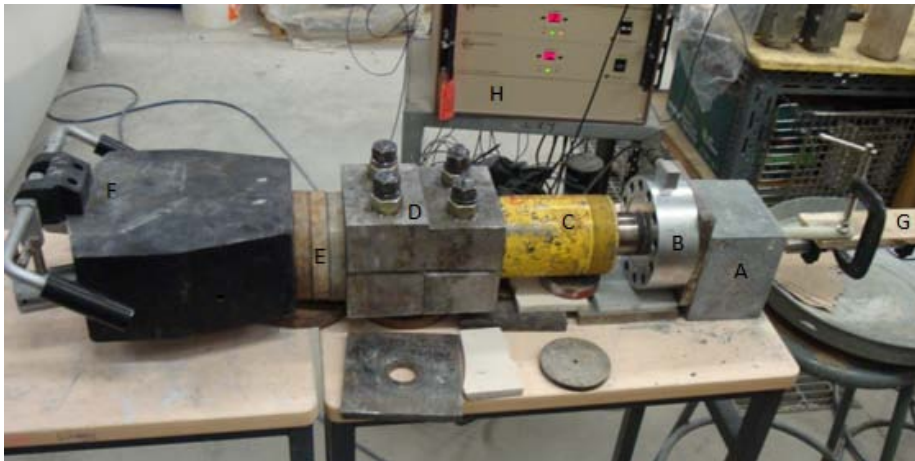
A   Test Specimen
B   Load Cell
C   Hydraulic Jack
D   Grip
E   Spacers
F   Wedge Grip
G   LVDT Measuring Free-End Slip
H   Data Aquisision System

Figure 3.23: Pullout test setup.

Chapter 4

RESULTS AND ANALYSIS

4.1   General

This chapter presents the results from the bond tests conducted in this experimental study.   The effects of the investigated parameters are discussed in this section.

Following the assumption of constant distribution of bond stress for each test specimen, the mean bond stress over the embedment length was determined by Equation 2.2.

$$\mu = \frac{A_b f_s}{l \pi d_b} = \frac{d_b f_s}{4l} \qquad\qquad\qquad\qquad \text{Equation 2.2}$$

The bar diameter used in Equation 2.2 was determined by averaging 10 diameter readings measured with a micrometer accurate to 0.001 mm for each GFRP bar.   The sand coating was included in the measurement since it affects the concrete surface area in contact with the GFRP bar. d_b used in Equation 2.2 is presented in Table 4.1.

Table 4.1: GFRP rebar actual diameters.

GFRP Rebar	Diameter Including Sand Coating
15.9 mm	17.494 mm
19.1 mm	20.763 mm

The bond test specimens with duplicate configurations (specimens with embedment lengths of five and ten times the bar diameter) had their results averaged for presentation in this section.   Appendix C and Appendix D provide a complete list of the test data for all of the tested specimens.

4.2   Beam Test Specimen Results

The beam tests specimens investigated the effects of the concrete compressive strength, rebar diameter, and the embedment length had on the bond behaviour of the GFRP rebar. In order to determine the bond strength of the beam specimens, the load in the GFRP rebar was first determined. Based on the geometry of the beam specimens, the locations of the applied loads, and supports (Figure 3.1), the load in the GFRP rebar was determined by the following expression:

$$P_A = 1.25F \qquad \text{for Type A specimens} \qquad\qquad\qquad \text{Equation 4.1a}$$
$$P_B = 1.50F \qquad \text{for Type B specimens} \qquad\qquad\qquad \text{Equation 4.1b}$$

where F was the applied load determined by the load cell. Figure 4.1 to Figure 4.4 show the relationship between bar load and embedment length for each type of concrete. As expected, it can be seen for each concrete that as the embedment length increased, the bar load also increased. This trend was evident for both bar diameters and each of the four concretes used in this study. Furthermore, the trend was fairly linear, indicating that the load required for rebar pullout was linearly proportional to the embedment length. The tensile force in the GFRP rebar for each specimen is presented Appendix C. All of the beam tests in this study exhibited the pullout mode of failure. No visual signs of splitting, shear, or moment cracks were observed on any of the beam test specimens. For all of the tested beams, bond failure was sudden. The LVDTs located at each of the free ends of the beams measured the GFRP rebar slip. Maximum slip values of the free ends at failure are given in Appendix C.
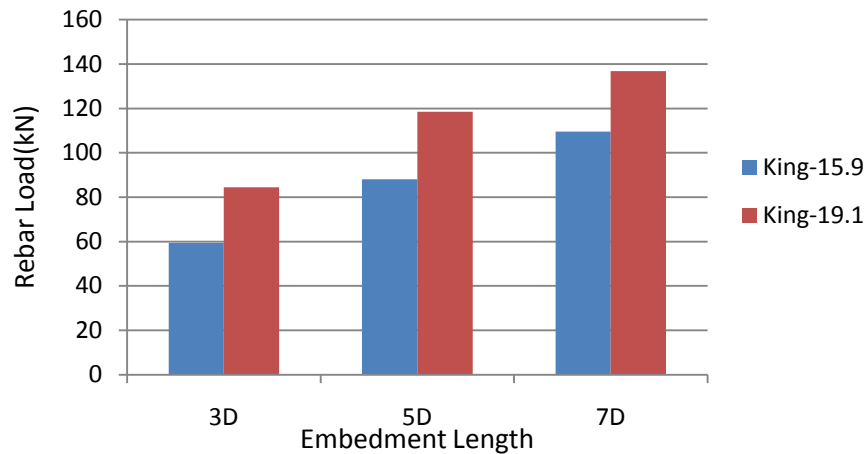
Figure 4.1: HP-S10 Concrete – rebar load vs. embedment length.
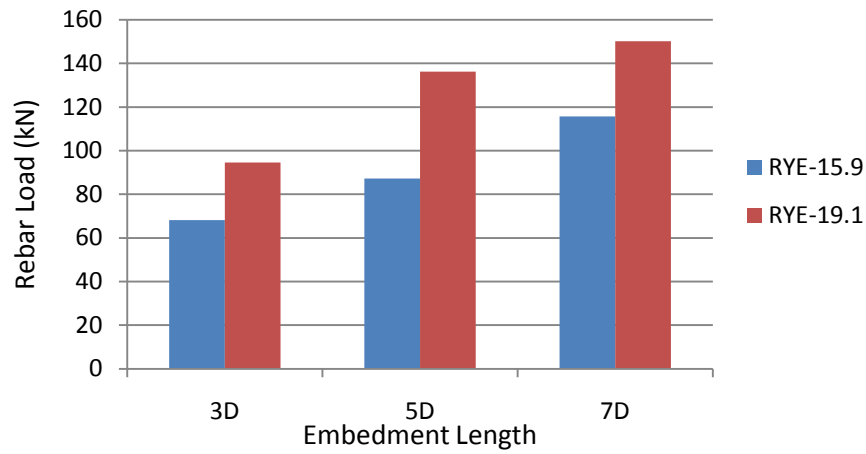
Figure 4.2: Ryerson Concrete – rebar load vs. embedment length.
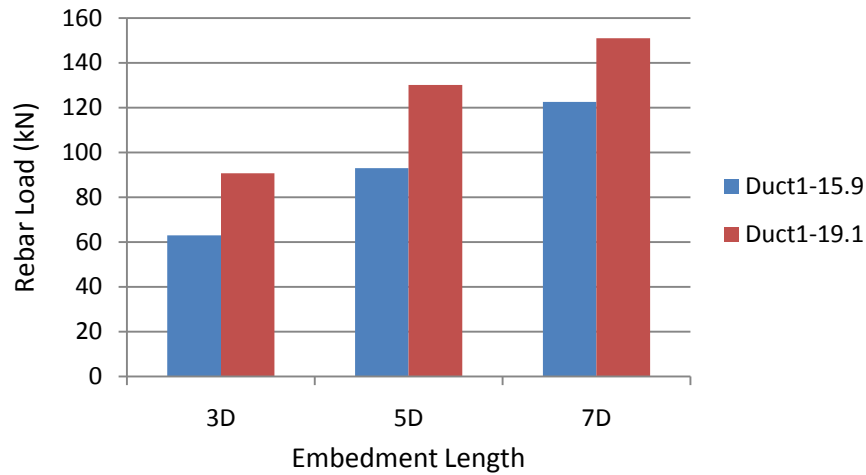
Figure 4.3: Duct1 – rebar load vs. embedment length.
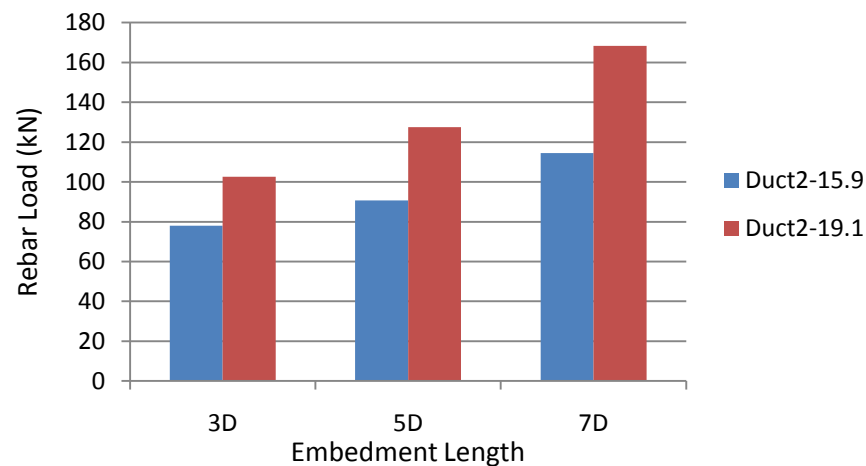
Figure 4.4: Duct2 – rebar load vs. embedment length.

In order to determine the bond strength using Equation 2.2, the stress in the GFRP bar was first determined. By dividing the pullout load by the area of the rebar, the bar stress f_s was obtained for each specimen. Figure 4.5 to Figure 4.8 shows the relationship between bond stress and embedment length for each type of concrete and GFRP bar size.
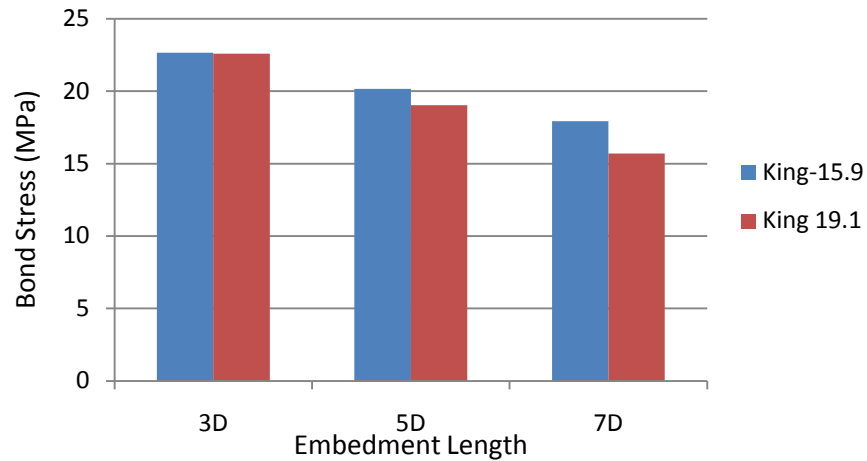
Figure 4.5: HP-S10 Concrete – bond stress vs. embedment length.
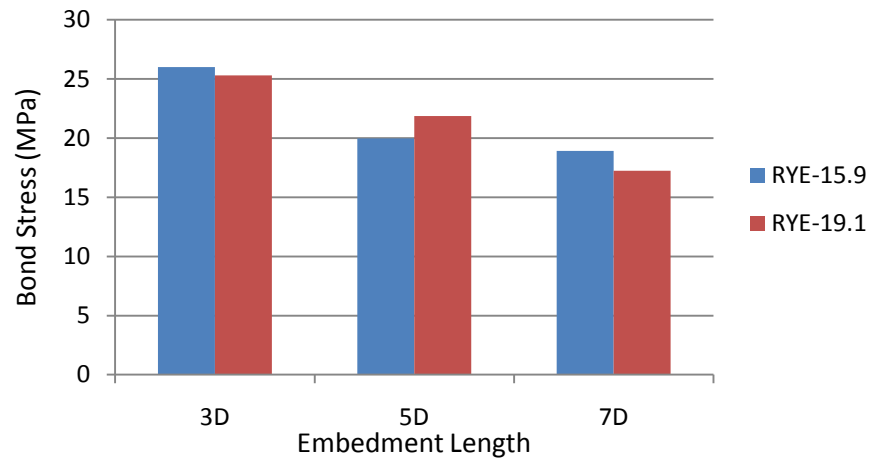
Figure 4.6: Ryerson Concrete – bond stress vs. embedment length.
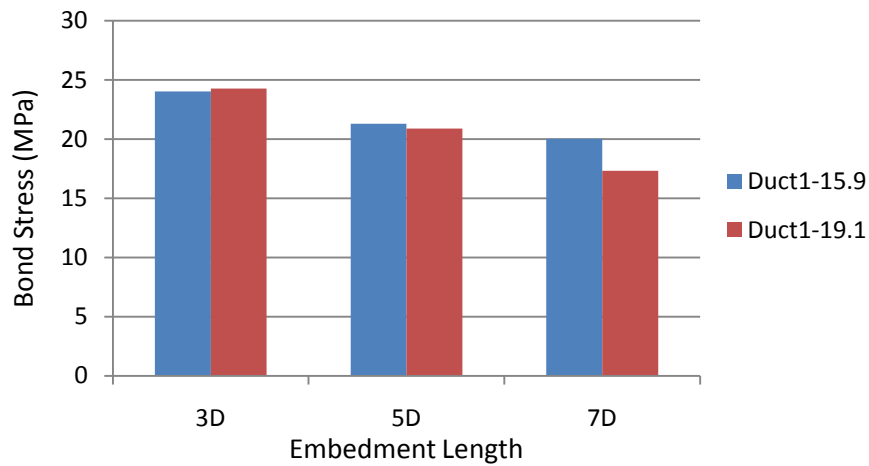
Figure 4.7: Duct1 – bond stress vs. embedment length.
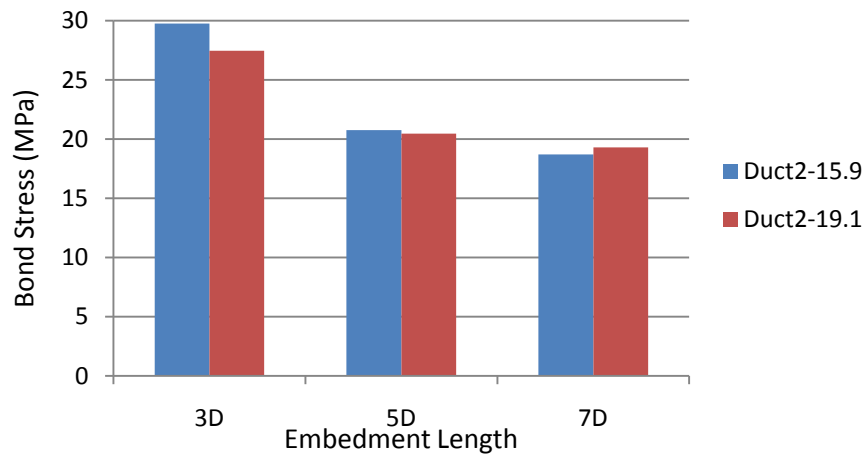
Figure 4.8: Duct2 – bond stress vs. embedment length.

Figure 4.9 shows the complete set of results for each concrete type on one graph. Figure 4.9 combines all of the parameters studied in the beam tests, thereby making it easier to observe any trends that are present, and to determine the effect that each variable parameter had on the bond strength on the beam specimens. The trends in Figure 4.9 with respect to the concrete strength, bar diameter and embedment length will be discussed in Section 4.4. Appendix C presents the bar loads and bond strengths for each of the beam specimens.
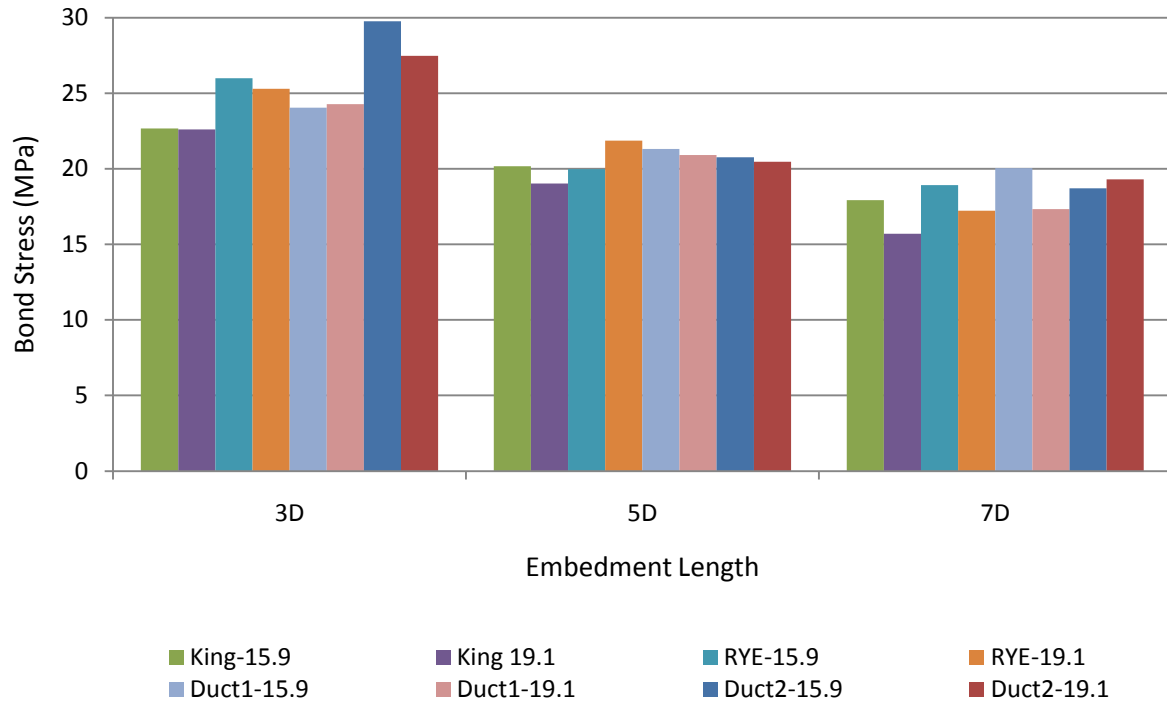
Figure 4.9: Bond stress vs. embedment length for beam specimens.

4.2.1 Stress vs. Strain Curve for GFRP Rebar

The strain values of the GFRP at bond failure from the strain gauges are presented in Appendix C. The maximum strain attained was well below the ultimate strain of the rebar, thus it can be concluded that all of the beam tests failed due to bond failure and not due to rebar rupture. Figure 4.10 shows the stress versus strain curve for the 15.9 mm GFRP rebar and the 19.1 mm GFRP rebar that attained the highest tensile load during the experiment. The highest load that was achieved in a 15.9 mm bar was 122.6 kN (in the Duct1-15.9-7D beam specimen). This translates into a stress of 617 MPa, which is less than the ultimate tensile strength of 751 MPa for the rebar. The highest load that was achieved in a 19.1 mm bar was 168.3 kN (in the Duct2-19.1-7D beam specimen). This translates into a stress of 587 MPa, which is less than the ultimate tensile strength of 728 MPa for the rebar. As expected, the strain curves are linear since the GFRP bar is a linear elastic material. The maximum strain attained in a 15.9 mm GFRP rebar was 9,362 με, which is 60% of the ultimate strain value of the GFRP rebar provided by the manufacturer, and the maximum strain attained in a 19.1 mm GFRP rebar was 10,014 με, which is 65% of the ultimate strain value of the GFRP rebar provided by the manufacturer.

(a)   (b)
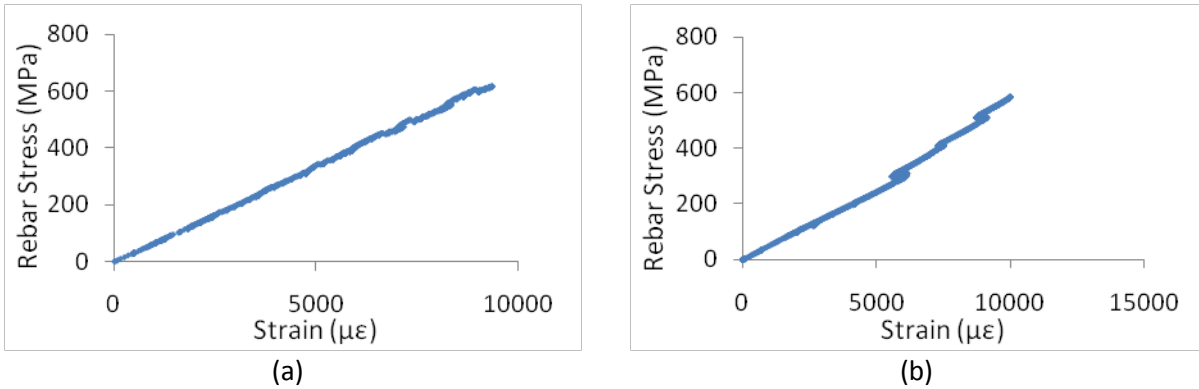
Figure 4.10: Stress vs. strain curve for GFRP rebar: (a) Duct1-15.9-7D specimen; (b) Duct2-19.1-7D specimen.

4.2.2 Stress vs. Slip Curve for Beam Specimen

As mentioned in Chapter 2, bond stress-slip curves can be used to determine the required development length for rebars to achieve their design stress prior to bond failure. Figure 4.11 shows the bond stress-slip curves for each concrete type embedded with a 15.9 mm GFRP bar with a development length of three times the bar diameter. Appendix C shows all of the bond stress-slip curves for the beam specimens. The stress-slip curves of the beam specimens will be used in the subsequent chapter to determine the required development length of the GFRP bars used in this study.
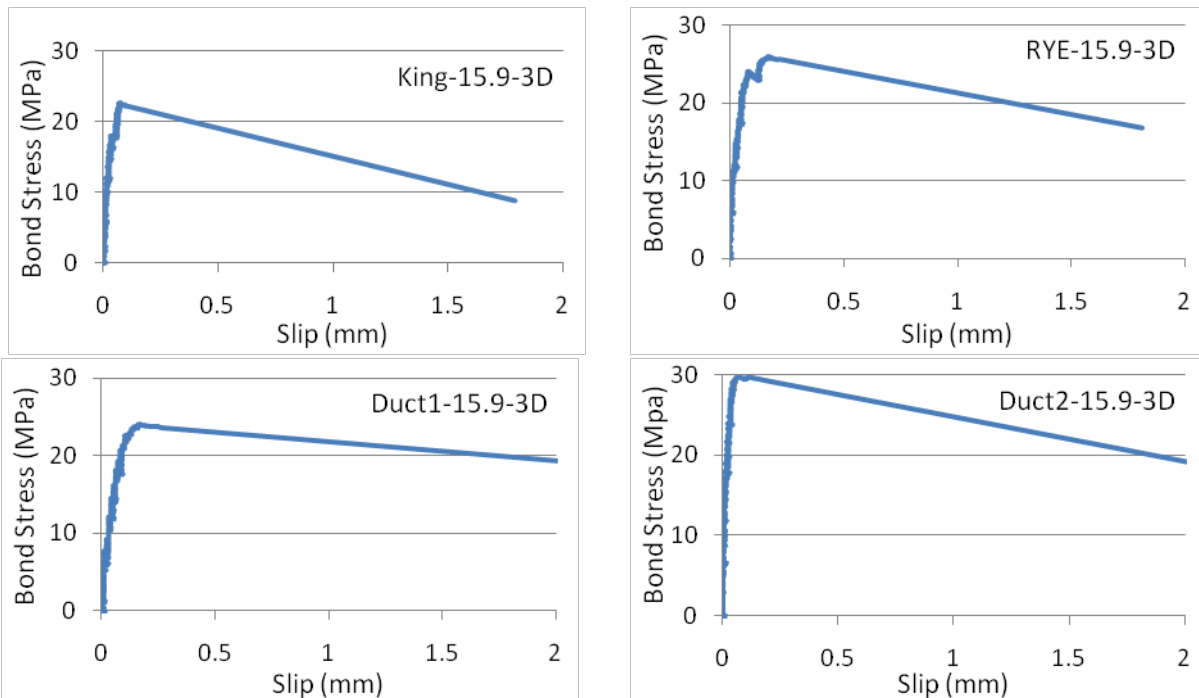
Figure 4.11: Bond stress – slip curves for beam test specimens.

It can be seen through the bond stress-slip curves for the beam test specimens that the sand coated GFRP rebars all exhibited a brittle bond failure. This is due to the interface between the sand grains and the rebar detaching abruptly, causing a brittle failure.

4.3   Pullout Test Specimen Results

The pullout tests specimens investigated the effect that the concrete compressive strength, rebar diameter, and the embedment length and concrete cover had on the bond behaviour of the GFRP rebar. Pullout test specimens made with concrete containing fibres all had bond failure due to rebar pullout. Pullout specimens made with HP-S10 Concrete exhibited both modes of bond failure. Appendix D specifies the failure mode for each pullout specimen along with a sketch of the cracking planes for the splitting mode of failure. Bond failure was sudden for the pullout specimens.

For the pullout specimens that had splitting bond failure, a visual inspection of the bond interface between the GFRP bar and the concrete was performed. It was observed that the sand coating had been partially sheared off of the GFRP rebar. The delaminated rebar surface indicated that the shear strength between the resin and bar fibre was less than the shear strength between the concrete and the resin. Figure 4.12 shows splitting bond failure for a pullout test specimen along with the delaminated rebar surface after execution of the test.

(a)

(b)

(c)
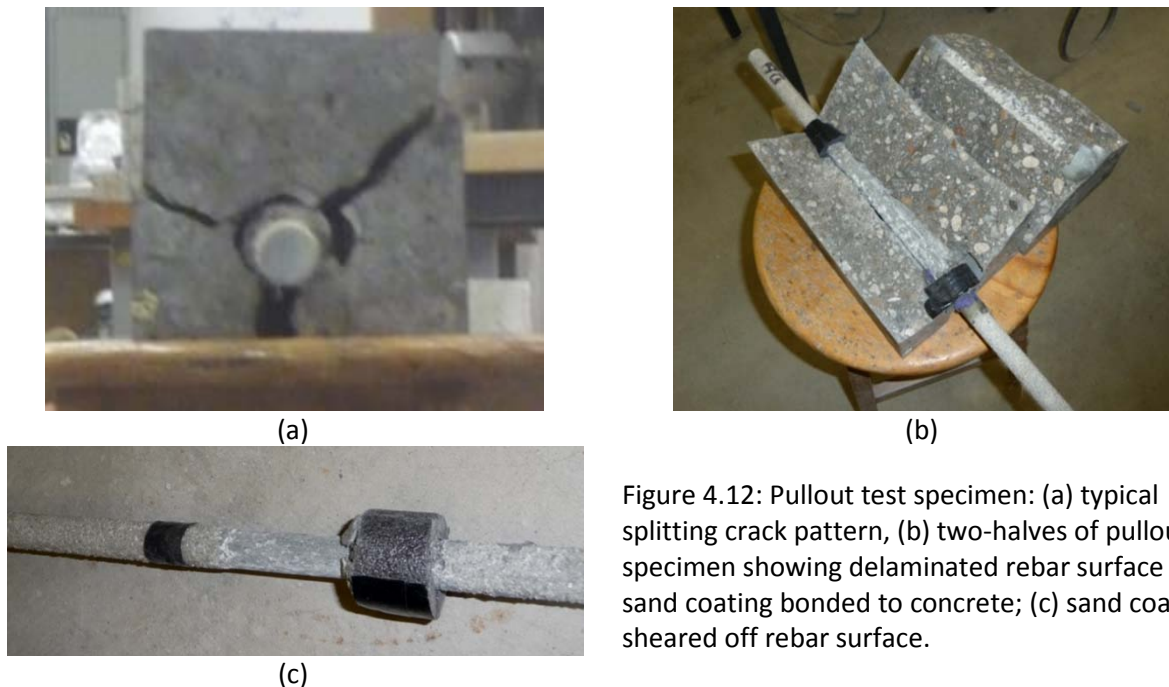
Figure 4.12: Pullout test specimen: (a) typical splitting crack pattern, (b) two-halves of pullout specimen showing delaminated rebar surface and sand coating bonded to concrete; (c) sand coating sheared off rebar surface.

Figure 4.13 to Figure 4.16 show the relationship between bar load and embedment length for each type of concrete, GFRP bar size, and amount of cover for the pullout test specimens. It can be seen in the following figures that for each concrete type and cover, as the embedment length increased, the bar load also increased (except for the specimen casted with HP-S10 Concrete, with a 19.1 mm diameter GFRP bar, an embedment length of 3D, and a cover of 40 mm - this was likely due to specimen irregularities). For all of the specimens that did exhibit this trend, the trend appeared to be linear for the vast majority of the data indicating that the load required for bond failure was linearly proportional to the embedment length. The tensile force in the GFRP rebar for each specimen is presented Appendix D.
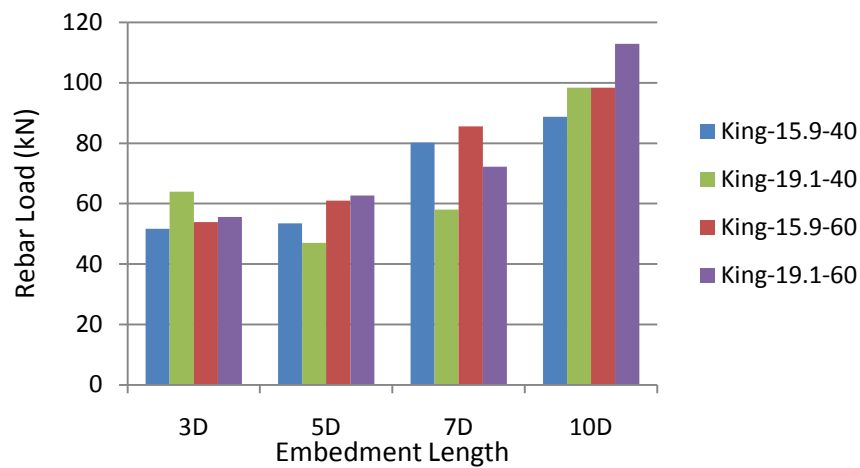
Figure 4.13: HP-S10 Concrete – rebar load vs. embedment length.
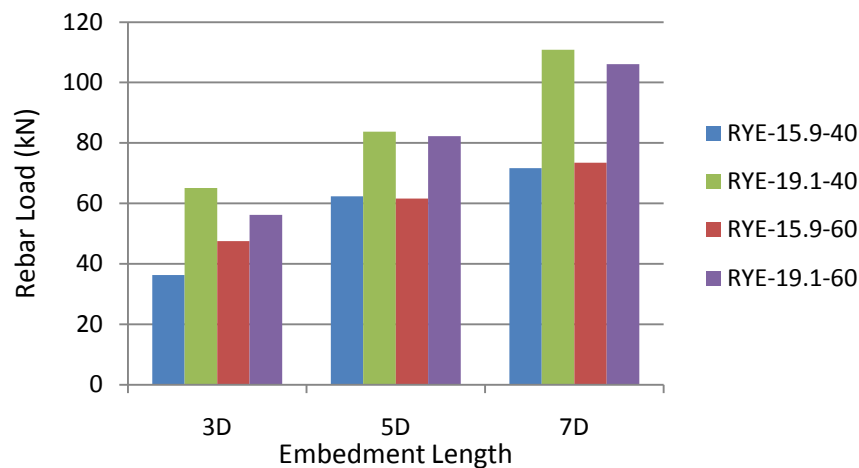
Figure 4.14: Ryerson Concrete – rebar load vs. embedment length.
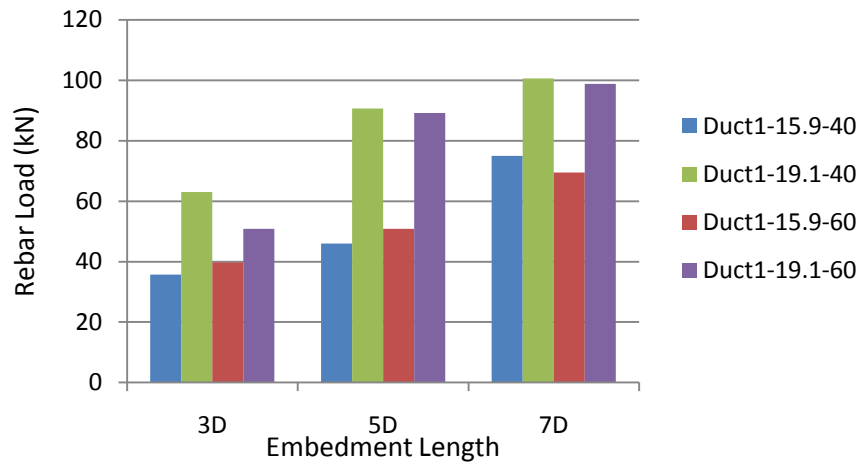
Figure 4.15: Duct1 – rebar load vs. embedment length.
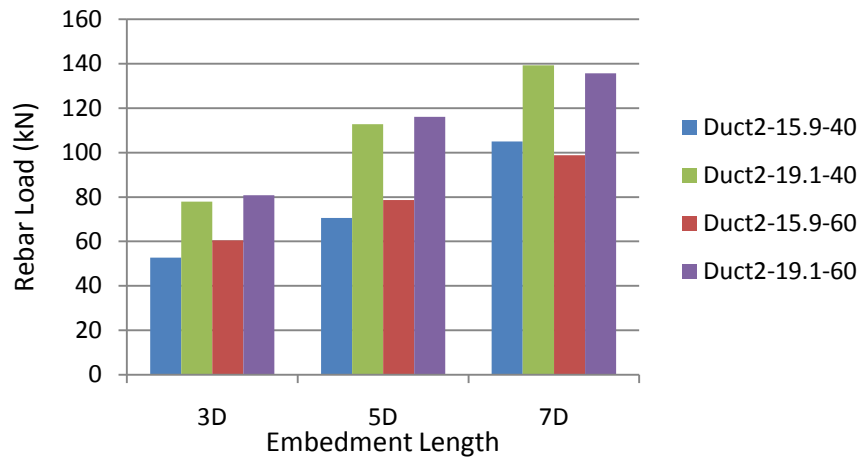
Figure 4.16: Duct2 – rebar load vs. embedment length.

Similar to the beam test specimens, the stress in the GFRP rebar was determined in order to ascertain the bond strength using Equation 2.2. Figure 4.17 to Figure 4.20 show the relationship between bond stress and embedment length for each type of concrete, GFRP bar size, and concrete cover. When compared to the beam tests specimens, the bond strength of the pullout tests was lower than the strength achieved by the beam tests. Since the pullout tests were performed in unconfined concrete, whereas the beam tests had a large amount of internal reinforcement which provided confinement, the bond strength achieved was lower in comparison.
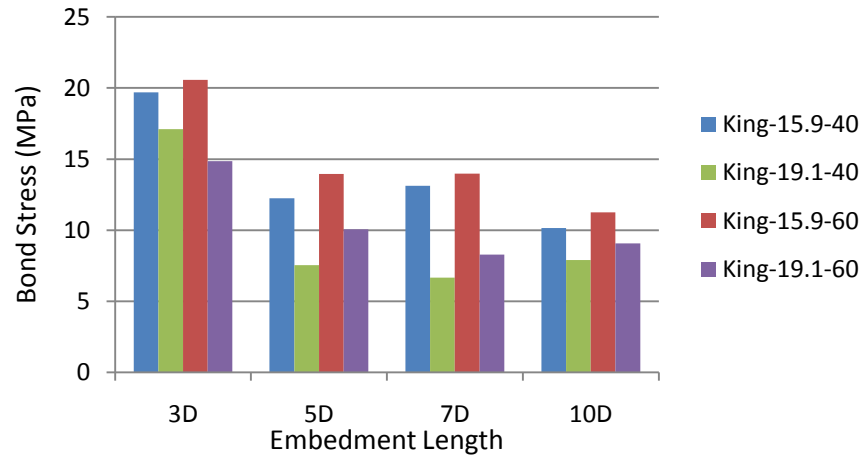
Figure 4.17: HP-S10 Concrete – bond stress vs. embedment length.
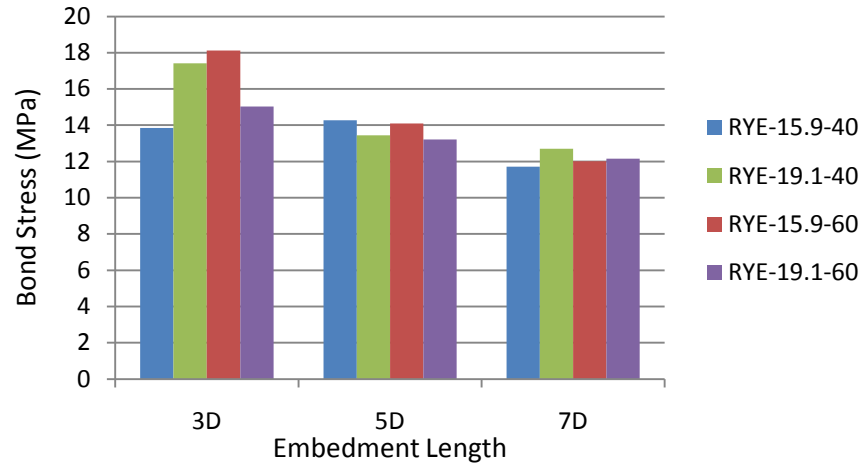
Figure 4.18: Ryerson Concrete – bond stress vs. embedment length.
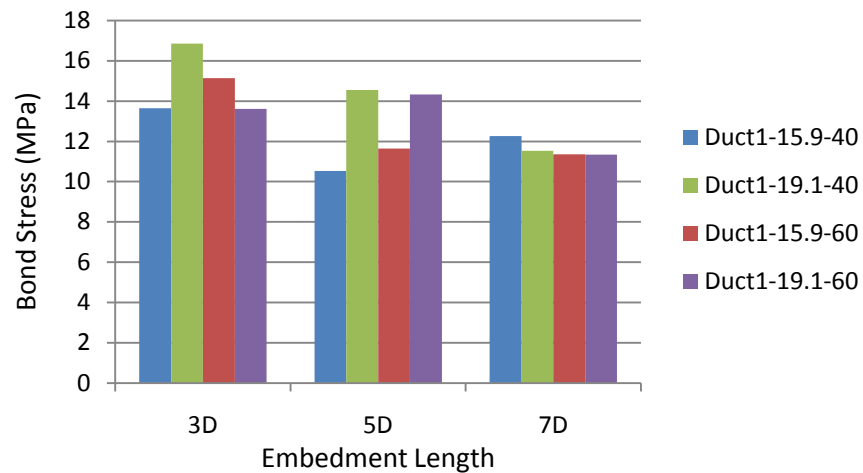
Figure 4.19: Duct1 – bond stress vs. embedment length.
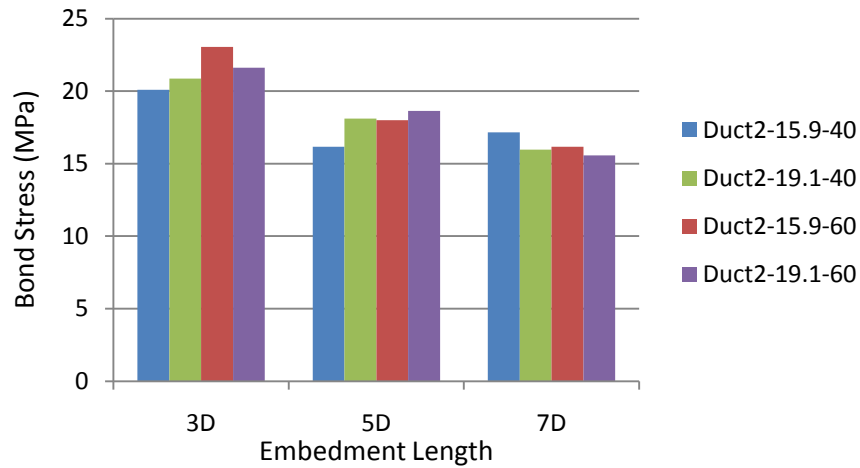
Figure 4.20: Duct2 – bond stress vs. embedment length.

Figure 4.21 and 4.22 show the pullout specimens grouped together according to their concrete cover. Similar to Figure 4.9, grouping the specimens in Figure 4.21 and Figure 4.22 makes it easier to observe any trends that are present within the data. The trends present in Figure 4.21 and Figure 4.22 with respect to the concrete strength, bar diameter and embedment length and concrete cover will be discussed in Section 4.4.
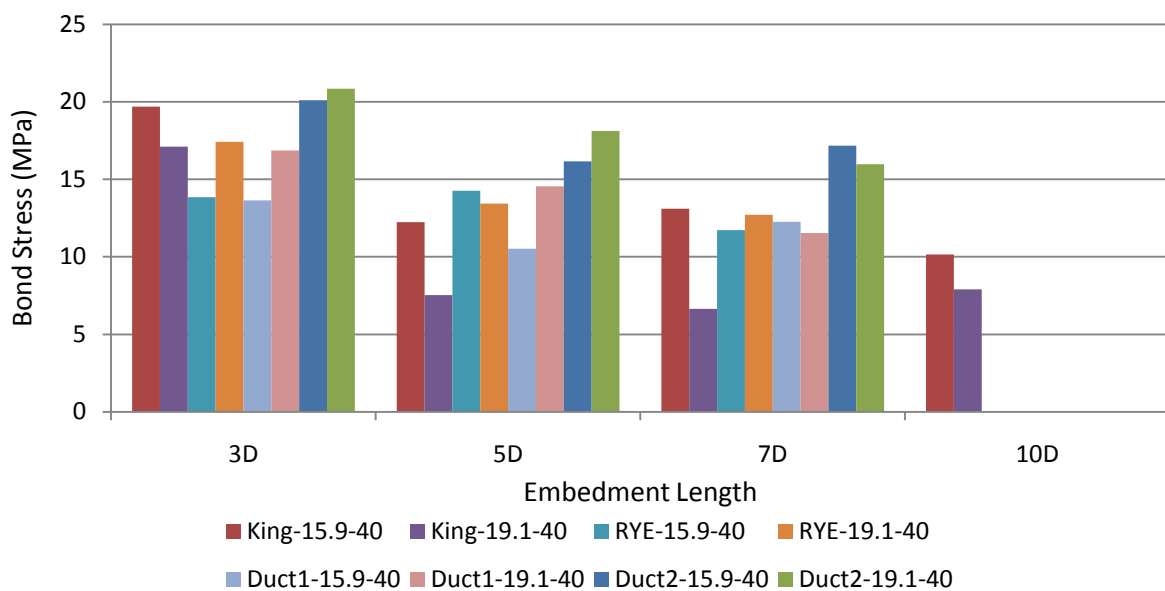
Figure 4.21: Bond strength vs. embedment length for pullout specimens with 40 mm cover.
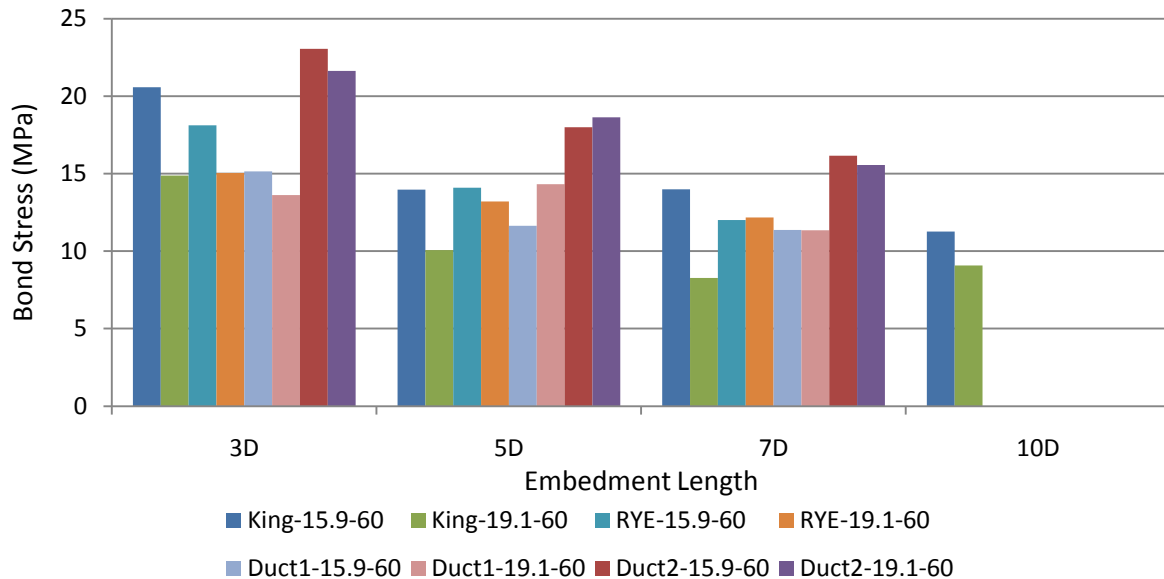
Figure 4.22: Bond strength vs. embedment length for pullout specimens with 60 mm cover.

4.3.1 Stress vs. Slip Curve for Pullout Specimen

The bond stress-slip curves shown in Figure 4.23 are for pullout specimens that failed due to rebar pullout, not splitting. In each graph, the bond strength increases until it reaches its maximum value, followed by a sudden loss of bond shown by the decreasing branch of the curve.   The 'scrambled' section in each graph is the result of the load cell and the LVDT stabilizing after the sudden shock, which jolted the test system at the instant of bond failure. Once the system stabilized, the bond stress reached a constant level and the slip values began to increase. The plateau represents the amount of bond created by the residual friction between the GFRP bar and the concrete once bond failure had occurred and the rebar was continuously pulled out from the specimen, as can be seen by the increasing slip. For specimens that failed due to splitting bond failure, the 'scrambled' and horizontal sections on the curves were non-existent.

Similar to the beam test specimens, it was noticed from the bond stress-slip curves for the pullout specimens (Figure 4.23), that the GFRP rebars all had brittle bond failure as a result of the sand coating abruptly detaching.
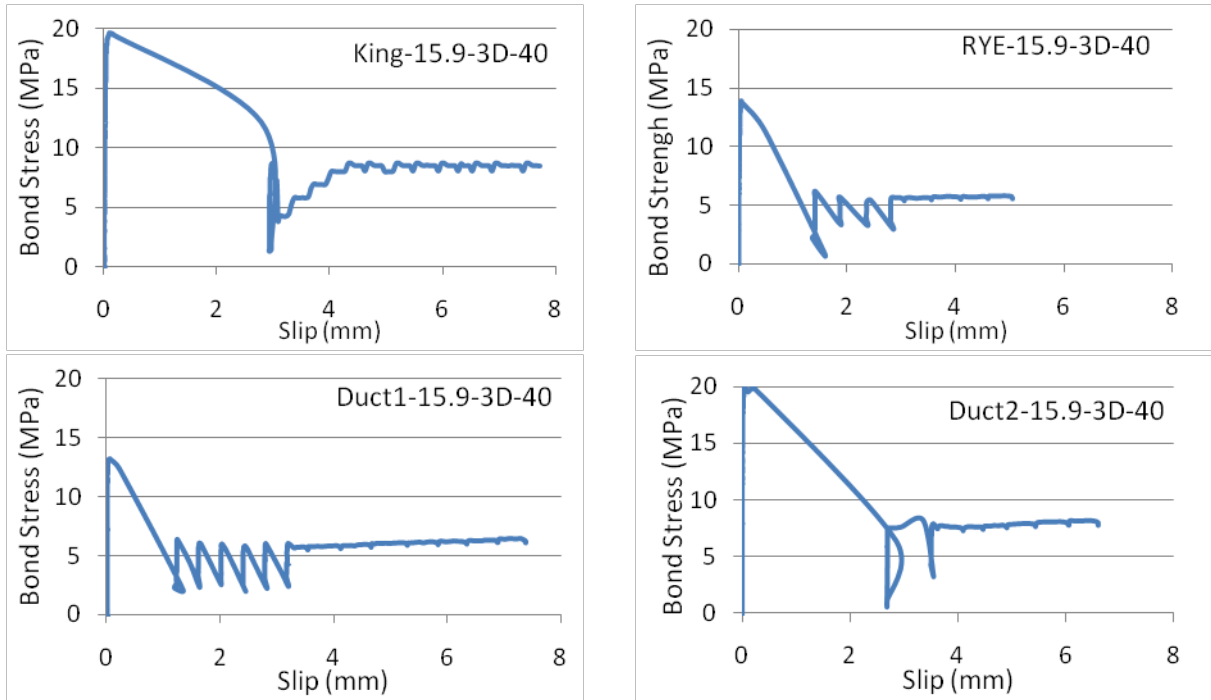
Figure 4.23: Bond stress-slip curves for pullout specimens.

4.4 Parameter Analysis

This section analyses the data and determines the effect of each of the investigated parameter in this study. The beam and pullout test data were analysed to determine the effect of the concrete compressive strength, the effect of the bar diameter, the effect of the embedment length, and the effect of the concrete cover.

When determining the effect of each parameter, it was decided that it was best not to normalize the bond strength results with the compressive strength of the concrete. Since the bond strength is related to the tensile properties of the concrete, code provisions modify the concrete compressive strength by raising it to a power such that the tensile properties of the concrete can be represented. CSA S86-02, CSA S6-06, and ACI 440.1R-06 express the bond strength as a function of the square root of the concrete compressive strength and JSCE Design Recommendation expresses the bond strength as a function of the compressive strength to the power of 2/3. However, the tensile properties of concrete are significantly affected when fibres are incorporated into the concrete mixture. Normalizing the bond strengths by the square root of the compressive strengths, as is most commonly done for normal strength concrete, or by the concrete compressive strength raised to the power of 2/3, would not be able to eliminate the effect of concrete strength equally for the concrete mixes

containing fibres and the concrete mixes without fibres. Furthermore, as discussed in Chapter 2, the effect of concrete strength should have minimal to negligible effects on the bond strength between the GFRP rebars and the high strength concrete. As a result, it was decided not to normalize the bond strengths as this would not have served a useful purpose since any variation in the test results could not be attributed to the variation in concrete strength. Above all, the effect of normalizing the bond strengths could not have been done equally for each type of concrete – mainly for the concrete without fibres versus the concretes containing fibres.

The beam bond strength ranges from 3D to 7D embedment lengths for each bar diameter and concrete type are shown in Table 4.2 for the beam test specimens. Table 4.3 shows the ranges of bond strengths for each bar diameter and concrete strength according to concrete cover from 3D to 7D embedment lengths. It can be seen that the beam test specimens achieved higher bond strengths than the pullout test specimens. Higher bond strength in the beam specimen is attributed to the auxiliary reinforcement providing confinement to the GFRP bars over the bonded length.

Table 4.2: Bond strength ranges of beam test specimens.

	15.9 mm GFRP	19.1 mm GFRP
	Range (MPa)	Range (MPa)
HP-S10	17.92 – 22.65	15.69 – 22.59
Ryerson Concrete	18.91 – 25.98	17.22 – 25.30
Duct1	20.04 – 24.04	17.33 – 24.28
Duct2	18.71 – 29.76	19.29 – 27.46

Table 4.3: Bond strength ranges of pullout test specimens.

	40 mm Concrete Cover		60 mm Concrete Cover	
	15.9 mm GFRP	19.1 mm GFRP	15.9 mm GFRP	19.1 mm GFRP
	Range (MPa)	Range (MPa)	Range (MPa)	Range (MPa)
HP-S10	12.44 – 19.69	6.65 – 17.11	13.96 – 20.58	8.28 – 14.87
Ryerson Concrete	11.72 – 14.27	12.71 – 17.42	12.01 – 18.12	12.16 – 15.04
Duct1	10.53 – 13.64	11.34 – 16.86	11.36 – 15.14	14.33 – 11.34
Duct2	16.16 – 20.10	15.97 – 20.85	16.15 – 23.05	15.56 – 21.62

4.4.1 Effect of Concrete Compressive Strength

As mentioned in Chapter 3, four different concrete strengths were used in this study, ranging from 70 MPa to 175 MPa. From Figure 4.9 and Table 4.2, it can be seen that the increase in compressive strength results in a marginally higher increase in bond strength for the beam specimens. From Figure

4.21, Figure 4.22 and Table 4.3, the increase in bond strength with the increase in compressive strength is more significant for the pullout specimens than for the beam specimens. As mentioned in Chapter 2, bond failure can occur in one of three locations: in the concrete matrix away from the FRP bar, partly on the surface between the concrete and the resin and partly between the resin and the fibres, or at the interface between the resin and the fibres. Once bond failure begins to occur between the resins and the fibres, and not in the concrete, any additional increase in compressive strength should theoretically have zero effect on the bond strength of the FRP bar. Analysing the data for the beam specimens showed that there was a slight increase in the bond strength, whereas for the pullout specimens, it was evident that there was a significant increase in the bond strength accompanying the increase in concrete strength. This phenomenon can be explained as a result of the increased hydrostatic pressure produced by the concrete as the compressive strength increased from 70 MPa to 175 MPa. The increase in hydrostatic pressure generated a high radial confinement, which in turn produced a stronger bond force. The presence of hydrostatic pressure was due to the autogenous shrinkage that occurs in high strength and ultra-high strength concrete. Since the water to cementitious materials ratio (w/c_m) is very low was these mixes, the likely hood of autogenous shrinkage occurring was quite high.

Typically when trying to increase the compressive strength of concrete, the w/c_m ratio is reduced. As a result, the autogenous shrinkage increases causing an increase in the hydrostatic pressure in the concrete. Although the amount of self dessication was not determined for each concrete type in this study, which would have given us a clear indication of which concrete produced a greater hydrostatic pressure, it can be safely assumed that between Duct1 and Duct2, Duct2 had a greater amount of autogenous shrinkage. This assumption is based on the fact that Duct2 had 10% less water and admixture in comparison to Duct1 whereas the cementitious material between the two concretes was kept constant. As a result the w/c_m ratio for Duct2 was lower than the w/c_m of Duct1. The lower w/c_m would have resulted in a higher amount of autogenous shrinkage which would have generated a higher hydrostatic pressure on the GFRP bar. Based on this principle, this theory can be assumed to be valid for the explanation of the bond strength increase accompanied by the compressive strength increase. Similar findings have been reported by Nanni *et* al. 1995; Cosenza *et al.* 1997 and Firas *et al.* 2010.

The increase in hydrostatic pressure appears to have affected the pullout specimens to a greater extent than the beam specimens as the increase in bond strength was far more pronounced for the

pullout specimens compared to a minimal increase for the beam specimens. For the pullout specimens, the concrete surrounding the GFRP bar was under compression and thus did not crack. In the beam specimens, the concrete surrounding the GFRP bar was under tension along with the GFRP bar, making the beam specimens highly more susceptible to micro-cracking than the pullout specimens prior to bond failure. At the instant of micro-crack development in the beam specimen, the hydrostatic pressure dissipated and had little effect on the bond strength for the concrete under tension. It was seen for the beam specimens that the 3D embedment lengths for both GFRP bar sizes had more of a bond strength increase than the 5D and 7D specimens (Figure 4.24). If a linear approximation is taken of the trend between the concrete type versus bond strength, it can be seen that the slope for the 3D specimens is greater than the 5D and 7D specimens. This is because fewer cracks developed along the 3D embedment length and the hydrostatic pressure did not dissipate to the same extent as in the 5D and 7D beams where the longer embedment lengths allowed for more cracks to develop along the embedded portion, causing the hydrostatic pressure to dissipate more readily. Since the hydrostatic pressure is a function of the crack development, it is expected that if no cracks develop, each embedment length should have similar increases in bond strength. This is shown to be true from the pullout specimen test results where the bond strength increase was the same for each embedment length (Figure 4.25). If a linear approximation is taken of the trend between the concrete type versus bond strength, it can be seen that the slopes for the 3D, 5D and 7D specimens are nearly the same. This indicated that the hydrostatic pressure affected the bond strength equally over the different embedment lengths.

Another explanation as to why the hydrostatic pressure seems to have affected the pullout specimens and not the beam specimens is because the pullout specimens were unconfined, whereas the beam specimens had a large amount of internal reinforcement. It is expected that the presence of reinforcement would contribute to resisting the hydrostatic forces, thereby causing them to influence the bond strength to a lower extent than if there was no internal reinforcement.

Since the conditions simulated by the pullout test specimens are rarely encountered in the field (reinforcement under tension and surrounding concrete under compression), it is possible to conclude that even if autogenous shrinkage occurs and hydrostatic pressure it produced, this pressure will dissipate once the concrete cracks and will not influence the bond of the GFRP rebar in high strength and ultra-high strength concrete. This theory validates the initial assumption that the concrete compressive strength has no effect on the bond strength of GFRP bars embedded in high strength and

ultra-high strength concrete. Table 4.4 and Table 4.5 show the relative increase of each concrete type using HP-S10 Concrete as a base for comparison for the beam test specimens and the pullout test specimens, respectively.
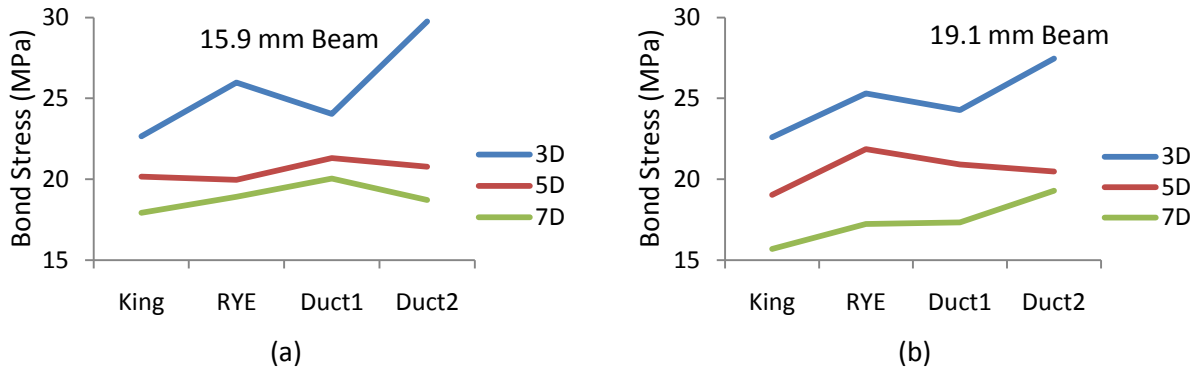
Figure 4.24: Bond stress vs. concrete strength for beam test specimens: (a) 15.9 mm beam specimens; (b) 19.1 mm beam specimens.
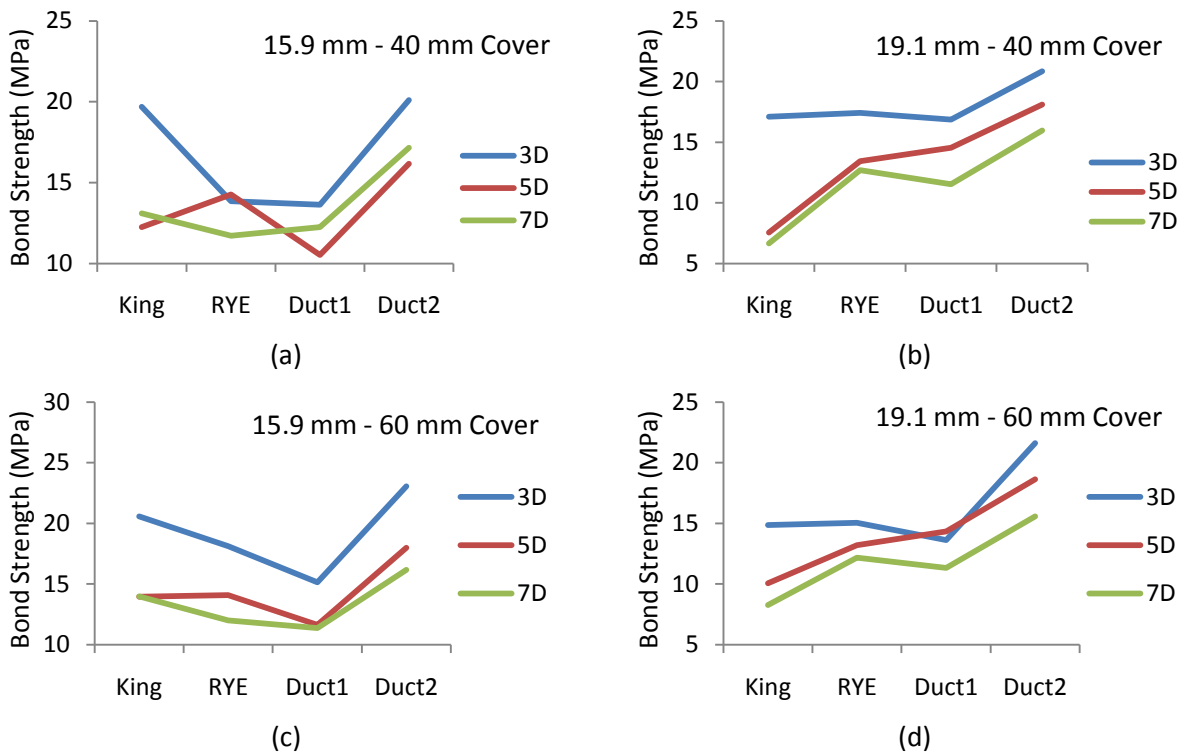
Figure 4.25: Bond stress vs. concrete strength for pullout test specimens: (a) 15.9 mm - 40 mm cover pullout specimens; (b) 19.1 mm - 40 mm cover pullout specimens; (c) 15.9 mm - 60 mm cover pullout specimens; (d) 19.1 mm - 60 mm cover pullout specimens.

Table 4.4: Bond strength increase for beam specimens.

Concrete	15.9 mm			19.1 mm		
	3D	5D	7D	3D	5D	7D
HP-S10	-	-	-	-	-	-
Ryerson Concrete	14.7%	-1.0%	5.5%	12.0%	14.9%	9.7%
Duct1	6.1%	5.7%	11.8%	7.5%	9.8%	10.4%
Duct2	31.4%	3.0%	4.4%	21.5%	7.5%	22.9%

Table 4.5: Bond strength increase for pullout specimens.

Concrete	40 mm Cover					
	15.9 mm			19.1 mm		
	3D	5D	7D	3D	5D	7D
HP-S10	-	-	-	-	-	-
Ryerson Concrete	-29.7%	16.5%	-10.6%	1.8%	78.2%	91.1%
Duct1	-30.8%	-14.0%	-6.5%	-1.5%	93.0%	73.5%
Duct2	2.1%	32.0%	30.9%	21.9%	140.3%	140.2%
Concrete	60 mm Cover					
	15.9 mm			19.1 mm		
	3D	5D	7D	3D	5D	7D
HP-S10	-	-	-	-	-	-
Ryerson Concrete	-11.9%	0.9%	-14.2%	1.2%	31.3%	46.9%
Duct1	-26.4%	-16.6%	-18.8%	-8.4%	42.4%	37.0%
Duct2	12.1%	28.9%	15.5%	45.4%	85.2%	88.0%

4.4.2 Effect of Bar Diameter

It can be seen that for a majority of the beam specimens, the larger bar diameter produced lower bond strengths. The effect of bar diameter for the pullout specimens remains to be inconclusive on the bond strength. Although the slight majority of the pullout specimens with the larger bar exhibited lower bond stress when compared to specimens of the same configuration using a smaller bar, the amount was not significant enough to make this conclusion with confidence. Although several researchers in the past have reported that there is a bond strength decrease with the increase of bar diameter, the same relationship cannot be as readily accepted for FRP bars in high strength and ultra-high performance concrete. Many studies have been performed to evaluate the effect of the bar diameter on the bond strength of GFRP embedded in ordinary and moderate strength concrete, and results have shown that the bond strength increased with the reduction in rebar diameter. This trend was attributed to the greater amount of bleed water, which became trapped beneath larger diameter bars producing voids. The presence of voids consequently reduces the contact area between the

concrete and the rebar lowering its bond capacity. However, in the case of high-strength concrete, especially ultra-high strength concrete, the amount of bleed water present in the fresh concrete is significantly lower than in ordinary and moderate strength concrete, therefore it is expected that this effect should be reduced. Furthermore, the depths of concrete below the bottom surface of the GFRP bar ranged only from 40 mm - 60 mm for the specimens tested in this study; hence in addition to the reduced amount of bleed water, there was insufficient concrete depth accumulate enough migrating water to be trapped beneath the surface to make a significant difference in the bond strength between the larger bars and the smaller bars. Perhaps if the difference between the two GFRP bar diameters was greater, the effect of the trapped bleed water would have been amplified and a more definite conclusion could have been made.

For the beam and pullout test specimens produced with HP-S10 Concrete, the trend of bond strength reduction with the increase in bar size is evident for each embedment length (Figure 4.26). An average bond strength reduction of 6% was noticed for the beam specimens casted with HP-S10 Concrete. An average bond strength reduction for pullout specimens casted with HP-S10 was 31% and 29% for pullout specimens with 40 mm and 60 mm covers, respectively. For the mixes that contained fibres, Ryerson Concrete and Ductal®, the reduction of bond strength with the increase in bar size did not seem as definite. This indicates that the addition of fibres created a local disturbance of the concrete matrix that prevented proper compaction in the vicinity of the rebar, which led to an affected bond strength. Figure 4.27 shows the bond strength comparison between the 15.9 mm GFRP bar and the 19.1 mm GFRP bar embedded in fibre reinforced concrete. The degree to which the fibres affect the bond strength is unknown and furthermore, it is unknown if the smaller bars or larger bars were affected more based on the data obtained from this study. It is hypothesized that the smaller diameter bars suffered a greater disturbance because the difference between the relative surface area between the fibre and the smaller bar is less than that of the fibre and the larger bar. Therefore, a fibre being trapped on the surface of smaller bar would have a greater effect than the same fibre being trapped on the surface of a larger bar.

(a)

(b)

(c)
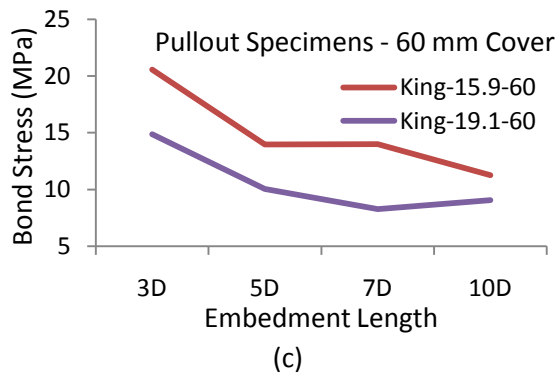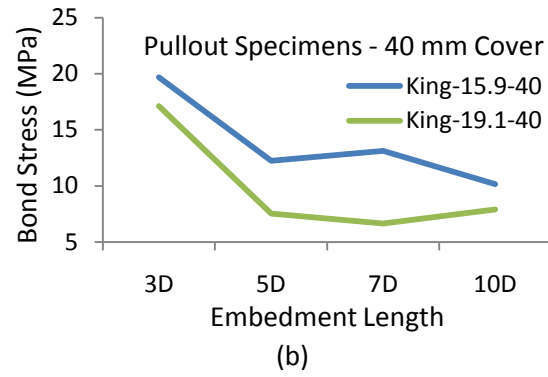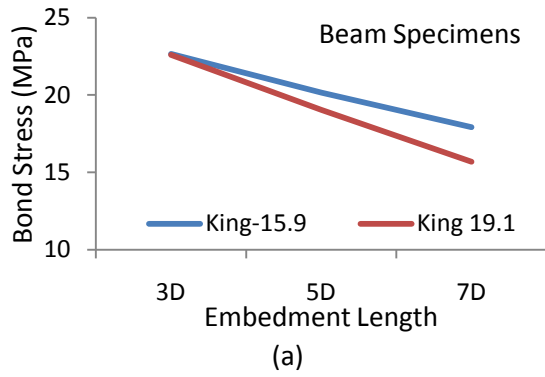
Figure 4.26: Bond strength of GFRP in HP-S10 Concrete: (a) beam test specimens; (b) pullout test specimens with 40 mm cover; (c) pullout test specimens with 60 mm cover.

(a)

(b)
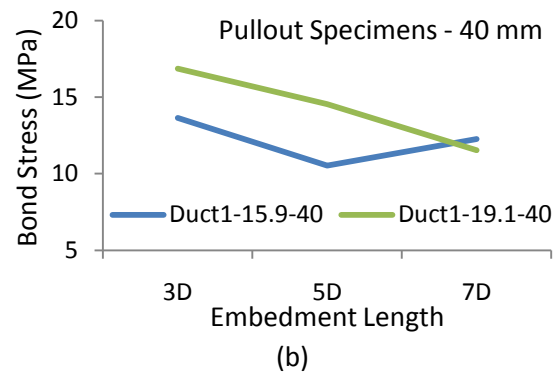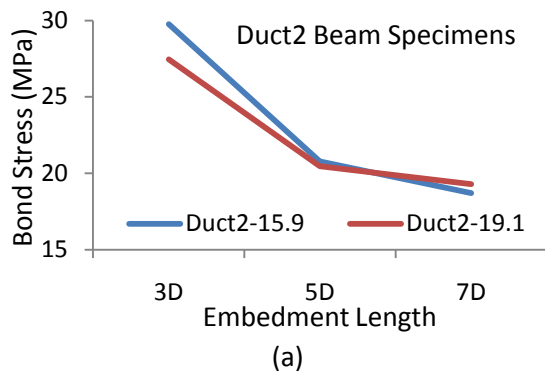
Figure 4.27: Bond strength between GFRP and fibre reinforced concrete: (a) Duct2 beam specimen; (b) Duct1 pullout specimen with 40 mm cover.

4.4.3 Effect of Embedment Length

It can be seen from Figure 4.28 that as the embedment length increases, the bond strength decreased for both the beam and pullout test specimens. This decrease was caused by the non-linear distribution of bond stresses along the GFRP bar embedded in concrete. For the beam tests, the bond strength of the 7D specimens ranged from 62 – 83% of the 3D specimens with 15.9 mm GFRP bars, and for the 19.1 mm bars, the 7D bond strength was 68 – 71% of the 3D specimens. For the pullout tests, the bond strength of the 7D specimens ranged from 66 – 90% of the bond strength of the 3D specimens with 15.9 mm GFRP bars, and for the 19.1 mm GFRP bars, the 7D bond strength was 38 – 83% of the 3D specimens. The average bond strength reductions of 7D specimens compared to 3D specimens for the beam tests were 25% and 30% for the 15.9 mm and the 19.1 mm diameter bars, respectively. The average bond strength reductions of 7D specimens compared to 3D specimens for the pullout tests were 24% and 31% for the 15.9 mm and the 19.1 mm diameter bars, respectively. This indicated that the providing confinement to the concrete did not affect the effect of the embedment length on the bond strength. It can be concluded that the bond behaviour of GFRP bars in high strength and ultra-high strength concrete is similar to that in conventional concrete.

(a)

(b)

(c)

(d)
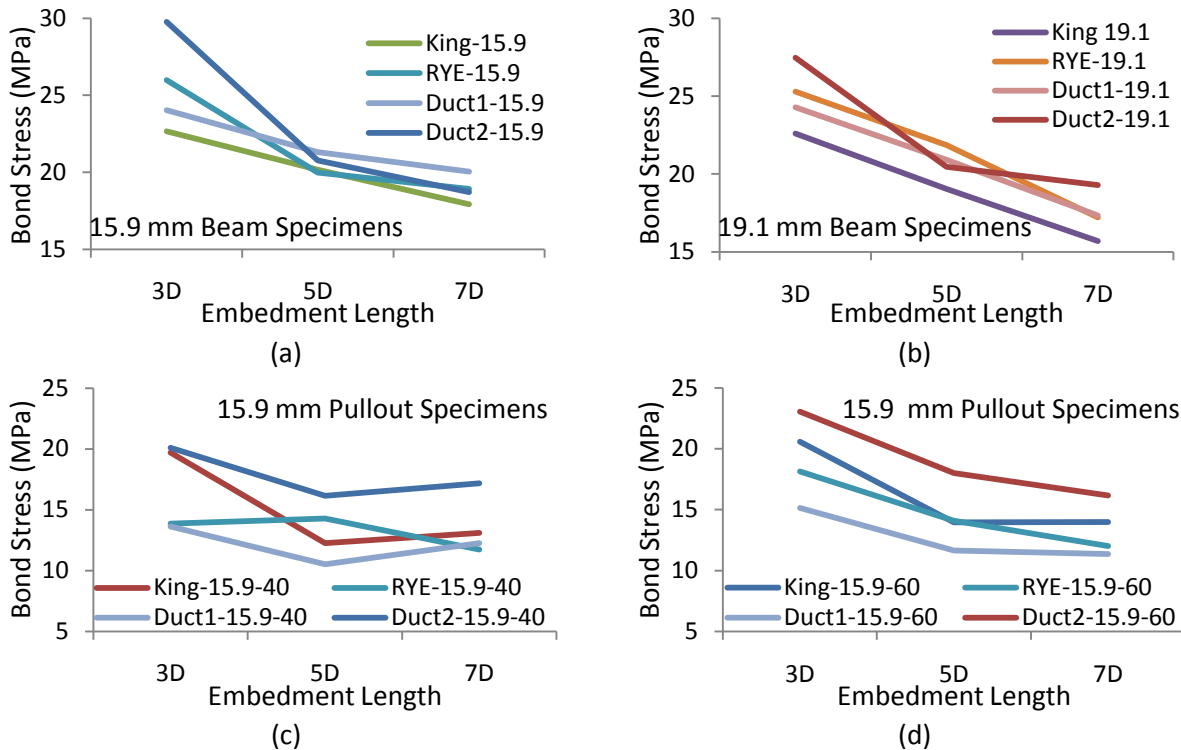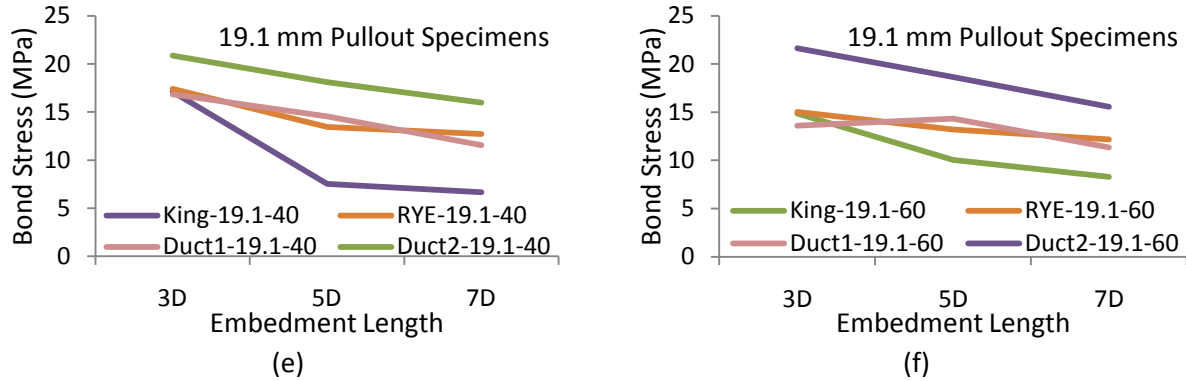
Figure 4.28: Bond stress vs. embedment length: (a) 15.9 mm beam specimens; (b) 19.1 mm beam specimens; (c) 15.9 mm pullout specimen with 40 mm cover; (d) 15.9 mm pullout specimens with 60 mm cover; 19.1 mm pullout specimen with 40 mm cover; (f) 19.1 mm pullout specimen with 60 mm cover.

4.4.4 Effect of Concrete Cover

The pullout tests were used to determine the effect of concrete cover on the bond behaviour of GFRP rebars in high strength and ultra-high strength concrete.   The effect of concrete cover was most noticeable for the specimens casted with HP-S10 concrete. Specimens casted with Ryerson Concrete and Ductal® showed no noticeable trends with regards to the concrete cover. The fibre reinforcement in Ryerson Concrete and Ductal® provided enough confinement such that the radial stresses produced by the GFRP bar under tensile loading was less than the capacity of the concrete; therefore, the pullout specimens casted with the fibre reinforced concrete all underwent the pullout mode of failure, rendering the concrete cover to have no effect on the bond strength. If two smaller concrete covers had been investigated, perhaps the pullout specimens produced with Ryerson Concrete and Ductal® would have failed due to splitting and the effect of concrete cover could have been investigated. The pullout test specimens casted with HP-S10 Concrete exhibited both pullout and splitting failure modes, therefore, the effect of concrete cover was evaluated in these specimens. All of the specimens, except for the 3D specimen with a 19.1 mm GFRP bar, with a cover of 60 mm, exhibited stronger bond strength than specimens of the same configuration with concrete covers of 40 mm. An average increase of 9% in bond strength was observed for 15.9 mm GFRP bars that went from 40 mm to 60 mm concrete covers. For 19.1 mm GFRP bars, an average increase of 15% in bond strength was observed for specimens that increased in cover from 40 mm to 60 mm. If the 3D-19.1 mm specimen was not included in this calculation, the average increase in bond strength would have been 24% as the cover

increased from 40 mm to 60 mm. Figure 4.29 shows the relationship between concrete cover and bond strength.
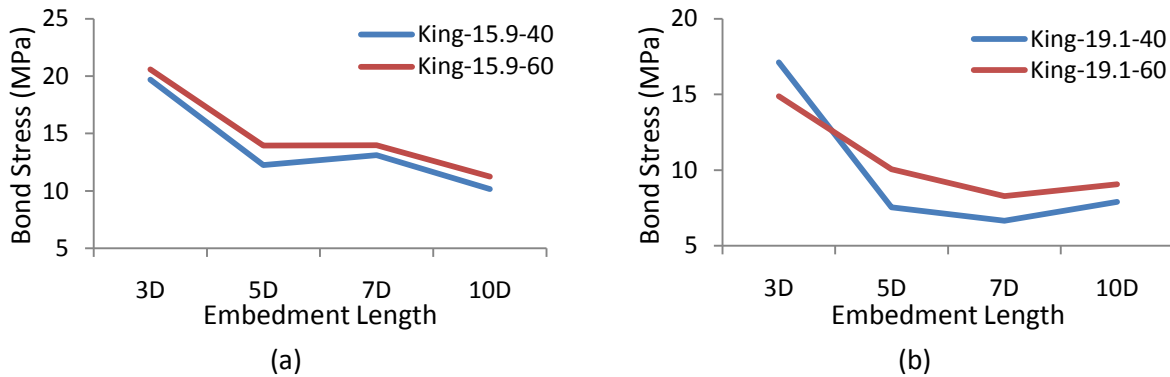
Figure 4.29: Bond stress vs. concrete cover for HP-S10 Concrete.

4.5   Summary

Based on the results presented in this chapter, the main conclusion drawn was that the bond behaviour of GFRP bars embedded in high strength and ultra-high strength concrete is very similar to the bond behaviour of GFRP bars embedded in conventional concrete. The increase in compressive strength when using high strength and ultra-high strength concrete has a negligible effect on the bond strength of the GFRP bars. Similar to conventional concrete, an increase in bar diameter leads to a decrease in bond strength – provided that no fibre reinforcement is used in the concrete matrix. The increase in embedment length is accompanied by a decrease in bond strength due to the non-uniform bond stress distribution over the length of the rebar, which is similar to the behaviour of GFRP bars in conventional concrete. The main difference between using conventional concrete or high strength and ultra-high strength concrete, especially when there are fibres present in the concrete matrix, is that the amount of cover needed to avoid splitting failure is less than the cover needed when using conventional concrete. Since high strength and ultra-high strength concrete has a greater resistance to splitting compared to the resistance of conventional concrete, this allows for the cover to be reduced while still achieving pullout failure when using GFRP bars.

Chapter 5

DEVELOPMENT LENGTH MODELING AND CODE REQUIREMENTS

5.1 General

This chapter presents the required development length based on the results obtained from the bond tests conducted in this study. As discussed in Chapter 2, beam tests simulate bond stress fields more accurately than pullout tests; therefore, a generalized bond stress-slip model will be proposed for each bar diameter and concrete type based on the experimental data obtained from the beam test specimens by using the peak bond stress and the corresponding slip. Using this model, the required development length was determined and these values were compared to the code provisions discussed in Chapter 2. The issues associated with determining the development length of the GFRP rebars from the pullout tests are discussed at the end of this chapter.

5.2 Modeling of Bond Stress-Slip Relationship

The assessment of the stress-slip law by means of experimental tests is not straightforward. Pullout or beam tests are performed to evaluate a constitutive law and tests are carried out on specimens with short embedment lengths, about five times the bar diameter or less (Cosenza *et al.* 2002). Furthermore, the stress is assumed to have a constant distribution along the embedded portion of the bar while the slips are measured at the unloaded end. In the case of FRP reinforcing bars, values of slips measured at the loaded and unloaded end of the rebar are very different, therefore the assumption of a constant bond stress distribution appears to be inadequate. In order to mitigate this problem, reducing the embedment length to very short values would result in a more uniform bond strength distribution and similar slips. However, shorter embedment lengths tend to amplify local irregularities causing test results to vary significantly, which subsequently increases the amount of tests needed to produce a more accurate average of the results. Increasing the embedment length

would significantly reduce the irregularities; but as a result, the bond stress distribution would be more non-uniform along the embedded portion of the rebar.

As discussed in Chapter 2, beam tests simulate bond stress fields more accurately, therefore, the beam tests were used to determine the development length required for the GFRP bars used in this study. The bond stress-slip curves for the beam specimens presented in Appendix C were used to determine the required embedment length of the GFRP bars. It was observed that all of the stress-slip curves consisted of two distinct branches. The first branch ascends to the peak bond stress and the other branch is a descending post-peak branch. It is evident from the bond stress-slip curves for each beam specimen presented in Appendix C that very low free-end slip amounts were measured corresponding to the peak bond stress. As a result, any irregularities would significantly affect the modeling results. Even though specimens with the shortest embedment lengths would produce the most uniform bond stress distribution over the embedded portion, the probability of irregularities was the greatest for these specimens due to their short embedment length. Specimens produced with embedment lengths equal to five times the bar diameter would still be greatly affected by irregularities. Although two duplicate specimens were casted with embedment lengths of five times the bar diameter, taking an average of only two specimens was determined to be insufficient for selection to produce the stress-slip curves. It was decided to model the beam specimens using the greatest embedment lengths as the amount of irregularities would be reduced and the model would be more representative of the true behaviour of the bond. Since the slip data was not available for the King-19.1-7D specimen, the data from the King-19.1-5D specimens was averaged and used in its place.

The BPE model was used to represent the stress-slip curves for the ascending branch produced from the data for $0 \leq s \leq s_m$. As seen from Chapter 2, the ascending branch of the BPE model is represented as:

$$\frac{\tau}{\tau_1} = \left(\frac{s}{s_1}\right)^\alpha$$

Equation 2.14

where τ_1= maximum bond stress; s_1= slip corresponding to maximum bond stress and α is a curve fitting parameter. The term α was calibrated from the experimental data by using the least-square error method. Figure 5.1 shows the stress-slip curves obtained from the experimental results along with the calibrated modeled curves for the test data. Table 5.1 summarizes the τ_1, s_1, α obtained from the test data and curve-fitting parameters. It can be seen from Figure 5.1 that the BPE model

underestimates the bond strength of the test specimens by providing a slightly conservative approximation.
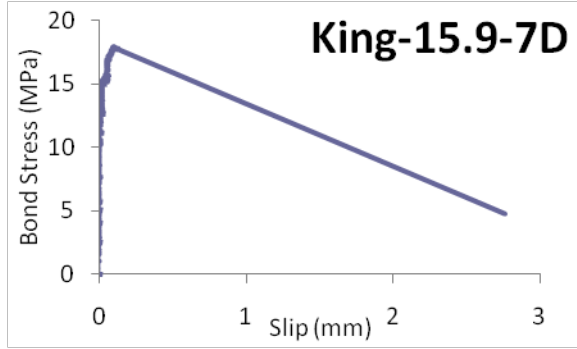
(a): $\tau_1 = 17.92, s_1 = 0.1, \alpha = 0.1512, R^2 = 0.1512$
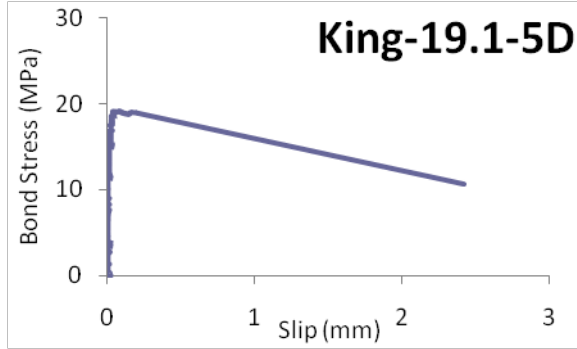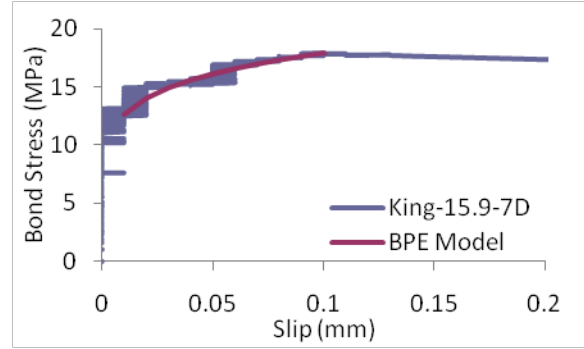
(b): $\tau_1 = 19.03, s_1 = 0.08, \alpha = 0.099, R^2 = 0.5852$
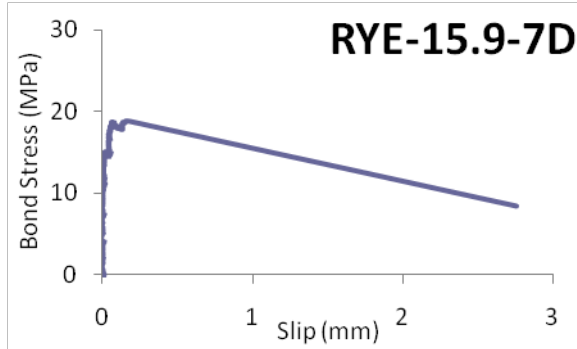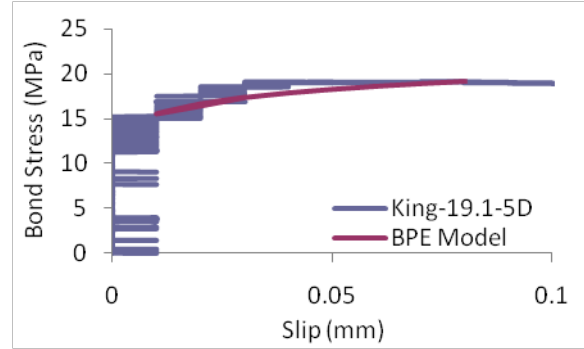
(c): $\tau_1 = 18.91, s_1 = 0.16, \alpha = 0.1298, R^2 = 0.833$
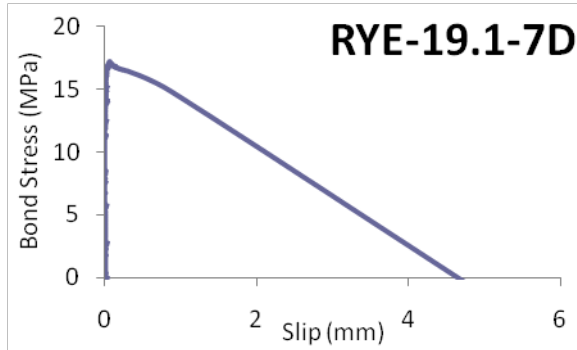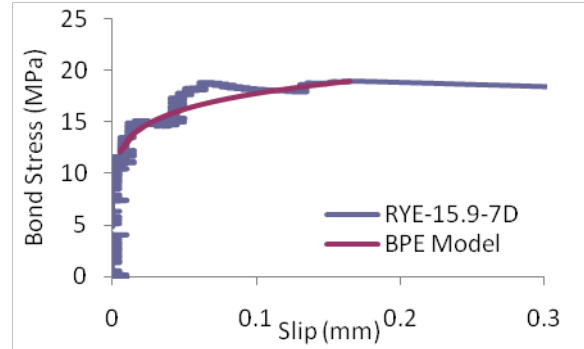
(d): $\tau_1 = 17.22, s_1 = 0.06, \alpha = 0.0319, R^2 = 0.7441$
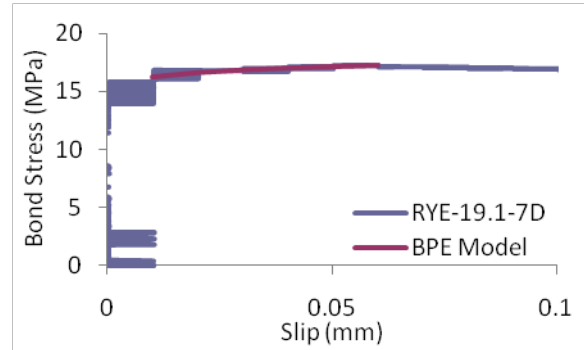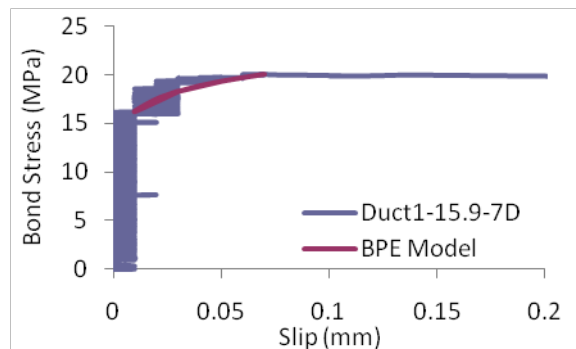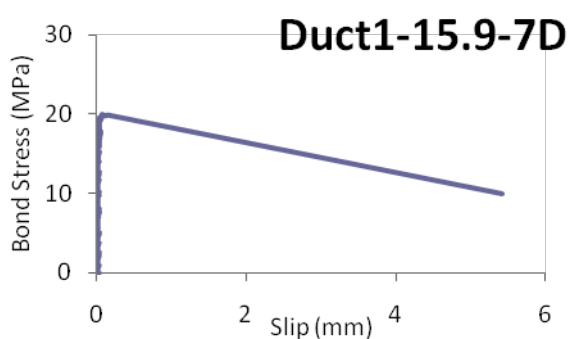
(e): $\tau_1 = 20.04, s_1 = 0.07, \alpha = 0.1086, R^2 = 0.1965$
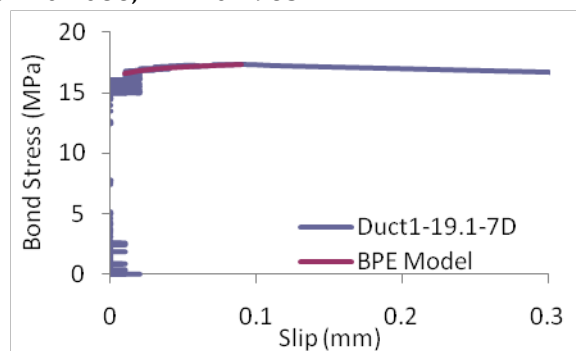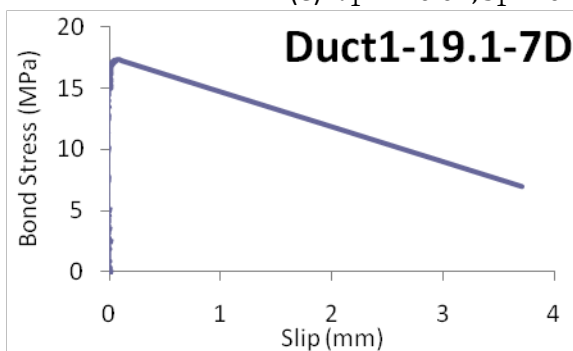
(f): $\tau_1 = 17.33, s_1 = 0.09, \alpha = 0.0197, R^2 = 0.7511$
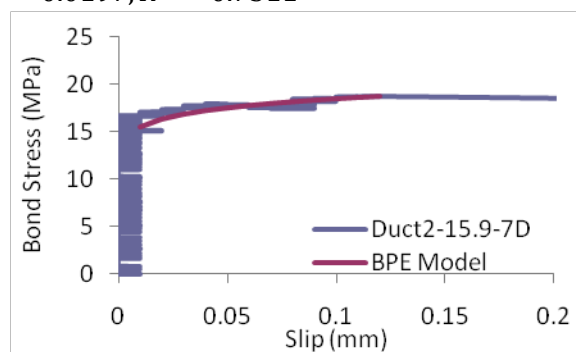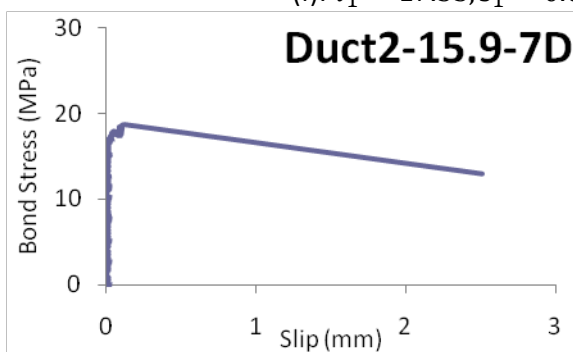
(g): $\tau_1 = 18.71, s_1 = 0.12, \alpha = 0.076, R^2 = 0.4489$
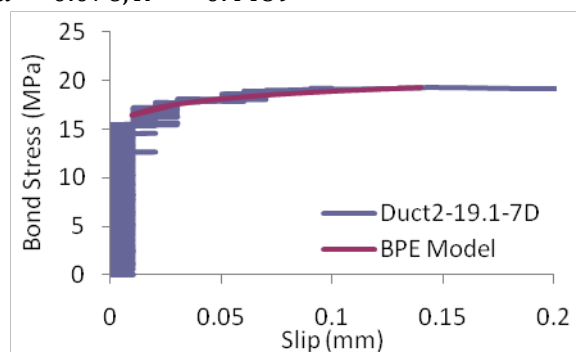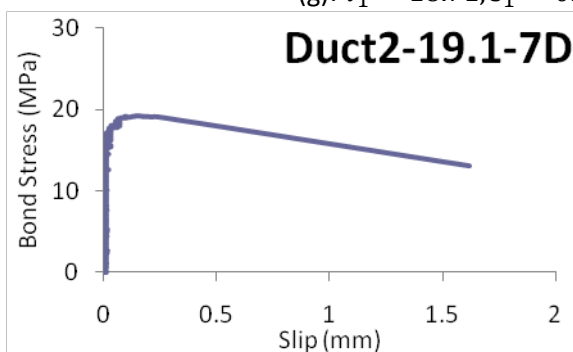
(h): $\tau_1 = 19.29, s_1 = 0.14, \alpha = 0.0618, R^2 = 0.8733$

Figure 5.1: Stress-slip curves for beam specimens showing raw and modeled data.

Table 5.1: Values used in the BPE model.

Specimen	τ_1	s_1	α
King-15.9-7D	17.92	0.1	0.1512
King-19.1-5D	19.03	0.08	0.099
RYE-15.9-7D	18.91	0.16	0.1298
RYE-19.1-7D	17.22	0.06	0.0319
Duct1-15.9-7D	20.04	0.07	0.1086
Duct1-19.1-7D	17.33	0.09	0.0197
Duct2-15.9-7D	18.71	0.12	0.076
Duct2-19.1-7D	19.29	0.14	0.0618

The accuracy of the model can be determined by how well the model approximates the test data. It can be seen that the R^2 values in Figure 5.1 are not all very close to 1. This is because the regression is compared to the entire ascending branch. The slip variation produced at low bond stresses oscillated between 0 and 0.01, which could not be produced from the models. However if the model was compared only to the upper portion of the ascending branch where the slip values constantly increased without oscillation, the R^2 values all exceed 0.8.

5.3   Determination of Development Length

From the values in Table 5.1 it is possible to determine the required development length on th GFRP bars used in this study. A method proposed by Focacci *et al.* (2000) was used to determine the required development lengths of the 15.9 mm and 19.1 mm bars in each type of concrete. This method involved finding parameters of a given bond-slip relationship such that the results of the bond tests could be predicted in terms of applied pullout force and consequent slip at the loaded end and at the free end.

Focacci *et al.* (2000) proposed the following relationship to relate the bar load of the FRP bar to the required development length of the bar to ensure zero slip at the unloaded end:

$$N(x) = \frac{2E_{lb}A_b}{1-\alpha}\left[\frac{2C(1-\alpha)^2}{E_{lb}d_b(1+\alpha)}\right]^{1/(1-\alpha)} x^{(1+\alpha)/(1-\alpha)} \qquad \text{Equation 5.1}$$

where:
N =   Bar load, N.
x =   Development length, mm.
E_{lb} =   Young's modulus, MPa.
A_b =   Area of FRP bar, mm^2
d_b =   Diameter of rebar, mm^2

α = Curve fitting parameter from BEP model.
C = τ_1, peak bond stress, MPa.

Focacci *et al.* (2000) also proposed another relationship to relate the development length to the slip at the loaded end of the FRP bar:

$$s(x) = \left[\frac{2C(1-\alpha)^2}{E_{lb}d_b(1+\alpha)}\right]^{1/(1-\alpha)} x^{2/(1-\alpha)}$$ Equation 5.2

Based on Equation 5.1, the required development length was determined for the GFRP bars used in this study. The parameters used in Equation 5.1 are shown in Table 5.2. Solving for x in Equation 5.1 yielded the required development length. Using Equation 2.2, the average bond stress was determined for each beam specimen. Substituting the development length obtained from Equation 5.1 into Equation 5.2, the slip at the loaded end of the bar was determined. The development length requirements, average bond stresses, and loaded end slips are presented in Table 5.3.

Table 5.2: Values for determining required development length.

Parameter:	For 15.9 mm Bar	For 19.1 mm Bar
E_{lb}	48,200 MPa	47,600 MPa
A_b	17.494 mm^2	20.763 mm^2
d_b	15.875 mm	19.05 mm
α	See Table 5.1	See Table 5.1
C	$= \tau_1$, MPa. See Table 5.1	$= \tau_1$, MPa. See Table 5.1
N	$= F_u \times A_b$ $= 751\text{MPa} \times 17.494\text{mm}^2 = 14{,}8623\text{N}$	$= F_u \times A_b$ $= 728\text{MPa} \times 20.763\text{mm}^2 = 20{,}7480\text{N}$
x	See Table 5.3	See Table 5.3

Table 5.3: Development length and corresponding bond strength and slip values.

Concrete	Bar	Development Length (mm)	No. of Bar Diameters	Bond Strength (MPa)	Slip (mm)
HP-S10	15.9	214.02	$14d_b$	15.35	1.415
HP-S10*	19.1	213.86	$12d_b$	17.67	1.474
RYE	15.9	197.10	$13d_b$	16.66	1.336
RYE	19.1	212.54	$12d_b$	17.86	1.566
Duct1	15.9	180.47	$12d_b$	18.20	1.253
Duct1	19.1	206.34	$11d_b$	18.31	1.547
Duct2	15.9	181.75	$12d_b$	18.07	1.308
Duct2	19.1	198.96	$11d_b$	18.99	1.427

*Bond strength value adjusted to 15.69 MPa. Development length becomes 221 mm = $12d_b$. See below for explanation.

The values provided by Table 5.3 correspond to 15.9 mm and 19.1 mm sand coated GFRP bars embedded in confined high strength and ultra-high strength concrete. The average bond strengths determined from the required development lengths agree with the experimental results obtained from the beam tests in this study. By extrapolating the data obtained from the beam tests results, it is apparent from the bond strength versus embedment length curves for the beam specimens that if the curves are extended, the bond stresses determined simultaneously from Equation 5.1 and Equation 2.2 correlate very well with the extrapolated results as shown in Figure 5.2 and Figure 5.3 for the 15.9 mm and 19.1 mm beam specimens, respectively.

All extrapolations from Figure 5.2 and Figure 5.3 appear to be smooth except for the King-19.1 specimen. This is because the data used to obtain the τ_1, s_1, α parameters for this specimen corresponded to the King-19.1-5D specimens. Since the bond strengths obtained from the 19.1-7D beam specimens (τ_1 values in Table 5.1) on average are equal to the bond strengths determined by the method proposed by Focacci *et al.* (2000), the bond strength can be taken as 15.69 MPa. Therefore the required development length now becomes 221 mm, which is equivalent to $12 - 19.1$ mm bar diameters. These values have been noted in Table 5.3.
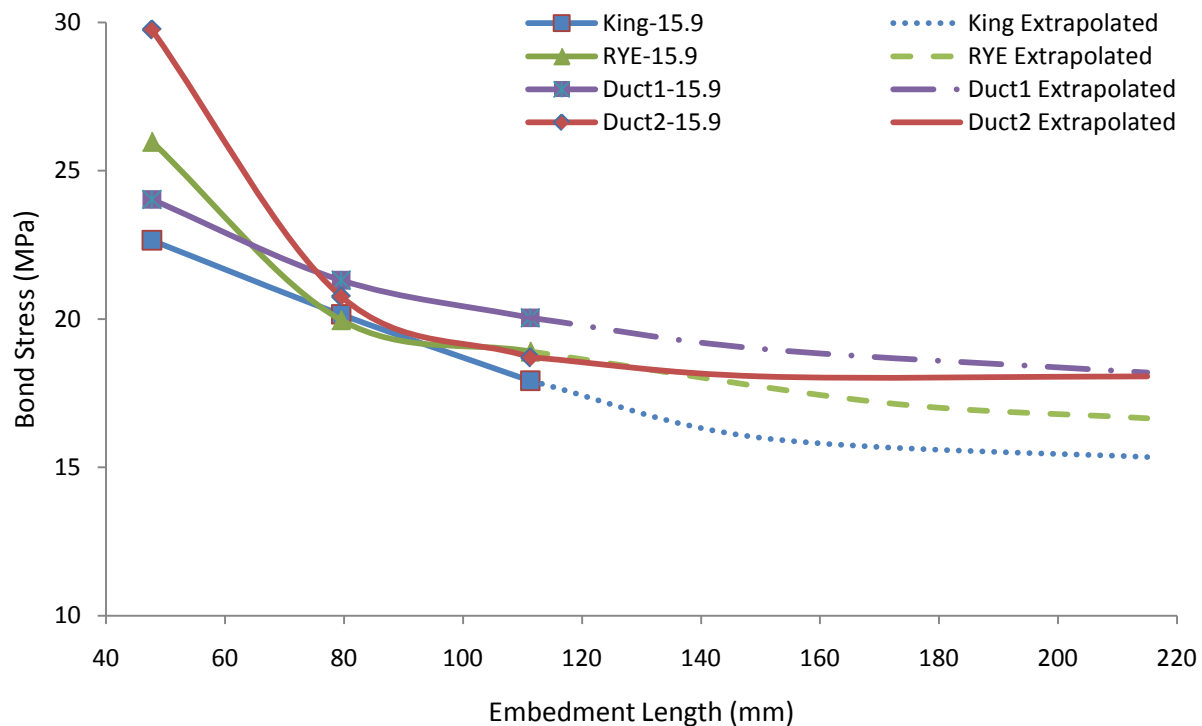
Figure 5.2: Extrapolated bond stress vs. embedment length curves for 15.9 mm beam specimens.
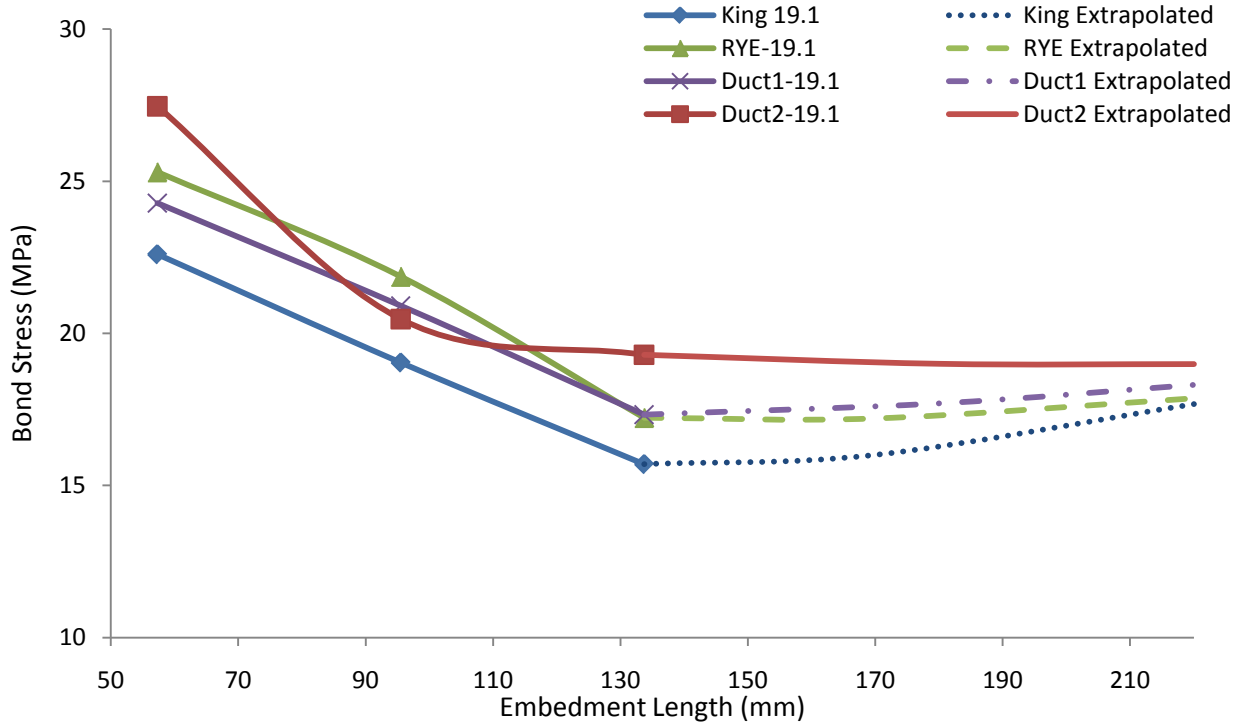
Figure 5.3: Extrapolated bond stress vs. embedment length curves for 19.1 mm beam specimens.

5.4   Comparison to Code Predictions

The design provisions and recommendations evaluated in this study were CSA S806-02, CSA S6-06, ACI 440.1R-06, and JSCE Design Recommendation. The development lengths provided by the codes will be compared to the development lengths determined from this study. It is important to note that the development lengths determined in this study do not have any factor of safety associated with them. Therefore, this will also be taken into consideration when comparing the values determined through experimentation and modeling to the values obtained from the code and provision requirements. For comparative purposes, the development lengths provided by the design codes and provisions will be determined based on the specimen configurations, in terms of bar size, concrete strength, concrete cover and reinforcement properties, used in the beam tests. The average bond strengths along the development lengths obtained in the following sections are determined using Equation 2.2 unless otherwise indicated.

$$\mu = \frac{d_b f_s}{4l}$$
<div align="right">Equation 2.2</div>

5.4.1 CSA S806-02 Development Length

The development length requirement for FRP bars provided by CSA S806-02 is shown in Equation 2.3. Table 5.4 shows the values of the parameters used in Equation 2.3 for each bar size and concrete strength used in this study. Table 5.5 shows the development length and corresponding bond strength determined from Equation 2.3 and Equation 2.2, respectively.

$$l_d = 1.15 \frac{k_1 k_2 k_3 k_4 k_5}{d_{cs}} \frac{f_F}{\sqrt{f'_c}} A_b$$

Equation 2.3

Table 5.5 shows that the effect of concrete strength and the bar size do not influence the bond strength. This correlates well to the experimental results discussed in Section 4.4.1 and Section 4.4.2 results obtained for the beam test specimens. The CSA-S806-02 requirement does not take into account the affect of transverse reinforcement. If there is transverse reinforcement provided, the bond strength will increase and reduce the required amount of development length needed for the FRP bar. It is clear from the results of the pullout and the beam specimens that the addition of transverse reinforcement increased the bond strength between the FRP bar and concrete. Without taking the amount of transverse reinforcement into account, this will lead to a conservative bond strength which in turn will increase the amount of development length needed for the rebar.

Table 5.4: Parameters for CSA S806-02 development length equation.

Parameter	15.9 mm GFRP Bar	19.1 mm GFRP Bar
k_1	1	1
k_2	1	1
k_3	1	1
k_4	1	1
k_5	1	1
d_{cs}	39.6875 mm	47.625 mm
f_F	751 MPa	728 MPa
A_b	197.9 mm^2	285 mm^2
d_b	15.875 mm	19.05 mm
f'_c	64 MPa*	64 MPa*

*Although the concrete used in this study exceeded 64 MPa, the maximum permissible value of f'_c is limited to 64 MPa by CSA S806-02 in this equation.

Table 5.5: CSA S806-02 development length requirement and computed bond stress.

Concrete	15.9 mm GFRP Bar		19.1 mm GFRP Bar	
	l_d (mm)	μ (MPa)	l_d (mm)	μ (MPa)
HP-S10	538.32	5.54	626.25	5.54
Ryerson Concrete	538.32	5.54	626.25	5.54
Ductal1	538.32	5.54	626.25	5.54
Ductal2	538.32	5.54	626.25	5.54

5.4.2   CSA S6-06 Development Length

The development length requirement for FRP bars provided by CSA S86-06 is shown in Equation 2.5. Table 5.6 shows the values of the parameters used in Equation 2.3 for each bar size and concrete strength used in this study. Table 5.7 shows the development length and corresponding bond strength determined from Equation 2.5 and Equation 2.2, respectively.

$$l_d = 0.45 \frac{k_1 k_4}{\left(d_{cs} + k_{tr}\frac{E_{frp}}{E_s}\right)} \left(\frac{f_{frp}}{f_{cr}}\right) A_{frp}$$

Equation 2.5

Similar to CSA S806-02, Table 5.7 shows that the effect of concrete strength and the bar size do not affect the bond strength as was shown with the explanations provided in Section 4.4.1 and Section 4.4.2. It is important to note that although the transverse reinforcement index, k_{tr}, accounts for the transverse reinforcement provided, because the distance from the center of the bar to the closest concrete surface was greater than two times the bar diameter, the effect of confinement provided by the transverse reinforcement was neglected. This will lead to a conservative bond strength which in turn will increase the amount of development length required.

Table 5.6: Parameters for CSA S6-06 development length equation.

Parameter	15.9 mm GFRP Bar	19.1 mm GFRP Bar
k_1	1	1
k_4	1	1
f_{frp}	751 MPa	728 MPa
A_{frp}	197.9 mm^2	285 mm^2
$d_{cs} + k_{tr}\dfrac{E_{frp}}{E_s}$	39.6875 mm	47.625 mm
f_{cr}	3.2 MPa*	3.2 MPa*

*Although the concrete used in this study exceeded 64 MPa, the maximum permissible value of f'_c is limited to 64 MPa by CSA S6-06 for calculating f_{cr}.

Table 5.7: CSA S6-06 development length requirement and computed bond stress.

Concrete	15.9 mm GFRP Bar		19.1 mm GFRP Bar	
	l_d (mm)	μ (MPa)	l_d (mm)	μ (MPa)
HP-S10	526.62	5.66	612.64	5.66
Ryerson Concrete	526.62	5.66	612.64	5.66
Ductal1	526.62	5.66	612.64	5.66
Ductal2	526.62	5.66	612.64	5.66

5.4.3 ACI 440.1-06 Development Length

The development length requirement for FRP bars provided by ACI 440.1-06 was determined by solving for l_e in Equation 2.8. The bond stress is determined from Equation 2.7. Table 5.8 shows the values of the parameters used in Equation 2.8 and Equation 2.7 for each bar size and concrete strength used in this study. Table 5.9 shows the development length and corresponding bond strength determined from Equation 2.8 and Equation 2.7, respectively.

$$f_{fe} = \frac{0.083\sqrt{f'_c}}{\alpha}\left(13.6\frac{l_e}{d_b} + \frac{C}{d_b}\frac{l_e}{d_b} + 340\right)$$

Equation 2.8

$$\mu = \left(0.33 + 0.025\frac{C}{d_b} + 8.3\frac{d_b}{l_e}\right)\sqrt{f'_c}$$

Equation 2.7

Unlike in CSA S806-02 and CSA S6-06, the bond strength appears to double as the concrete strength is increased from 71.2 MPa to 174.5 MPa as seen in Table 5.9. This does not correlate with the results from the experimental data discussed in Section 4.4.1. A limit should be placed on the value of f'_c for use in Equation 2.8 such that the effect of concrete strength can be properly represented by the design equation. Since Equation 2.7 and Equation 2.8 was developed based on tests results using concrete between 28-45 MPa, it cannot be assumed to be accurate for extrapolating values using concrete strengths significantly higher than this range.

It can be seen that effect of bar size on the bond strength reduces as the embedment length increases according to Equation 2.7. It can be concluded that with an embedment length equal to the development length of the bar, the effect of the bar size to the contribution to the bond strength is very minimal. This correlates with the results discussed in Section 4.4.2 and also the CSA S806-02 and CSA S6-06 codes.

Table 5.8: Parameters for ACI 440.1-06 developable bar stress equation.

Parameter	15.9 mm GFRP Bar	19.1 mm GFRP Bar
f_{fe}	751MPa	728 MPa
f'_c	*See Below	*See Below
α	1	1
d_b	15.875 mm	19.05 mm
C	50 mm	50 mm

*f'_c = 71.2 MPa (HP-S10), 128.6 MPa (Ryerson Concrete), 147.8 MPa (Ductal1), 174.5 MPa (Ductal2).

Table 5.9: ACI 440.1-06 development length requirement and computed bond stress.

Concrete	15.9 mm GFRP Bar		19.1 mm GFRP Bar	
	l_d (mm)	μ (MPa)	l_d(mm)	μ (MPa)
HP-S10	694.07	5.05	821.278	4.96
Ryerson Concrete	433.978	8.08	508.931	8.01
Ductal1	383.1508	9.15	447.894	9.10
Ductal2	326.945	10.72	380.398	10.72

5.4.4 JSCE Development Length

The development length requirement for FRP bars provided by JSCE Recommendation is shown in Equation 2.9. Table 5.10 shows the values of the parameters used in Equation 2.9 for each bar size and concrete and Table 5.10 shows the development length and corresponding bond strength determined from Equation 2.9 and Equation 2.2, respectively.

$$l_d = \alpha_1 \frac{f_d}{4\,f_{bod}}\,d_b \qquad \text{provided that } l_d > 20d_b \qquad \text{Equation 2.9}$$

Similar to CSA S806-02 and CSA S6-06, from Table 5.11 it is evident that the effect of concrete strength and the bar size do not influence the bond strength. The JSCE Recommendation takes into account the effect of transverse reinforcement on the bond strength. For the 15.9 mm GFRP bar, because the distance of the downward cover from the GFRP bar to the closest concrete surface was greater than 2.5 times the bar diameter, any effect that the reinforcement had was neglected in the determination of the development length and the value of α_1 was equal to 0.6. For the 19.1 mm GFRP bar, because the distance of the downward cover from the GFRP bar to the closest concrete surface was less than 2.5 times the bar diameter, the transverse reinforcement was taken into account and the value of α_1 was equal to 0.6. It can be seen that the same bond strength was achieved for both the 15.9 mm

and the 19.1 mm GFRP bars; however, one takes into account the effect of reinforcement, whereas the other does not and the bond strength achieved for both of them was the same. This led to a conservative bond strength which in turn increased the amount of development length required for the GFRP bar.

Table 5.10: Parameters for JSCE development length equation.

Parameter	15.9 mm GFRP Bar	19.1 mm GFRP Bar
α_1	0.6	0.6
f_d	751 MPa	728 MPa
d_b	15.875 mm	19.05 mm
f_{bod}	3.2 MPa	3.2 MPa

Table 5.11: JSCE development length requirement and computed bond stress.

Concrete	15.9 mm GFRP Bar		19.1 mm GFRP Bar	
	l_d (mm)	μ (MPa)	l_d (mm)	μ (MPa)
HP-S10	558.85	5.33	650.08	5.33
Ryerson Concrete	558.85	5.33	650.08	5.33
Ductal1	558.85	5.33	650.08	5.33
Ductal2	558.85	5.33	650.08	5.33

5.4.5 Experimental Results and Design Code Requirements

The development length requirement obtained from the test results for the sand coated GFRP bars were far less than the requirements provided in the design codes and provisions. Table 5.12 organizes all of the required development lengths from shortest to longest and Table 5.13 organizes all of the average bond strengths from strongest to weakest. The development length requirements provided by the codes and provisions are all greater than the minimum requirements determined from the test results. This shows that the code provides the minimum amount of anchorage needed plus a large margin for safety.

Table 5.12: Experimental and code based development length requirements.

Concrete	Test Results		ACI 440.1R-06		CSA S6-06		CSA S806-02		JSCE	
	15.9	19.1	15.9	19.1	15.9	19.1	15.9	19.1	15.9	19.1
HP-S10	214.02	240.84	694.07	821.28	526.62	612.64	538.32	626.25	558.85	650.08
RYE	197.10	212.54	433.98	508.93	526.62	612.64	538.32	626.25	558.85	650.08
Duct1	180.47	206.34	383.15	447.89	526.62	612.64	538.32	626.25	558.85	650.08
Duct2	181.75	198.96	326.95	380.40	526.62	612.64	538.32	626.25	558.85	650.08

*All values in mm

Table 5.13: Experimental and code based bond strengths.

Concrete	Test Results		ACI 440.1R-06		CSA S6-06		CSA S806-02		JSCE	
	15.9	19.1	15.9	19.1	15.9	19.1	15.9	19.1	15.9	19.1
HP-S10	15.35	15.69	5.05	4.96	5.66	5.66	5.54	5.54	5.33	5.33
RYE	16.66	17.86	8.08	8.01	5.66	5.66	5.54	5.54	5.33	5.33
Duct1	18.20	18.31	9.15	9.10	5.66	5.66	5.54	5.54	5.33	5.33
Duct2	18.07	18.99	10.72	10.72	5.66	5.66	5.54	5.54	5.33	5.33

*All values in MPa

Since the ACI 440.1 Code does not provide a limit to the compressive strength used in determining the development length or bond strength, and because the relationships derived for determining these values are based on test results using compressive strengths of 28-45 MPa, the development lengths determined from ACI 440.1 will not be reduced further. However, applying a factor of safety of two on the development lengths determined from the test results, the development lengths provided by the codes and provisions still exceeded the required development lengths determined through the experimental results. Table 5.14 shows the reduction factors that can be applied to the codes and provisions while still maintaining a factor of safety of least two.

Table 5.14: Reduction factors for required development lengths.

Concrete	CSA S6-06		CSA S806-02		JSCE	
	15.9	19.1	15.9	19.1	15.9	19.1
HP-S10	0.81	0.79	0.80	0.77	0.77	0.74
RYE	0.75	0.69	0.73	0.68	0.71	0.65
Duct1	0.69	0.67	0.67	0.66	0.65	0.63
Duct2	0.69	0.65	0.68	0.64	0.65	0.61

Based on Table 5.14, it can be concluded that the development lengths determined from CSA S806-02, CSA S6-06 and JSCE Recommendation can be reduced by 20% and still provide a minimum factor of safety of two except for the CSA S6-06 development length determined for the 15.9 mm GFRP bar embedded in HP-S10 Concrete where the factor of safety is 1.99. A reduction in the development length will lead to a reduction in the material costs of the structure and promote the use of GFRP bars.

5.5   Development Length Determination from Pullout Tests

As discussed in Chapter 2, bond strengths obtained from pullout tests are typically higher than bond strengths obtained from beam tests with similar configurations. Since beam tests can accurately simulate the stress conditions encountered in the field and pullout tests cannot, results from pullout tests may over predict the bond strength of rebars in concrete which may lead to inadequate design and premature failure of the structure. The literature review in Chapter 2 discussed that the bond strength of FRP rebars does not depend on the compressive strength of concrete when $f_c' > 30$ MPa. It was seen from the beam test results that as the concrete compressive strength increased from 71.2 MPa to 174.5 MPa, there was a minimal increase in the bond strength (Table 4.4); however, this was not the case for the pullout tests where a significant increase was observed (Table 4.5), with the greatest increase in bond strength being 140%. The development length determined from Equation 2.2 for specimens casted with 174.5 MPa concrete would be 2.4 times shorter than the development length for specimen casted with 71.2 MPa concrete. This could result in a significant over estimation of the bond strength for the GFRP bar embedded in the 174.5 MPa concrete and as a result, the development length provided may not be adequate and cause the bond to fail.

The previous sections modeled the bond stress-slip curves and determined the development length based on curve fitting parameters, the slip corresponding to the peak bond stress, and the peak bond stress itself. The peak bond stress used to determine the development lengths from Table 5.1 had small relative ranges between 17.92 − 20.02 MPa and 17.22 − 19.29 MPa for the 15.9 mm and 19.1 mm GFRP bars, respectively. If the same approach was taken to model the pullout specimens (by modeling the specimens with embedment lengths of seven times the bar diameter), the peak bond stresses used for specimens would have much greater relative ranges. For specimens with 40 mm covers, the ranges would have been between 11.72 − 17.17 MPa and 10.43 − 15.97 MPa for 15.9 mm and 19.1 mm GFRP bars, respectively. For specimens with 60 mm covers, the ranges would have been between 11.36 − 16.15 MPa and between 8.23 − 15.56 MPa for 15.9 mm and 19.1 mm GFRP bars, respectively. Table 5.15 shows the peak bond stress for the pullout specimens having embedment lengths of seven times the bar diameter. It can be seen that the relative ranges for the peak bond stresses are far greater than those of the beam tests. Consequently, the development lengths would vary significantly, as would the average bond strengths. Since it has been shown that the bond strength is not dependent on the concrete strength, the development lengths determined as a function of the experimental bond strength results would not be accurate; therefore, modeling the

experimental results for data obtained from the pullout tests would serve no purpose. This section will only provide a comparative analysis of the bond strengths determined from the code provisions and compare them to the bond strengths determined from the pullout tests to ascertain whether the design codes over estimate the bond stress which would lead to an insufficient development length for concrete without transverse reinforcement.

Table 5.15: Peak bond stress for pullout specimens.

Concrete Type	40 mm Cover		60 mm Cover	
	15.9 mm	19.1 mm	15.9 mm	19.1 mm
HP-S10	13.11	6.65	13.99	8.28
Ryerson Concrete	11.72	12.71	12.01	12.16
Duct1	12.26	11.54	11.36	11.34
Duct2	17.17	15.97	16.15	15.56

*All values in MPa.

5.5.1 CSA S806-02 Bond Strength

The bond strength achieved by FRP bars provided by CSA S806-02 was determined by Equation 2.4. Table 5.16 shows the values of the parameters used in Equation 2.4 for each bar size, concrete cover and concrete strength used in this study. Table 5.17 shows the bond strengths determined from Equation 2.4.

$$\mu = \frac{d_{cs}\sqrt{f'_c}}{1.15k_1k_2k_3k_4k_5\pi d_b}$$

Equation 2.4

Table 5.16: Parameters for CSA S806-02 bond strength equation.

Parameter	40 mm Cover		60 mm Cover	
	15.9 mm GFRP Bar	19.1 mm GFRP Bar	15.9 mm GFRP Bar	19.1 mm GFRP Bar
k_1	1	1	1	1
k_2	1	1	1	1
k_3	1	1	1	1
k_4	1	1	1	1
k_5	1	1	1	1
d_{cs}	39.6875	47.625	39.6875	47.625
f_F	751	728	751	728
A_b	197.9	285	197.9	285
d_b	15.875	19.05	15.875	19.05
f'_c	64*	64*	64*	64*

*Although the concrete used in this study exceeded 64 MPa, the maximum permissible value of f'_c is limited to 64 MPa by CSA S806-02 in this equation.

Table 5.17: Bond strengths determined from CSA S806-02.

Concrete	40 mm Cover		60 mm Cover	
	15.9 mm GFRP Bar	19.1 mm GFRP Bar	15.9 mm GFRP Bar	19.1 mm GFRP Bar
HP-S10	5.54	5.54	5.54	5.54
Ryerson Concrete	5.54	5.54	5.54	5.54
Ductal1	5.54	5.54	5.54	5.54
Ductal2	5.54	5.54	5.54	5.54

*All values in MPa

Table 5.17 shows that the bond stresses for specimens with 40 mm and 60 mm covers are the same. This is because the d_{cs} value is limited to 2.5 times the bar diameter and therefore this becomes the governing factor. Once the distance from the closest concrete surface to the center of the bar being developed exceeds 2.5 times the bar diameter, an increase in cover will have no effect on the bond strength. This was verified by the results obtained for the specimens casted with Ryerson Concrete, Ductal1 and Ductal2; however the same cannot be said for the specimens casted with HP-S10 Concrete where the bond strength increased with the increase in concrete cover.

5.5.2 CSA S6-06 Bond Strength

The bond strength achieved by FRP bars provided by CSA S6-06 was determined by Equation 2.6. Table 5.18 shows the values of the parameters used in Equation 2.4 for each bar size, concrete cover and concrete strength used in this study. Table 5.19 shows the bond strengths determined from Equation 2.6.

$$\mu = \frac{\left(d_{cs} + k_{tr} \frac{E_{frp}}{E_s} \right) f_{cr}}{0.45 k_1 k_4 \pi d_b}$$

Equation 2.6

Table 5.18: Parameters for CSA S86-06 bond strength equation.

Parameter	40 mm Cover		60 mm Cover	
	15.9 mm GFRP Bar	19.1 mm GFRP Bar	15.9 mm GFRP Bar	19.1 mm GFRP Bar
k_1	1	1	1	1
k_4	1	1	1	1
f_{frp}	751 MPa	728 MPa	751 MPa	728 MPa
A_{frp}	197.9 mm^2	285 mm^2	197.9 mm^2	285 mm^2
$d_{cs} + k_{tr} \frac{E_{frp}}{E_s}$	39.6875 mm	47.625 mm	39.6875 mm	47.625 mm
f_{cr}	3.2 MPa*	3.2 MPa*	3.2 MPa*	3.2 MPa*

*Although the concrete used in this study exceeded 64 MPa, the maximum permissible value of f'_c is limited to 64 MPa by CSA S6-06 for calculating f_{cr}.

Table 5.19: Bond strengths determined from CSA S6-06.

Concrete	40 mm Cover		60 mm Cover	
	15.9 mm GFRP Bar	19.1 mm GFRP Bar	15.9 mm GFRP Bar	19.1 mm GFRP Bar
HP-S10	5.66	5.66	5.66	5.66
Ryerson Concrete	5.66	5.66	5.66	5.66
Ductal1	5.66	5.66	5.66	5.66
Ductal2	5.66	5.66	5.66	5.66

*All values in MPa

Similar to CSA S806-02, the bond stress for specimens with 40 mm and 60 mm covers are the same. Once again this is because the d_{cs} value is limited to 2.5 times the bar diameter and therefore this becomes the governing factor. Also as in CSA S806-02, this was verified by the results obtained for the specimens casted with Ryerson Concrete, Ductal1 and Ductal2; however the same trend was not observed for specimens casted with HP-S10 Concrete where the bond strength increased as the concrete cover increased.

5.5.3 ACI 440.1-06 Bond Strength

The bond strength achieved by FRP bars provided by ACI 440.1-06 can be determined by Equation 2.8 and Equation 2.7, which are both shown in sections 2.5.3 and 5.4.3. Using Equation 2.8, the development length was first determined and then substituted into Equation 2.7 to determine the bond strength. Table 5.20 shows the values of the parameters used in Equation 2.8 and Equation 2.7 for each bar size, concrete cover, and concrete strength used in this study. Table 5.21 shows the bond strengths determined from Equation 2.7.

The results from Table 5.21 show that as the concrete cover increases, so does the bond strength. This trend was observed for the specimens casted with HP-S10 Concrete; however, for specimens casted with Ryerson Concrete, Ductal1, and Ductal2, this was not the case. Although the C/d_b ratio is limited to 3.5 in Equation 2.8, care should be taken when determining the bond strength of FRP bars embedded in fibre reinforced concrete. It was seen that the lowest C/d_b ratio used in this study corresponded to specimens with covers of 40 mm embedded with 19.1 mm GFRP bars where this ratio was around 2.5. Using the bond equation provided by ACI 440.1-06, the bond strength should increase as the C/d_b ratio increases up to a value of 3.5; however, it was observed that the bond strength did not increase for the fibre reinforced concrete with C/d_b ratios as little as 2.5. Therefore, assuming that the bond strength increases up until the C/d_b ratio reaches 3.5 is not accurate for fibre reinforced concrete.

Table 5.20: Parameters for ACI 440.1-06 bond strength equation.

Parameter	40 mm Cover		60 mm Cover	
	15.9 mm GFRP Bar	19.1 mm GFRP Bar	15.9 mm GFRP Bar	19.1 mm GFRP Bar
f_{fe}	751MPa	728 MPa	751MPa	728 MPa
f'_c	*See Below	*See Below	*See Below	*See Below
α	1	1	1	1
d_b	15.875 mm	19.05 mm	15.875 mm	19.05 mm
C	47.9375 mm	49.525 mm	67.9375 mm	69.525 mm

*f'_c = 71.2 MPa (HP-S10), 128.6 MPa (Ryerson Concrete), 147.8 MPa (Ductal1), 174.5 MPa (Ductal2).

Table 5.21: Bond strengths determined from ACI 440.1-06.

Concrete	40 mm Cover		60 mm Cover	
	15.9 mm GFRP Bar	19.1 mm GFRP Bar	15.9 mm GFRP Bar	19.1 mm GFRP Bar
HP-S10	5.01	4.95	5.40	5.28
Ryerson Concrete	8.01	8.00	8.63	8.52
Ductal1	9.08	9.09	9.78	9.68
Ductal2	10.64	10.70	11.46	11.40

*All values in MPa

5.5.4 JSCE Bond Strength

The bond strength achieved by FRP bars provided by JSCE Recommendation can be determined by Equation 2.10. Table 5.22 shows the values of the parameters used in Equation 2.10 for each bar size, concrete cover and concrete strength used in this study. Table 5.23 shows the bond strengths determined from Equation 2.10.

$$\mu = \frac{f_{bod}}{\alpha_1}$$

Equation 2.10

Table 5.22: Parameters for JSCE bond strength equation.

Parameter	40 mm Cover		60 mm Cover	
	15.9 mm GFRP Bar	19.1 mm GFRP Bar	15.9 mm GFRP Bar	19.1 mm GFRP Bar
α_1	0.6	0.7	0.6	0.6
f_{bod}	3.2 MPa	3.2 MPa	3.2 MPa	3.2 MPa

Table 5.23: Bond strengths determined from JSCE Recommendation.

Concrete	40 mm Cover		60 mm Cover	
	15.9 mm GFRP Bar	19.1 mm GFRP Bar	15.9 mm GFRP Bar	19.1 mm GFRP Bar
HP-S10	5.33	4.57	5.33	5.33
Ryerson Concrete	5.33	4.57	5.33	5.33
Ductal1	5.33	4.57	5.33	5.33
Ductal2	5.33	4.57	5.33	5.33

*All values in MPa

It can be seen in Table 5.23 that JSCE Recommendation does not show an increase in bond strength with the increase in concrete cover for the 15.9 mm GFRP bars; however, for the 19.1 mm bars, an increase in bond strength is observed with the increase in concrete cover.

5.5.5 Experimental Bond Strength and Design Code Bond Strength

Results from the previous sections show that the bond strengths achieved from the pullout tests are greater than the bond strengths provided by the design codes and provisions for the sand coated GFRP bars.   Table 5.24 organizes all of the bond strengths from strongest to weakest.

Table 5.24: Experimental and code based bond strengths for pullout specimens.

Concrete	Test Results		ACI 440.1R		CSA S6-06		CSA S806-02		JSCE	
	15.9	19.1	15.9	19.1	15.9	19.1	15.9	19.1	15.9	19.1
40 mm Cover										
HP-S10	13.11	6.65	5.01	4.95	5.66	5.66	5.54	5.54	5.33	4.57
RYE	11.72	12.71	8.01	8.00	5.66	5.66	5.54	5.54	5.33	4.57
Duct1	12.26	11.54	9.08	9.09	5.66	5.66	5.54	5.54	5.33	4.57
Duct2	17.17	15.97	10.64	10.70	5.66	5.66	5.54	5.54	5.33	4.57
60 mm Cover										
HP-S10	13.99	8.28	5.40	5.28	5.66	5.66	5.54	5.54	5.33	5.33
RYE	12.01	12.16	8.63	8.52	5.66	5.66	5.54	5.54	5.33	5.33
Duct1	11.36	11.34	9.78	9.68	5.66	5.66	5.54	5.54	5.33	5.33
Duct2	16.15	15.56	11.46	11.40	5.66	5.66	5.54	5.54	5.33	5.33

*All values in MPa

Based on the results from Table 5.24, the bond strengths provided by the codes and provisions are all less than the bond strengths obtained from the experimental results. This indicates that the development lengths provided by the design codes are adequate such that the FRP bars can reach their ultimate stress prior to bond failure. Unlike for the beam test specimens, a reduction factor cannot be applied to the design codes to reduce the required development lengths because an accurate development length could not be determined from the pullout test specimens. It can only be concluded that the design codes provide conservative bond strengths and as a result, a sufficient development length requirement as shown from the results of this study.

Chapter 6

CONCLUSION

6.1   General

The objective of the present study was to investigate the effects of different parameters on the bond behaviour of sand coated GFRP rebars in high strength, high performance concrete (HPC) and ultra-high strength, ultra-high performance concrete (UHPC). The objective was to also determine the required development length for the GFRP bars, and to compare these results with the requirements provided by design codes and provisions. For this purpose, an experimental investigation was conducted using beam test specimens and pullout test specimens such that the effects of the concrete compressive strength, ranging between 70 to 175 MPa, the GFRP bar diameter, the embedment length, and the concrete cover on the bond strength could be determined. Based on the analysis of the experimental results, the development length was determined using a bond stress-slip law. The results from the experimental data lead to the following conclusions:

- As is the case for conventional concrete, the concrete compressive strength had a negligible effect on the bond behaviour of GFRP bars embedded in high strength and ultra-high strength concrete as determined from the beam test specimens. Though the pullout specimens exhibited an increase in bond strength with the increase in concrete strength, this was due to the increase in hydrostatic pressure within the concrete. However, since the stress conditions created in the concrete and the GFRP bar during the pullout test are not encountered in practice, where the concrete surrounding the rebar is in compression while the rebar is under tension, the effect of hydrostatic pressure would not occur in practical structures. In reality, when the reinforcement is under tension, the surrounding concrete would also be under tension, causing it to crack. These cracks would cause the

internal hydrostatic pressure to dissipate and become ineffective. Therefore, it can be concluded that the compressive strength of concrete has no affect on the bond strength of GFRP bars in high strength and ultra-high strength concrete.

- It was concluded that when bleed water was trapped beneath the bottom surface of the rebar, it created void spaces and as a result, it reduced the bond strength. The effect of water was more pronounced in the specimens casted with HP-S10 Concrete because no fibres were present to cause further disturbance in the bonded region. Test results showed that larger amounts of bleed water became trapped under the larger bar and therefore, produced lower bond strength than the smaller bar.

- The addition of fibres to the concrete created a local disturbance at the bond interface that consequently reduced the bond strength. Smaller diameter bars were affected by the addition of fibres to a greater extent than larger diameter bars. This assumption was based on the fact that there is a greater relative area of local disturbance caused by the fibres for the smaller bars compared to the relative area of local disturbance for the larger bars.

- The effect of the embedment length was similar for the beam and pullout test specimens. Due to the non-uniform distribution of stresses along the surface of the rebar, the increase in embedment length was accompanied by a decrease in bond strength. The non-uniform bond distribution can be verified by the slip values at the loaded end of the bar being greater than the slip values at the unloaded end of the bar.

- The amount of concrete cover only affected the concrete which did not contain fibre reinforcement. A noticeable trend in the concrete specimens which did not contain fibre reinforcement was that the increase in cover was accompanied by an increase in bond strength. As the cover was increased, the amount of confinement provided by the concrete was increased and, as a result, the bond strength increased.

- The addition of fibres to the concrete matrix increased the amount of confinement provided by the concrete to the GFRP bar. With the addition of fibres, the concrete cover had no effect on the bond strength of the GFRP bars. The confinement provided by the

105

fibres was sufficient in preventing the splitting of the concrete cover; and in doing so, it eliminated the effect of cover by producing equal bond strengths between specimens with 40 mm and 60 mm concrete covers.

- Results from the beam specimens allowed for the derivation of a bond stress-slip law which was used to model the test results and to determine the requirement for the development length. It was concluded that CSA S806-02, CSA S6-06, ACI 440.1R-06, and JSCE Design Recommendation provide sufficient development lengths, plus a large margin for safety. It was determined that the development lengths provided by CSA S806-02, CSA S6-06, and JSCE Design Recommendation could be reduced by 20% provided that there is sufficient transverse reinforcement surrounding the bar being developed, such that adding additional transverse reinforcement has no affect on the bond strength. This reduction would still maintain a factor of safety of two over the development lengths determined from the test results.

- Although the bond strength of GFRP bars is not influenced by the compressive strength of concrete, the use of high strength and ultra-high strength concrete with sand coated GFRP bars shows that the development length requirement and amount of concrete cover needed to prevent splitting, provided by design codes, can be reduced in certain cases. A reduction in the development length and concrete cover leads to a reduction in material costs, which in turn will decrease the overall cost of construction. Reduced construction costs will encourage the use of GFRP in the construction of reinforced concrete structures.

6.2   Limitations of the Study

The development lengths for concrete without transverse reinforcement could not be determined because the pullout tests did not provide adequate results for this purpose. Results from the pullout tests do not represent the stress fields encountered in practice and tend to overestimate the bond stress, hence, they could not be used. Furthermore, the hydrostatic pressure present in the pullout tests caused the bond strength to increase as the concrete strength increased and consequently, the results could not be used to determine the development lengths as these situations are not encountered in practice. As a result, only the bond stresses from the design codes were compared to

the experimental results to determine whether the design codes underestimated or overestimated the bond stress of GFRP bars in concrete without transverse reinforcement. Although the bond strengths from the code predictions were less than the bond strengths from the pullout tests, a reduction factor could not be applied since it was unclear to what extent the development lengths could be reduced.

6.3   Recommendations for Future Work

Both the literature review and this research study show that our knowledge of the use of GFRP in high strength and ultra-high strength concrete is still very limited.   The following are some recommendations for future investigation:

- Conduct beam tests without any auxiliary reinforcement to determine the bond strength of GFRP bars in unconfined high strength and ultra-high strength concrete and compare the results to this study.

- Produce bond test specimens with similar configurations using steel rebar as opposed to GFRP rebars for comparison.

- Conduct further research on the effect of transverse/auxiliary reinforcement so that the limits in the design codes can be modified and provide less conservative development length requirements.

- Conduct further research to determine the amount of concrete cover needed for fibre reinforced concrete such that the bond strength does not increase with the increase in cover beyond this amount.

- Conduct long term bond behaviour of deteriorated GFRP bars in high strength and ultra-high strength concrete.

- Accumulate more test data so that the bond properties of GFRP bars in high strength and ultra-high strength concrete could be further understood and eventually included in design codes either by modifying the existing equations or by creating new ones, with and without fibre reinforcement.

REFERENCES

Achillides, Z. (1998). *Bond behaviour of FRP bars in concrete.* PhD Thesis, University of Sheffield, Centre for Cement and Concrete, Dept. of Civil and Structural Engineering, Sheffield, UK.

Achillides, Z., & Pilakoutas, K. (2004). Bond behaviour of fibre reinforced polymer bars under direct pullout conditions. *Journal of Composites for Construction , 8* (2), 173-181.

ACI Committee 318. (2002). *Building Code Requirements for Structural Concrete (ACI 318-02) and Commentary (ACI 318R-02).* Farmington Hills, MI: American Concrete Institute.

ACI Committee 408. (2003). *Bond and development of straight reinforcing bars in tension (ACI 408R-03).* Farmington Hills, MI: American Concrete Institute.

ACI Committee 440. (2003). *Guide for the Design and Construction of Concrete Reinforced with FRP Bars.* Farmington Hills, MI: American Concrete Institute.

ACI Committee 440. (2006). *Guide for the Design and Construction of Structural Concrete Reinforced with FRP Bars (ACI 440.1R-06).* Farmington Hills, MI: American Concrete Institute.

ACI Committee 440. (2007). *Report on fibre-reinforced polymer (FRP) reinforcement for concrete structures (ACI 440R-07).* Farmington Hills, MI: American Concrete Institute.

ACI Committee 440. (1996). *State of the art report on fibre reinforced plastic (FRP) reinforcement for concrete structures.* Farmington Hills, MI: American Concrete Institute.

Alavi-Fard, M. (1999). *Bond Characteristics of High Strength Concrete.* MASc. Thesis, Memorial University, St. John's, Nfld.

Alunno Rossetti, V., Galeota, V., & Giammatteo, M. M. (1995). Local bond stress-slip relationships of glass fibre reinforced plastic bars embedded in concrete . *Materials and Structures , 28* (6), 340-344.

Aly, R. S., & Benmokrane, B. (2005). Flexural Behaviour of Lap Splicing CFRP Bars in Concrete: Bundled Bars. *Proceedings of the Third International Conference on Composites in Constructions*, (pp. 807-814). Lyon.

Aly, R., Benmokrane, B., & Ebead, U. (2005). Bond splitting strength of lap splicing of GFRP bars in concrete. *Proc., 33rd Annual General Conference of the Canadian Society for Civil Engineering*, (pp. 1-10). Toronto.

Aly, R., Benmokrane, B., & Ebead, U. (2006). Tensile lap splicing of fibre-reinforced polymer reinforcing bars in concrete. *ACI Structural Journal , 103* (6), 857-864.

ASTM Committee C09. (2000). *ASTM C 143: Standard Test Method for Slump of Hydraulic-Cement Concrete.* West Conshohocken, PA: ASTM.

ASTM Committee C09. (2000). *ASTM C 192: Standard Practice for Making and Curing Concrete Test Specimens in the Laboratory.* West Conshohocken, PA: ASTM.

ASTM Committee C09. (2001). *ASTM C 39: Standard Test Method for Compressive Strength of Cylindrical Concrete Specimens.* West Conshohocken, PA: ASTM.

ASTM Committee C-9. (1997). *ASTM C 231: Standard Test Method for Air Content of Freshly Mixed Concrete by the Pressure Method.* West Conshohocken, PA: ASTM.

ASTM Committee C-9. (1998). *ASTM C 617: Standard Practice for Capping Cylindrical Concrete Specimens.* West Conshohocken, PA: ASTM.

Azizinamini, A., Pavel, R., Hatfield, E., & Ghosh, S. K. (1999). Behavior of Spliced Reinforcing Bars Embedded in High Strength Concrete. *ACI Structural Journal , 96* (5), 826-835.

Azizinamini, A., Stark, M., Roller, J. J., & Ghosh, S. K. (1993). Bond Performance of Reinforcing Bars Embedded in High-Strength Concrete. *ACI Structural Journal , 90-5*, 554-561.

Azizinamini, M., Chisala, M., & Ghosh, S. K. (1995). Tension dedvelopment length of reinforcing bars embedded in high-strength concrete. *Engineering Structures , 17* (7), 512-522.

Baena, M., Torres, L., Turon, A., & Barris, C. (2009). Experimental study of bond behaviour between concrete and FRP bars using a pull-out test. *Composites: Part B , 40* (8), 784-797.

Benmokrane, B., & Masmoudi, R. (1996). FRP C-bar as reinforcing rod for concrete structures. *Proceedings of the 2nd Intern. Conf. on Advanced Composite Materials in Bridges and Structures (ACMBS II)* (pp. 181-188). Montreal: Canadian Society of Civil Engineering.

Benmokrane, B., Tighiouart, B., & Chaallal, O. (1996). Bond strength and load distribution of composite GFRP reinforcing bars in concrete. *ACI Materials Journal , 93* (3), 246-253.

Bisby, L. A. (2006). *ISIS Canada Educational Module No. 2: FRP Composites for Construction.* Winnipeg: ISIS Canada Corporation.

Bisby, L. A. (2006). *ISIS Canada Educational Module No. 3: FRP Composites for Construction.* Winnipeg: ISIS Canada Corporation.

CAN/CSA S6-06. (2006). *Canadian highway bridge design code.* Rexdale, ON: Canadian Standards Association.

CAN/CSA S806-02. (2002). *Design and construction of building components with fibre reinforced polymers.* Rexdale, ON: Canadian Standards Association.

Chaallal, O., & Benmokrane, B. (1993). Pullout and bond of glass fibre rods embedded in concrete and cement grout. *Materials and Structures , 26* (3), 167-175.

Cosenza, E., Manfredi, G., & Realfonzo, R. (1995). Analytical modelling of bond between FRP reinforcing bars and concrete. *Proc., 2nd Int.RILEM Symp*, (pp. 164-171).

Cosenza, E., Manfredi, G., & Realfonzo, R. (1997). Behaviour and modelling of bond of FRP rebars to concrete. *Journal of Composites for Construction , 1* (2), 40-51.

Cosenza, E., Manfredi, G., & Realfonzo, R. (1996). Bond characteristics and anchorage length of FRP rebars. *Proc., 2nd Int. Conf. on Advanced Compos. Mat. in Bridge Structures* (pp. 909-916). Montreal: The Canadian Society of Civil Engineering.

Cosenza, E., Manfredi, G., & Realfonzo, R. (2002). Development length of FRP straight rebars. *CompositesbPart B: Engineering , 33* (7), 493-504.

Dancygier, A. N., Katz, A., & Wexler, U. (2010). Bond between deformed reinforcement and normal and high-strength concrete with and without fibers. *Materials and Structures , 43* (6), 839-856.

Dancygier, A., Katz, A., & Wexler, U. (2006). Bond-slip behavior of reinforcement in NSC and HSC with and without steel fibers. *Measuring, Monitoring and Modeling Concrete Properties* , 145-150.

Darwin, D., & Graham, E. K. (1993b). *Effect of Deformation Height and Spacing on Bond Strength of Reinforcing Bars.* SL Report, University of Kansas Center for Research, Lawrence, Kans.

Darwin, D., Tholen, M. L., Idun, E. K., & Zuo, J. (1996). Splice Strength of High Relative Rib Area Reinforcing Bars. *ACI Structural Journal, , 93* (1), 95-107.

Dawrin, D., & Graham, E. K. (1993a). Effect of Deformation Height and Spacing on Bond Strength of Reinforcing Bars. *ACI Structural Journal , 90* (6), 646-657.

Ehsani, M. R., Saadatmanesh, H., & Tao, S. (1996). Bond Behavior and Design Recommendations for Fiber-Glass Reinforcing Bars. *Proceedings of the First International Conference on Composites in Infrastructure*, (pp. 466-476). Tucson, Ariz.

Ehsani, M. R., Saadatmanesh, H., & Tao, S. (1995). Bond of hooked glass fibre reinforced plastic (GFRP) reinforcing bars to concrete. *ACI Materials Journal , 92* (4), 391-400.

Ehsani, M. R., Saadatmanesh, H., & Tao, S. (1996). Design recommendations for bond of GFRP rebars to concrete. *Journal of Structural Engineering , 122* (3), 247-254.

Eligehausen, R. (1979). *Bond in Tensile Lapped Splices of Ribbed Bars with Straight Anchorages.* German Institute for Reinforced Concrete. Berlin: Publication 301.

Eligehausen, R., Popov, E. P., & Bertero, V. V. (1983). *Local bond stress-slip relationships of deformed bars under generalized excitations.* Earthquake Engineering Research Center, University of California, Berkeley.

Erki, M. A., & Rizkalla, S. (1993). Anchorages for FRP reinforcement. *Concrete International , 15* (6), 54-59.

Faoro, M. (1992). Bearing and deformation behaviour of structural components with reinforcements comprising resin bounded glass fibre bars and conventional ribbed steel bars. *Proc., Int. Conf. on Bond in Concrete.*

Focacci, F., Nanni, A., & Bakis, C. E. (2000). Local Bond-Slip Relationship for FRP Reinforcement in Concrete. *Journal of Composites for Construction , 4* (1), 24-31.

Hamad, B. S., Harajli, M. H., & Jumaa, G. (2001). Effect of fiber reinforcement on bond strength of tension-lap splices in high strength concrete. *ACI Structural Journal , 98* (5), 638-647.

Hao, Q. D., Wang, B., & Ou, J. P. (2006). Fibre reinforced polymer rebar's application to civil engineering. *Concrete , 9*, 38-40.

Hao, Q., Wang, Y., He, Z., & Ou, J. (2009). Bond strength of glass fiber reinforced polymer ribbed rebars in normal strength concrete. *Construction and Building Materials , 23* (2), 865-871.

Harajli, M. H., & Salloukh, K. A. (1997). Effect of fibers on development/splice strength of reinforcing bars in tension. *ACI Materials Journal , 94* (4), 317-324.

Harajli, M. H., Hamad, B. S., & Rteil, A. A. (2004). Effect of Confinement on Bond Strength between Steel Bars and Concrete. *ACI Structural Journal , 101* (5), 595-603.

Harajli, M., Hamad, B., & Karam, K. (2002). Bond-slip Response of Reinforcing Bars Embedded in Plain and Fiber Concrete. *Journal of Materials in Civil Engineering , 14* (6), 503-511.

Japanese Society of Civil Engineers (JSCE). (1997). *Recommendations for design and construction for concrete structures using continuous fibre reinforcing materials.* Tokyo: Concrete Engineering Series.

Larralde, J., & Silva-Rodriguez, R. Bond and slip of FRP reinforcing bars in concrete. *Journal of Materials in Civil Engineering , 5* (1), 30-40.

Lee, J. Y., Kim, T. Y., Yi, C. K., Park, J. S., You, Y. C., & Park, Y. H. (2008). Interfacial bond strength of glass fiber reinforced polymer bars in high-strength concrete. *Composites: Part B , 39* (2), 258-270.

Makitani, E., Irisawa, I., & Nishiura, N. (1993). Investigation of bond in concrete member with fibre reinforced plastic bars. *Fibre-Reinforced-Plastic Reinforcement for Concrete Structures-Int. Symp* (pp. 315-331). ACI SP138-20.

Malvar, L. J. (1994). *Bond stress-slip characteristics of FRP rebars.* Report TR- 2013-SHR, Naval facilities Engineering Service Center, Port Hueneme.

Mazloom, M., Ramezanianpour, A. A., & Brooks, J. J. (2004). Effect of silica fume on mechanical properties of high strength concrete. *Cement and Concrete Composites , 26* (4), 347-357.

Mosley, C. P., Tureyen, A. K., & Frosch, R. J. (2008). Bond Strength of Nonmetallic Reinforcing Bars. *ACI Structural Journal , 105* (5), 634-642.

Newhook, J., & Svecova, D. (2006). *Reinforcing Concrete Structures with Fibre-Reinforced Polymers.* Winnipeg: ISIS Canada Corporation.

Okelo, R. (2007). Realistic bond strength of FRP rebars in NSC from beam specimens. *Journal of Aerospace Engineering , 20* (3), 133-140.

Okelo, R., & Yuan, R. L. (2005). Bond strength of fibre reinforced polymer rebars in normal strength concrete. *Journal of Composites for Construction , 9* (3), 203-213.

Orangun, C. O., Jirsa, J. O., & Breen, J. E. (1977). Reevaluation of Test Data on Development Length and Splices. *ACI Proceedings , 74* (3), 114-122.

Pecce, M., Manfredi, G., Realfonzo, R., & Cosenza, E. (2001). Experimental and analytical evaluation of bond properties of GFRP bars. *Journal of Materials in Civil Engineering , 13* (4), 282-290.

Pultrall Inc. (2007). *Product Guide Specifications.* Retrieved from VRod Product Guide Specification: http://www.pultrall.com/Site2008/Docs/V-RODSpecificationsMar2007.pdf

RILEM TC. (1994). RC 5 Bond test for reinforcement steel. 1. Beam test, 1982. In *RILEM Recommendations for the Testing and Use of Constructions Materials* (pp. 213 - 217). London: E & FN SPON.

RILEM TC. (1994). RC 6 Bond test for reinforcement steel. 2. Pull-out test, 1983. In *RILEM Recommendations for the Testing and Use of Constructions Materials* (pp. 218-220). London: E & FN SPON.

Self-Compacting Concrete European Project Group. (2005, May). *The European Guidelines for Self Compacting Concrete.* Retrieved November 2010, from European Concrete Platform: http://www.europeanconcrete.eu/

Shield, C. K., French, C. W., & Retika, A. (1997). Thermal and mechanical fatigue effects on GFRP rebar-concrete bond. *Proc., Third Int. Symp. on Non-Metallic Reinforcement for Concrete Structures*, (pp. 381-388). Sapporo, Japan.

Tepfers, R. (1973). *A Theory of Bond Applied to Overlapping Tensile Reinforcement Splices for Deformed Bars.* Chalmers University of Technology, Division of Concrete Structures, Goteborg.

Tepfers, R. (2006). Bond clause proposal for FRP-bars/rods in concrete based on CEB/FIP Model Code 90. Part 1: design bond stress for FRP reinforcing bars. *Structural Concrete , 7* (2), 47-55.

Tighiouart, B., Benmokrane, B., & Gao, D. (1998). Investigation of bond in concrete member with fibre reinforced polymer (FRP) bars. *Construction and Building Materials , 12*, 453-462.

Tighiouart, B., Benmokrane, B., & Mukhopadhyaya, P. (1999). Bond strength of glass FRP rebar splices in beams under static loading. *Construction and Building Materials , 13* (7), 383-392.

Untrauer, R. E. (1965). Development Length for Large High Strength Reinforcing Bars. *ACI Journal , 62* (9), 1153-1154.

Wafa, F. F., & Ashour, S. A. (1992). Mechanical Properties of High-Strength Fiber Reinforced Concrete. *ACI Materials Journal , 89* (5), 449-455.

Wambeke, B. W. (2003). *Development length of glass fibre reinforced polymer bars in concrete.* MS Thesis, University of Minnesota, Minneapolis.

Wambeke, B. W., & Shield, C. K. (2006). Development length of glass fibre-reinforced polymer bars in concrete. *ACI Structural Journal , 103* (1), 11-17.

Won, J. P., Park, C. G., Kim, H. H., Lee, S. W., & Jang, C. I. (2008). Effect of fibers on the bonds between FRP reinforcing bars and high-strength concrete. *Composites Part B: Engineering , 39* (5), 747-755.

Appendix

APPENDIX A

Test Configurations

Beam test specimens:

There were a total of 32 beam test specimens produced in this investigation. Example notation for beam test: RYE-19.1-5D indicates that Ryerson Concrete was used to cast the beam specimen, bar diameter was 19.1 mm and the embedment length was five times the bar diameter.

Test No.	Specimen	Test No.	Specimen	Test No.	Specimen	Test No.	Specimen
1	KING-15.9-3D	9	RYE-15.9-3D	17	Duct1-15.9-3D	25	Duct2-15.9-3D
2	KING-15.9-5D	10	RYE-15.9-5D	18	Duct1-15.9-5D	26	Duct2-15.9-5D
3	KING-15.9-5D	11	RYE-15.9-5D	19	Duct1-15.9-5D	27	Duct2-15.9-5D
4	KING-15.9-7D	12	RYE-15.9-7D	20	Duct1-15.9-7D	28	Duct2-15.9-7D
5	KING-19.1-3D	13	RYE-19.1-3D	21	Duct1-19.1-3D	29	Duct2-19.1-3D
6	KING-19.1-5D	14	RYE-19.1-5D	22	Duct1-19.1-5D	30	Duct2-19.1-5D
7	KING-19.1-5D	15	RYE-19.1-5D	23	Duct1-19.1-5D	31	Duct2-19.1-5D
8	KING-19.1-7D	16	RYE-19.1-7D	24	Duct1-19.1-7D	32	Duct2-19.1-7D

Pullout test specimens:

There were a total of 72 pullout test specimens produced in this investigation. Example notation for pullout test: KING-15.9-10D indicates that HP-S10 Concrete was used to cast the pullout specimen, bar diameter was 15.9 mm and the embedment length was ten times the bar diameter.

Test No.	Specimen	Test No.	Specimen
1	KING-15.9-3D-40	13	KING-19.1-3D-40
2	KING-15.9-5D-40	14	KING-19.1-5D-40
3	KING-15.9-5D-40	15	KING-19.1-5D-40
4	KING-15.9-7D-40	16	KING-19.1-7D-40
5	KING-15.9-10D-40	17	KING-19.1-10D-40
6	KING-15.9-10D-40	18	KING-19.1-10D-40
7	KING-15.9-3D-60	19	KING-19.1-3D-60
8	KING-15.9-5D-60	20	KING-19.1-5D-60
9	KING-15.9-5D-60	21	KING-19.1-5D-60
10	KING-15.9-7D-60	22	KING-19.1-7D-60
11	KING-15.9-10D-60	23	KING-19.1-10D-60
12	KING-15.9-10D-60	24	KING-19.1-10D-60

Test No.	Specimen	Test No.	Specimen	Test No.	Specimen
25	RYE-15.9-3D-40	41	Duct1-15.9-3D-40	57	Duct2-15.9-3D-40
26	RYE-15.9-5D-40	42	Duct1-15.9-5D-40	58	Duct2-15.9-5D-40
27	RYE-15.9-5D-40	43	Duct1-15.9-5D-40	59	Duct2-15.9-5D-40
28	RYE-15.9-7D-40	44	Duct1-15.9-7D-40	60	Duct2-15.9-7D-40
29	RYE-15.9-3D-60	45	Duct1-15.9-3D-60	61	Duct2-15.9-3D-60
30	RYE-15.9-5D-60	46	Duct1-15.9-5D-60	62	Duct2-15.9-5D-60
31	RYE-15.9-5D-60	47	Duct1-15.9-5D-60	63	Duct2-15.9-5D-60
32	RYE-15.9-7D-60	48	Duct1-15.9-7D-60	64	Duct2-15.9-7D-60
33	RYE-19.1-3D-40	49	Duct1-19.1-3D-40	65	Duct2-19.1-3D-40
34	RYE-19.1-5D-40	50	Duct1-19.1-5D-40	66	Duct2-19.1-5D-40
35	RYE-19.1-5D-40	51	Duct1-19.1-5D-40	67	Duct2-19.1-5D-40
36	RYE-19.1-7D-40	52	Duct1-19.1-7D-40	68	Duct2-19.1-7D-40
37	RYE-19.1-3D-60	53	Duct1-19.1-3D-60	69	Duct2-19.1-3D-60
38	RYE-19.1-5D-60	54	Duct1-19.1-5D-60	70	Duct2-19.1-5D-60
39	RYE-19.1-5D-60	55	Duct1-19.1-5D-60	71	Duct2-19.1-5D-60
40	RYE-19.1-7D-60	56	Duct1-19.1-7D-60	72	Duct2-19.1-7D-60

APPENDIX B

Ryerson Concrete Fresh Property Evaluations

B1: Slump-Flow and T_{500}:

The slump-flow and T_{500} time is a test to assess the flowability and the flow rate of self-consolidating concrete in the absence of obstructions. The slump-flow is an indication of the filling ability of the self-compacting concrete. The T_{500} time is also a measure of the speed of flow and therefore the viscosity of the self-compacting concrete.

Apparatus:

- Slump cone that conformed to ASTM C143.
- A baseplate made from a flat plate with a plane area of at least 900 mm x 900 mm on which the concrete was placed. The base plate was flat, smooth and non-absorbant and had a minimum thickness of 2 mm. The centre of the plate was marked with a cross whose lines ran parallel with the edge of the plate and circles of 200 mm diameter and 500 mm diameter were drawn about the centre point of the plate. (Figure A.1)
- A measuring tape.
- A stop watch capable of measuring to the nearest 0.1 seconds.
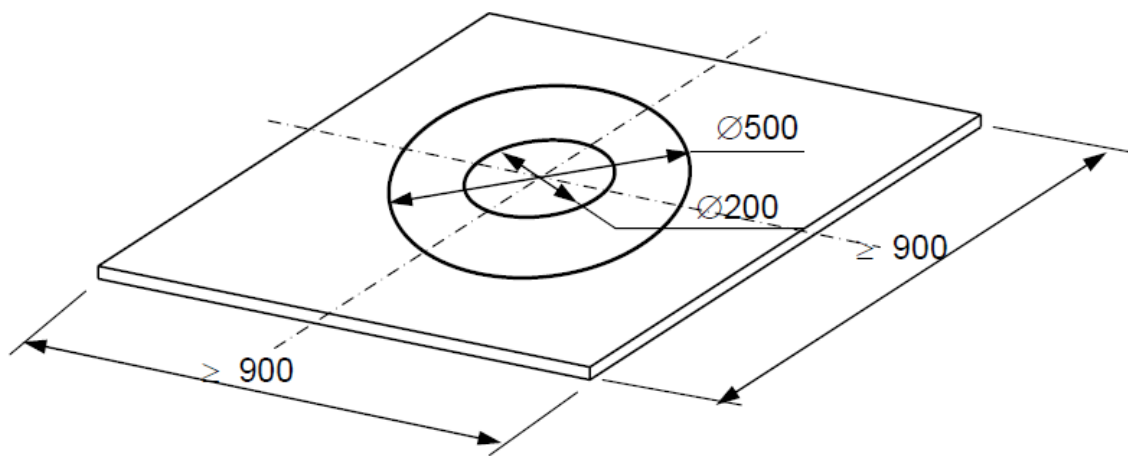
Figure B.1: Baseplate used for slump flow test. (Source: European Guidlines for Self Compacting Concrete. 2005)

Procedure:

The bottom of the slump cone was placed over the 200 mm diameter circle on the base plate and held in position. The cone was filled with concrete and was not allowed to stand for more than 30 seconds, which in this time, the spilled concrete was removed from the base plate. The cone was lifted vertically in one movement without interfering with the flow of the concrete. As soon as the cone was lifted, the stop watch was started and the time was recorded it took for the concrete to spread to a diameter of 500 mm and recorded to the nearest 0.1 seconds. Once the concrete stopped flowing, the diameter of the flow spread was recorded. Figure B.2 shows images from the slump-flow test and flow time tests conducted on Ryerson Concrete.

| (a) | (b) | (c) |

Figure B.2: Slump-flow and T_{500} test for Ryerson Concrete: (a) Slump cone and base plate; (b) lifting of the slump cone allowing concrete to flow; (c) measurement of the largest diameter of spread.

Results:

Slump-Flow	T_{500}
910 cm	1.8 seconds

It was observed that the concrete spread uniformly and that the it formed a nearly perfect circle.

B2: V-funnel Test:

The V-funnel test was used to assess the viscosity and filling ability of Ryerson Concrete.

Apparatus:

- A V-funnel with the dimensions shown in Figure B3 was used. It was fitted with a quick release, watertight gate at its base and supported such that the top of the funnel was horizontal.
- A container having a larger volume than the volume of the funnel was used to hold the test sample and was not less than 12 L.
- A stop watch capable of measuring to the nearest 0.1 seconds.
- A straight edge was used for striking off the concrete at the top of the funnel such that it was level with the top of the funnel.
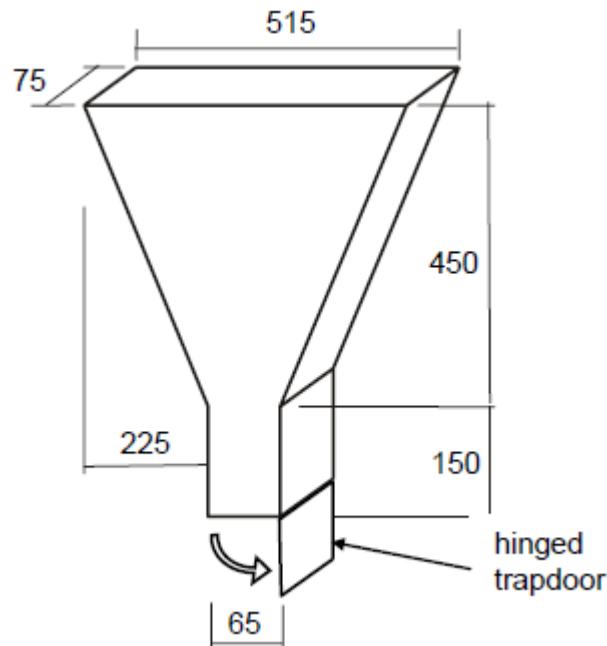
Figure B.3: V-funnel. (Source: European Guidlines for Self Compacting Concrete. 2005)

Procedure:

The funnel and the bottom gate were cleaned and all surfaces were dampened with water. The gate was then closed and the concrete was poured into the funnel without using any agitation or rodding. Once the funnel was filled, the excess concrete was struck off of the top using the straight edge such

that the concrete level was flush with the top of the funnel. The container was positioned under the funnel in order to retain the concrete that was passed. 8-12 seconds after the funnel was filled, the gate was opened and the time, measured to the nearest 0.1 seconds, it took from opening the gate to when it was possible to see vertically through the funnel into the container below was recorded. Figure B.4 shows images from the V-funnel test.

(a)   (b)
Figure B.4: V-funnel test: (a) During Discharge; (b) V-Funnel Time.

Results:

V-Funnel Time = 4.6 seconds

B3: L-Box Test:

The L-box test was used to assess the passing ability of Ryerson Concrete to flow through tight openings including reinforcing bars and other obstructions without segregation or blocking. The three bar test was used to simulate more congested reinforcement.

Apparatus:

- An L-Box with the dimensions shown in Figure B.5 was used.
- The L-Box had 3 smooth bars of 12 mm diameter with a gap of 41 mm for the three bar test.
- A measuring tape.
- A container having a volume greater than 14 L was used to hold the sample.
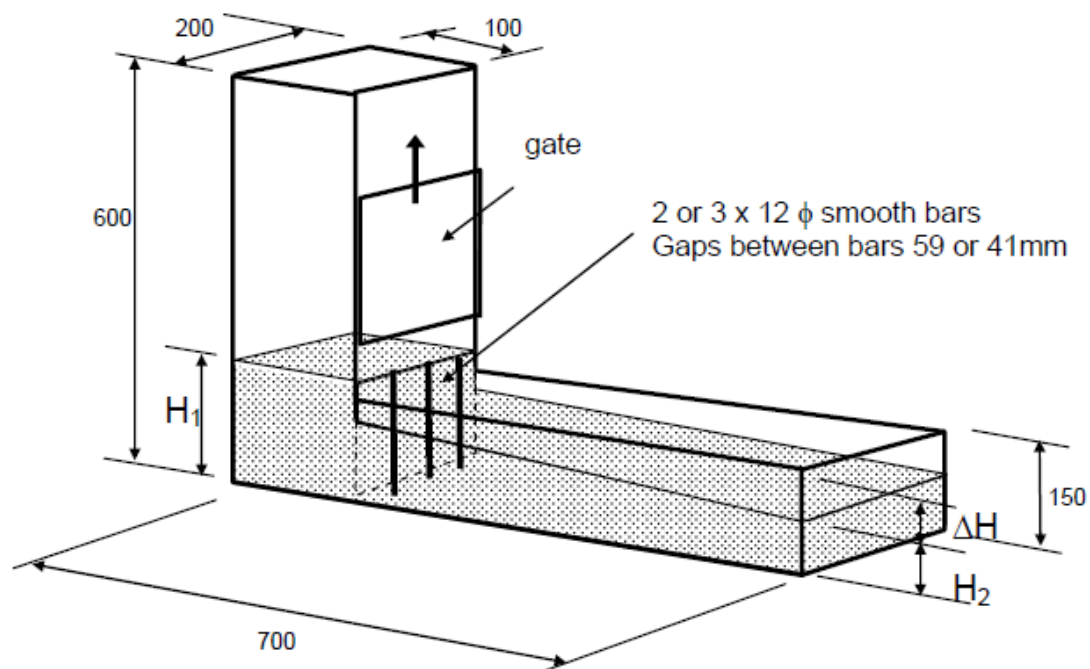
Figure B.5: L-box. (Source: European Guidlines for Self Compacting Concrete. 2005)

Procedure:

With the gate in the closed position, the concrete was poured from the container into the filling hopper of the L-Box and was allowed to stand for 60±10 seconds. The gate was then lifted and the concrete flowed into the horizontal section of the box. After the movement stopped, the depth of the concrete was measured at the end of the horizontal section of the L-box and the depth of the concrete

was directly behind the gate was measured. The passing ability was calculated as the ratio of the height of the concrete at the front of the horizontal section of the box to the height of the concrete directly behind the gate. Figure B.6 shows images from the L-Box test.

(a)	(b)

Figure B.6: L-box test: (a) immediately after opening the gate; (b) while concrete flow has reached the end of the box.

Results:

H1 = 7.6; H_2 7.1; Passing Ability = 7.1/7.6 = 0.93

There were no blockages or segregation of Ryerson Concrete observed during this test.

APPENDIX C

Beam Test Experimental Results

C1: Beam Test Results

	Test No.	Specimen	Nominal Dia (mm)	Act Dia w Sand (mm)	Emb. Len (3,5,7)xD	Emb. Len (mm)	Load (kN)	LVDT (1) (mm)	LVDT (2) (mm)	Strain (με)	Bar Load (kN)	Bond Stress (MPa)
HP-S10	1	KING-15.9-3D	15.9	17.494	3D	47.7	47.52	-0.08	-0.07	2506	59.400	22.658
	2	KING-15.9-5D	15.9	17.494	5D	79.5	74.22	-0.43	-0.17	7060	92.775	21.234
	3	KING-15.9-5D	15.9	17.494	5D	79.5	66.72	-0.1	-0.3	4511	83.400	19.088
	4	KING-15.9-7D	15.9	17.494	7D	111.3	87.7	-0.1	-0.09	6981	109.625	17.922
	5	KING-19.1-3D	19.1	20.763	3D	57.3	56.3	N/A	N/A	6711	84.450	22.595
	6	KING-19.1-5D	19.1	20.763	5D	95.5	75.32	-0.06	-0.08	4864	112.980	18.137
	7	KING-19.1-5D	19.1	20.763	5D	95.5	82.78	-0.08	-0.1	7554	124.170	19.933
	8	KING-19.1-7D	19.1	20.763	7D	133.7	91.25	N/A	N/A	7331	136.875	15.695

	Test No.	Specimen	Nominal Dia (mm)	Act Dia w Sand (mm)	Emb. Len (3,5,7)xD	Emb. Len (mm)	Load (kN)	LVDT (1) (mm)	LVDT (2) (mm)	Strain (με)	Bar Load (kN)	Bond Stress (MPa)
Ryerson Concrete	1	RYE-15.9-3D	15.9	17.494	3D	47.7	54.49	-0.15	-0.18	N/A	68.113	25.982
	2	RYE-15.9-5D	15.9	17.494	5D	79.5	69.61	-0.14	-0.18	6604	87.013	19.915
	3	RYE-15.9-5D	15.9	17.494	5D	79.5	69.99	-0.26	-0.11	6483	87.488	20.023
	4	RYE-15.9-7D	15.9	17.494	7D	111.3	92.53	-0.16	-0.16	5923	115.663	18.909
	5	RYE-19.1-3D	19.1	20.763	3D	57.3	63.03	-0.06	-0.08	3638	94.545	25.296
	6	RYE-19.1-5D	19.1	20.763	5D	95.5	90.6	-0.07	-0.07	6201	135.900	21.816
	7	RYE-19.1-5D	19.1	20.763	5D	95.5	90.97	-0.08	-0.06	6159	136.455	21.905
	8	RYE-19.1-7D	19.1	20.763	7D	133.7	100.13	-0.06	-0.05	7362	150.195	17.222

	Test No.	Specimen	Nominal Dia (mm)	Act Dia w Sand (mm)	Emb. Len (3,5,7)xD	Emb. Len (mm)	Load (kN)	LVDT (1) (mm)	LVDT (2) (mm)	Strain (με)	Bar Load (kN)	Bond Stress (MPa)
Ductal1	1	Duct1-15.9-3D	15.9	17.494	3D	47.7	50.41	-0.14	-0.2	4884	63.013	24.036
	2	Duct1-15.9-5D	15.9	17.494	5D	79.5	72.61	-0.06	-0.1	6398	90.763	20.773
	3	Duct1-15.9-5D	15.9	17.494	5D	79.5	76.37	-0.01	-0.05	6997	95.463	21.849
	4	Duct1-15.9-7D	15.9	17.494	7D	111.3	98.08	-0.06	-0.07	9362	122.600	20.043
	5	Duct1-19.1-3D	19.1	20.763	3D	57.3	60.5	-0.19	-0.05	3569	90.750	24.280
	6	Duct1-19.1-5D	19.1	20.763	5D	95.5	86.09	-0.05	-0.6	6973	129.135	20.730
	7	Duct1-19.1-5D	19.1	20.763	5D	95.5	87.54	-0.08	-0.01	5904	131.310	21.079
	8	Duct1-19.1-7D	19.1	20.763	7D	133.7	100.75	-0.09	-0.09	9163	151.125	17.329

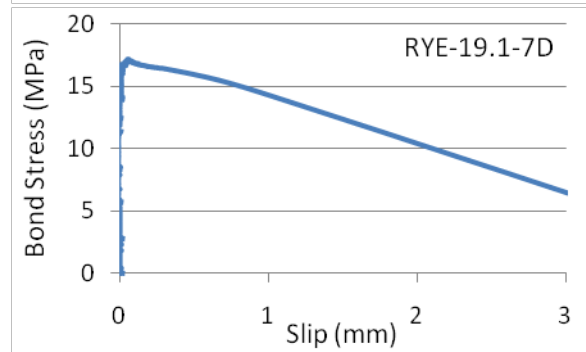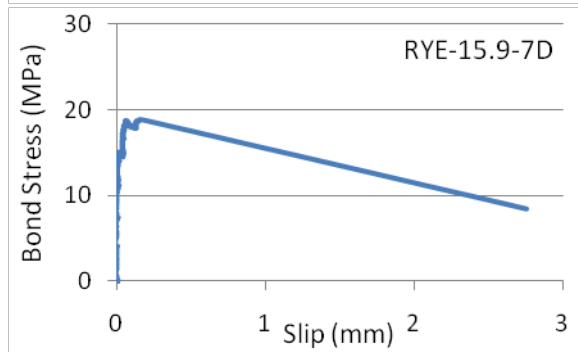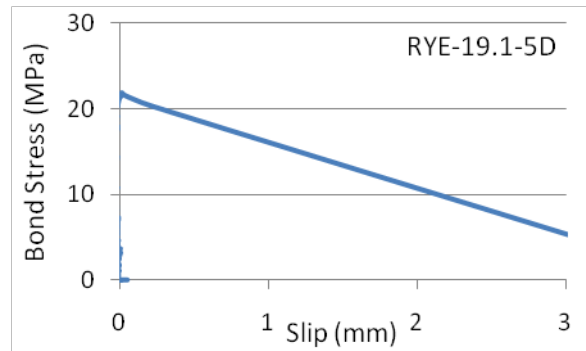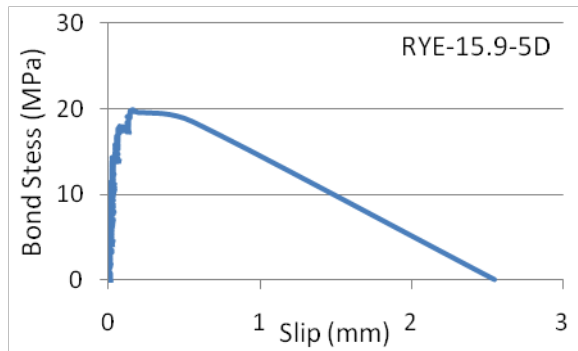|	Test No.	Specimen	Nominal Dia (mm)	Act Dia w Sand (mm)	Emb. Len (3,5,7)xD	Emb. Len (mm)	Load (kN)	LVDT (1) (mm)	LVDT (2) (mm)	Strain (με)	Bar Load (kN)	Bond Stress (MPa)
Ductal2	1	Duct2-15.9-3D	15.9	17.494	3D	47.7	62.42	-0.05	-0.08	5571	78.025	29.763
	2	Duct2-15.9-5D	15.9	17.494	5D	79.5	70.8	-0.22	-0.28	6634	88.500	20.255
	3	Duct2-15.9-5D	15.9	17.494	5D	79.5	74.36	-0.1	-0.09	7682	92.950	21.274
	4	Duct2-15.9-7D	15.9	17.494	7D	111.3	91.56	-0.1	-0.12	8169	114.450	18.710
	5	Duct2-19.1-3D	19.1	20.763	3D	57.3	68.43	-0.06	-0.1	6038	102.645	27.463
	6	Duct2-19.1-5D	19.1	20.763	5D	95.5	84.07	-0.17	-0.04	7503	126.105	20.244
	7	Duct2-19.1-5D	19.1	20.763	5D	95.5	85.92	-0.04	-0.13	7702	128.880	20.689
	8	Duct2-19.1-7D	19.1	20.763	7D	133.7	112.17	-0.14	-0.14	10014	168.255	19.293

C2: Bond Stress-Slip Curves
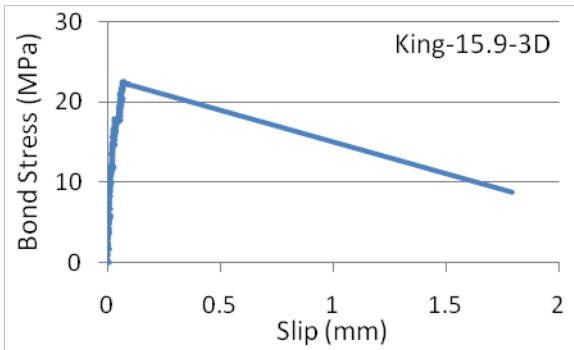
No data available for King-19.1-3D specimen.
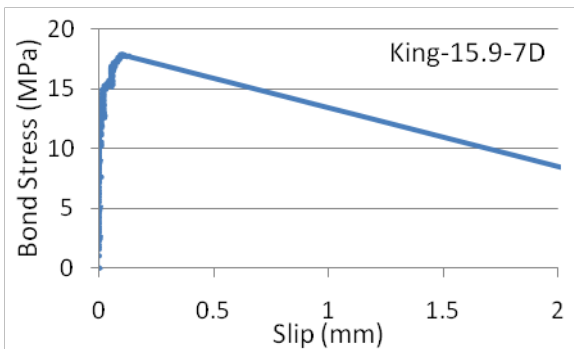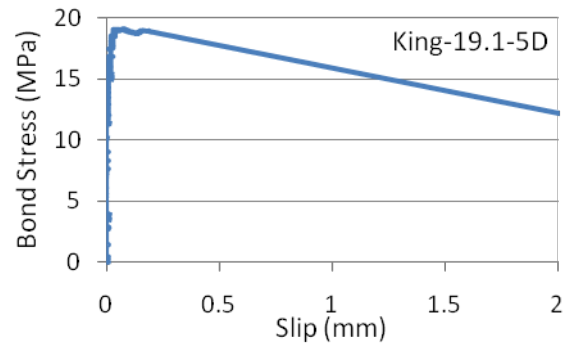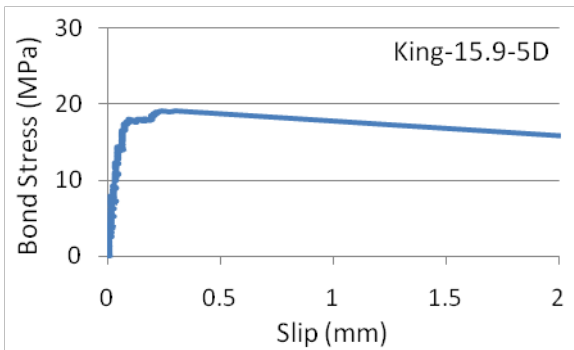
No data available for King-19.1-7D specimen.
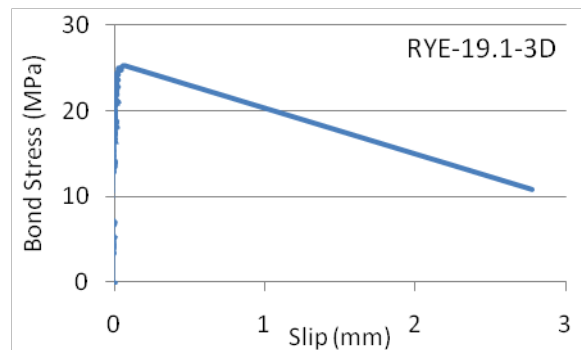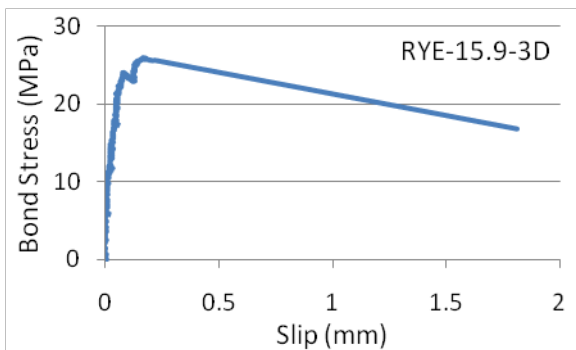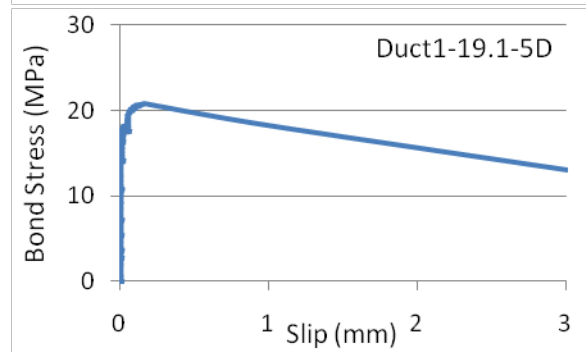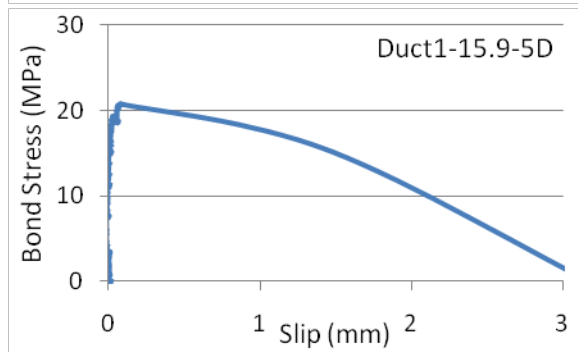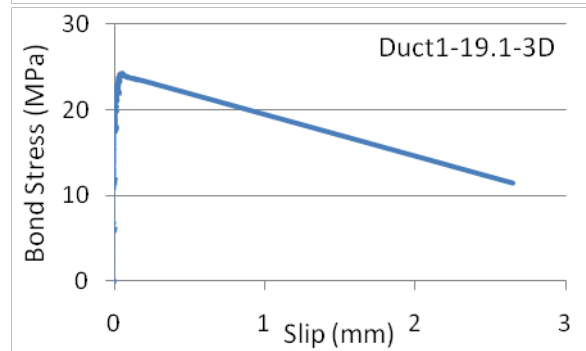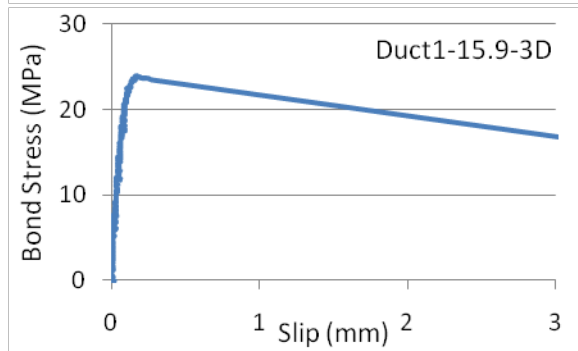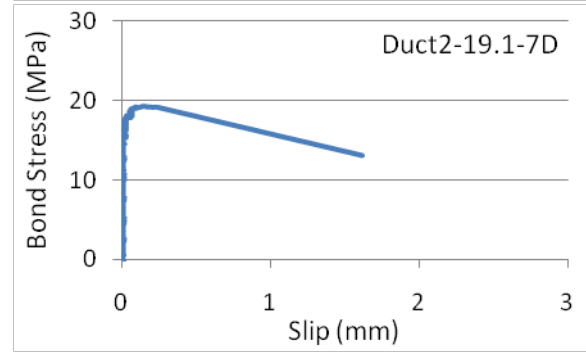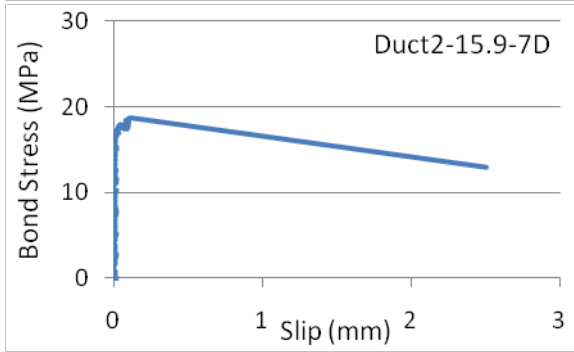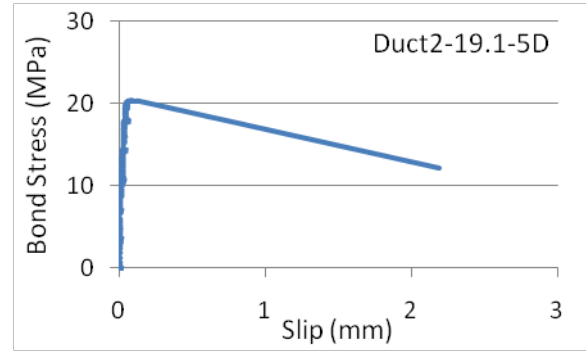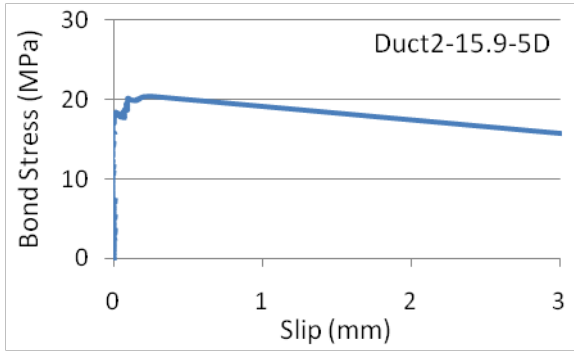
APPENDIX D

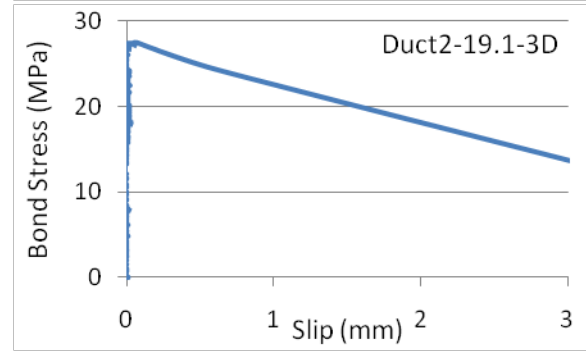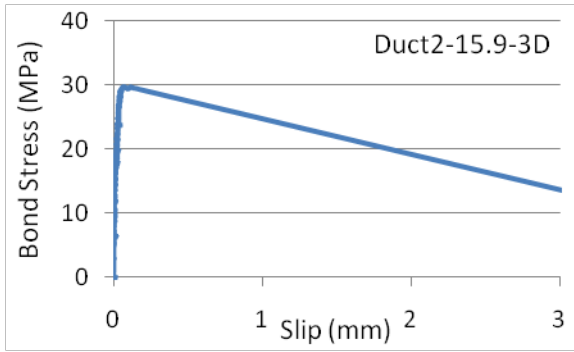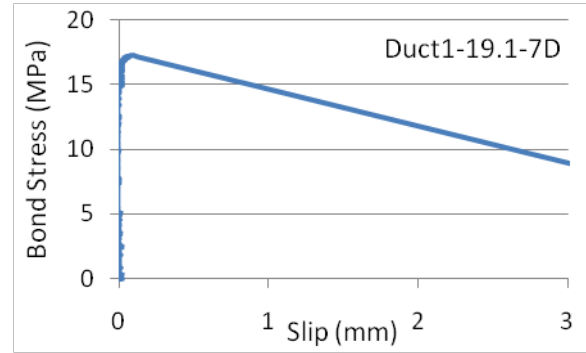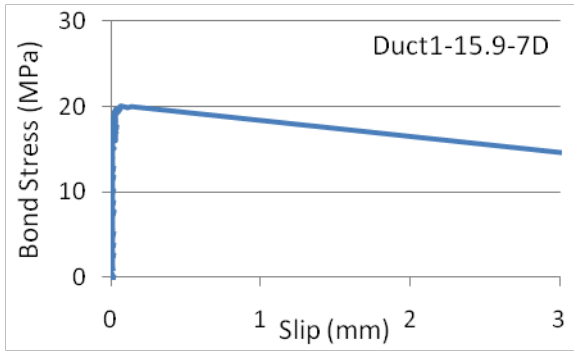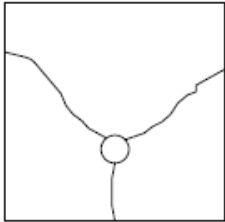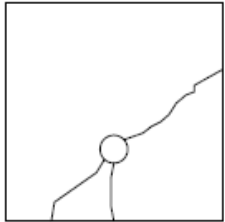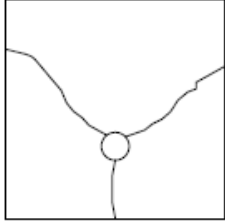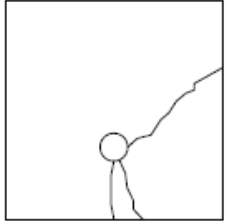# Pullout Test Experimental Results

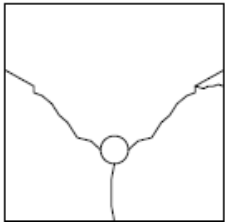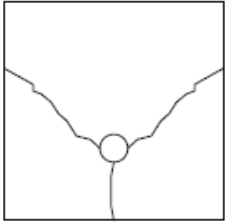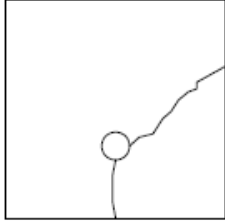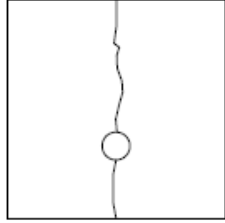## *D1: Pullout Test Results*
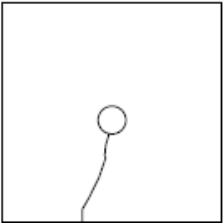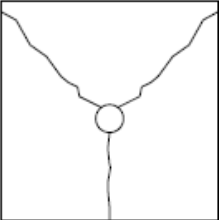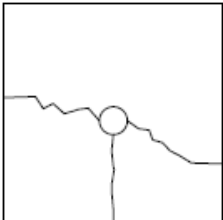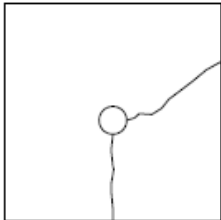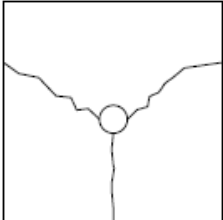
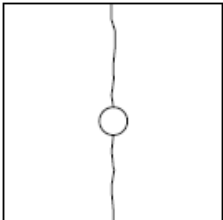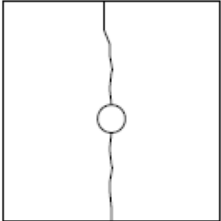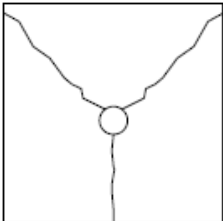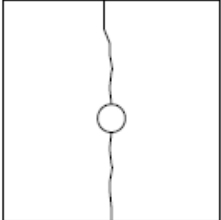| Test No.	Specimen	Nominal Dia (mm)	Act Dia w Sand (mm)	Emb. Len 3,5,7,10xD	Emb. Len (mm)	Cover (mm)	Pullout Force (kN)	Bond Stress (Mpa)	Failure Mode
1	KING-15.9-3D-40	15.9	17.494	3D	47.7	40	51.63	19.694	Pullout
2	KING-15.9-5D-40	15.9	17.494	5D	79.5	40	53.06	12.144	Splitting
3	KING-15.9-5D-40	15.9	17.494	5D	79.5	40	53.94	12.345	Splitting
4	KING-15.9-7D-40	15.9	17.494	7D	111.3	40	80.20	13.111	Pullout
5	KING-15.9-10D-40	15.9	17.494	10D	159	40	92.25	10.557	Splitting
6	KING-15.9-10D-40	15.9	17.494	10D	159	40	85.31	9.763	Splitting
7	KING-15.9-3D-60	15.9	17.494	3D	47.7	60	53.94	20.576	Pullout
8	KING-15.9-5D-60	15.9	17.494	5D	79.5	60	60.69	13.890	Splitting
9	KING-15.9-5D-60	15.9	17.494	5D	79.5	60	61.31	14.032	Splitting
10	KING-15.9-7D-60	15.9	17.494	7D	111.3	60	85.56	13.987	Pullout
11	KING-15.9-10D-60	15.9	17.494	10D	159	60	103.69	11.866	Splitting
12	KING-15.9-10D-60	15.9	17.494	10D	159	60	93.07	10.651	Splitting
13	KING-19.1-3D-40	19.1	20.763	3D	57.3	40	63.94	17.107	Pullout
14	KING-19.1-5D-40	19.1	20.763	5D	95.5	40	47.00	7.545	Splitting
15	KING-19.1-5D-40	19.1	20.763	5D	95.5	40	46.94	7.535	Splitting
16	KING-19.1-7D-40	19.1	20.763	7D	133.7	40	58.00	6.651	Pullout
17	KING-19.1-10D-40	19.1	20.763	10D	191	40	95.76	7.686	Splitting
18	KING-19.1-10D-40	19.1	20.763	10D	191	40	100.99	8.106	Splitting
19	KING-19.1-3D-60	19.1	20.763	3D	57.3	60	55.56	14.865	Splitting
20	KING-19.1-5D-60	19.1	20.763	5D	95.5	60	60.56	9.722	Splitting
21	KING-19.1-5D-60	19.1	20.763	5D	95.5	60	64.75	10.394	Splitting
22	KING-19.1-7D-60	19.1	20.763	7D	133.7	60	72.19	8.278	Splitting
23	KING-19.1-10D-60	19.1	20.763	10D	191	60	114.00	9.150	Splitting
24	KING-19.1-10D-60	19.1	20.763	10D	191	60	111.87	8.979	Splitting

HP-S10

	Test No.	Specimen	Nominal Dia (mm)	Act Dia w Sand (mm)	Emb. Len (3,5,7)xD	Emb. Len (mm)	Cover (mm)	Pullout Force (kN)	Bond Stress (Mpa)	Failure Mode
Ryerson Concrete	1	RYE-15.9-3D-40	15.9	17.494	3D	47.7	40	36.31	13.851	Pullout
	2	RYE-15.9-5D-40	15.9	17.494	5D	79.5	40	64.84	14.840	Pullout
	3	RYE-15.9-5D-40	15.9	17.494	5D	79.5	40	59.85	13.698	Pullout
	4	RYE-15.9-7D-40	15.9	17.494	7D	111.3	40	71.69	11.720	Pullout
	5	RYE-15.9-3D-60	15.9	17.494	3D	47.7	60	47.50	18.119	Pullout
	6	RYE-15.9-5D-60	15.9	17.494	5D	79.5	60	63.45	14.522	Pullout
	7	RYE-15.9-5D-60	15.9	17.494	5D	79.5	60	59.69	13.661	Pullout
	8	RYE-15.9-7D-60	15.9	17.494	7D	111.3	60	73.44	12.006	Pullout
	9	RYE-19.1-3D-40	19.1	20.763	3D	57.3	40	65.12	17.423	Pullout
	10	RYE-19.1-5D-40	19.1	20.763	5D	95.5	40	81.06	13.013	Pullout
	11	RYE-19.1-5D-40	19.1	20.763	5D	95.5	40	86.38	13.867	Pullout
	12	RYE-19.1-7D-40	19.1	20.763	7D	133.7	40	110.81	12.706	Pullout
	13	RYE-19.1-3D-60	19.1	20.763	3D	57.3	60	56.20	15.036	Pullout
	14	RYE-19.1-5D-60	19.1	20.763	5D	95.5	60	78.78	12.647	Pullout
	15	RYE-19.1-5D-60	19.1	20.763	5D	95.5	60	85.78	13.770	Pullout
	16	RYE-19.1-7D-60	19.1	20.763	7D	133.7	60	106.06	12.161	Pullout

	Test No.	Specimen	Nominal Dia (mm)	Act Dia w Sand (mm)	Emb. Len (3,5,7)xD	Emb. Len (mm)	Cover (mm)	Pullout Force (kN)	Bond Stress (Mpa)	Failure Mode
Ductal1	1	Duct1-15.9-3D-40	15.9	17.494	3D	47.7	40	35.75	13.637	Pullout
	2	Duct1-15.9-5D-40	15.9	17.494	5D	79.5	40	45.31	10.370	Pullout
	3	Duct1-15.9-5D-40	15.9	17.494	5D	79.5	40	46.69	10.686	Pullout
	4	Duct1-15.9-7D-40	15.9	17.494	7D	111.3	40	75.00	12.261	Pullout
	5	Duct1-15.9-3D-60	15.9	17.494	3D	47.7	60	39.69	15.140	Pullout
	6	Duct1-15.9-5D-60	15.9	17.494	5D	79.5	60	50.06	11.457	Pullout
	7	Duct1-15.9-5D-60	15.9	17.494	5D	79.5	60	51.69	11.830	Pullout
	8	Duct1-15.9-7D-60	15.9	17.494	7D	111.3	60	69.50	11.362	Pullout
	9	Duct1-19.1-3D-40	19.1	20.763	3D	57.3	40	63.00	16.856	Pullout
	10	Duct1-19.1-5D-40	19.1	20.763	5D	95.5	40	94.10	15.106	Pullout
	11	Duct1-19.1-5D-40	19.1	20.763	5D	95.5	40	87.15	13.990	Pullout
	12	Duct1-19.1-7D-40	19.1	20.763	7D	133.7	40	100.63	11.539	Pullout
	13	Duct1-19.1-3D-60	19.1	20.763	3D	57.3	60	50.88	13.613	Pullout
	14	Duct1-19.1-5D-60	19.1	20.763	5D	95.5	60	90.70	14.560	Pullout
	15	Duct1-19.1-5D-60	19.1	20.763	5D	95.5	60	87.80	14.095	Pullout
	16	Duct1-19.1-7D-60	19.1	20.763	7D	133.7	60	98.88	11.338	Pullout

	Test No.	Specimen	Nominal Dia (mm)	Act Dia w Sand (mm)	Emb. Len (3,5,7)xD	Emb. Len (mm)	Cover (mm)	Pullout Force (kN)	Bond Stress (Mpa)	
	1	Duct2-15.9-3D-40	15.9	17.494	3D	47.7	40	52.69	20.099	Pullout
	2	Duct2-15.9-5D-40	15.9	17.494	5D	79.5	40	73.75	16.879	Pullout
	3	Duct2-15.9-5D-40	15.9	17.494	5D	79.5	40	67.44	15.435	Pullout
	4	Duct2-15.9-7D-40	15.9	17.494	7D	111.3	40	105.00	17.165	Pullout
	5	Duct2-15.9-3D-60	15.9	17.494	3D	47.7	60	60.44	23.055	Pullout
	6	Duct2-15.9-5D-60	15.9	17.494	5D	79.5	60	74.50	17.051	Pullout
Ductal2	7	Duct2-15.9-5D-60	15.9	17.494	5D	79.5	60	82.69	18.925	Pullout
	8	Duct2-15.9-7D-60	15.9	17.494	7D	111.3	60	98.81	16.154	Pullout
	9	Duct2-19.1-3D-40	19.1	20.763	3D	57.3	40	77.94	20.853	Pullout
	10	Duct2-19.1-5D-40	19.1	20.763	5D	95.5	40	118.75	19.063	Pullout
	11	Duct2-19.1-5D-40	19.1	20.763	5D	95.5	40	106.94	17.167	Pullout
	12	Duct2-19.1-7D-40	19.1	20.763	7D	133.7	40	139.31	15.974	Pullout
	13	Duct2-19.1-3D-60	19.1	20.763	3D	57.3	60	80.81	21.621	Pullout
	14	Duct2-19.1-5D-60	19.1	20.763	5D	95.5	60	113.50	18.220	Pullout
	15	Duct2-19.1-5D-60	19.1	20.763	5D	95.5	60	118.63	19.044	Pullout
	16	Duct2-19.1-7D-60	19.1	20.763	7D	133.7	60	135.69	15.559	Pullout

D2: Crack Patterns for HP-S10 Pullout Specimens

Specimen	Failure Mode	Specimen	Failure Mode
KING-15.9-3D-40	Pullout Failure	KING-19.1-3D-40	Pullout Failure
KING-15.9-5D-40		KING-19.1-5D-40	
KING-15.9-5D-40		KING-19.1-5D-40	
KING-15.9-7D-40	Pullout Failure	KING-19.1-7D-40	Pullout Failure
KING-15.9-10D-40		KING-19.1-10D-40	
KING-15.9-10D-40		KING-19.1-10D-40	

Specimen	Failure Mode	Specimen	Failure Mode
KING-15.9-3D-60	Pullout Failure	KING-19.1-3D-60	
KING-15.9-5D-60		KING-19.1-5D-60	
KING-15.9-5D-60		KING-19.1-5D-60	
KING-15.9-7D-60	Pullout Failure	KING-19.1-7D-60	
KING-15.9-10D-60		KING-19.1-10D-60	
KING-15.9-10D-60		KING-19.1-10D-60	